UNIVERSIDADE ESTADUAL DE CAMPINAS

Instituto de Matemática, Estatística e Computação Científica

ARTUR CÉSAR FASSONI

# Modelos matemáticos em câncer abordando fase inicial e tratamento de tumor avascular

Campinas

2016

Artur César Fassoni

# Modelos matemáticos em câncer abordando fase inicial e tratamento de tumor avascular

Tese apresentada ao Instituto de Matemática, Estatística e Computação Científica da Universidade Estadual de Campinas como parte dos requisitos exigidos para a obtenção do título de Doutor em Matemática Aplicada.

Orientador: Hyun Mo Yang

Este exemplar corresponde à versão final da Tese defendida pelo aluno Artur César Fassoni e orientada pelo Prof. Dr. Hyun Mo Yang.

Campinas

2016

**Agência(s) de fomento e nº(s) de processo(s):** CAPES

Ficha catalográfica
Universidade Estadual de Campinas
Biblioteca do Instituto de Matemática, Estatística e Computação Científica
Ana Regina Machado - CRB 8/5467

Fassoni, Artur César, 1988-
F264m Modelos matemáticos em câncer abordando fase inicial e tratamento de tumor avascular / Artur César Fassoni. – Campinas, SP : [s.n.], 2016.

Orientador: Hyun Mo Yang.
Tese (doutorado) – Universidade Estadual de Campinas, Instituto de Matemática, Estatística e Computação Científica.

1. Câncer. 2. Carcinogênese. 3. Quimioterapia. 4. Equações diferenciais ordinárias. 5. Dinâmica não-linear. I. Yang, Hyun Mo,1959-. II. Universidade Estadual de Campinas. Instituto de Matemática, Estatística e Computação Científica. III. Título.

Informações para Biblioteca Digital

**Título em outro idioma:** Mathematical modeling in cancer addressing the early stage and treatment of avascular tumors
**Palavras-chave em inglês:**
Cancer
Carcinogenesis
Chemotherapy
Ordinary differential equations
Nonlinear dynamics
**Área de concentração:** Matemática Aplicada
**Titulação:** Doutor em Matemática Aplicada
**Banca examinadora:**
Hyun Mo Yang [Orientador]
Paulo Regis Caron Ruffino
Luis Fernando de Osório Mello
Paulo Fernando de Arruda Mancera
Harley Francisco de Oliveira
**Data de defesa:** 08-04-2016
**Programa de Pós-Graduação:** Matemática Aplicada

**Tese de Doutorado defendida em 08 de abril de 2016 e aprovada**

**Pela Banca Examinadora composta pelos Profs. Drs.**

**Prof(a). Dr(a). HYUN MO YANG**

**Prof(a). Dr(a). PAULO REGIS CARON RUFFINO**

**Prof(a). Dr(a). LUIS FERNANDO DE OSÓRIO MELLO**

**Prof(a). Dr(a). PAULO FERNANDO DE ARRUDA MANCERA**

**Prof(a). Dr(a). HARLEY FRANCISCO DE OLIVEIRA**

A Ata da defesa com as respectivas assinaturas dos membros
encontra-se no processo de vida acadêmica do aluno.

*À Andréia...*

# Agradecimentos

A Deus pela sua misericórdia e pela vida, ontem, hoje e amanhã.

À Andréia pelo companheirismo. Este doutorado é seu também. Não caberiam aqui os relatos das inúmeras vezes em que me animaste, tiveste paciência e sofreste comigo para concluir esta etapa.

À nossa filha Ana pela alegria indizível que trouxe ao nosso lar.

À nossa segunda filha, vindo em breve.

Aos meus pais Délio e Lora pela herança de vida e formação.

Aos meus irmãos, cunhados, familiares e amigos.

Ao meu tio Edson pela amizade e por me receber em sua casa inúmeras vezes, desde o dia da prova de seleção até o dia da defesa.

Ao Prof. Hyun pelo exemplo, confiança e pela orientação que nos prepara para as etapas posteriores ao doutorado.

Aos membros da banca, professores Paulo Ruffino, Luis Fernando Mello, Paulo Mancera e Harley de Oliveira, pela participação na banca, comentários e sugestões.

Ao Prof. Wilson Castro Ferreira Jr. pelos ensinamentos transmitidos nas disciplinas de Biomatemática e conversas, que mudaram a maneira como enxergo a Matemática e o Ensino de Matemática.

Ao Prof. Boldrini pelos ensinamentos transmitidos na disciplina Tópicos em Biomatemática.

Ao Prof. Eduardo Abreu pelo exemplo de didática transmitido na disciplina Análise Numérica.

Aos amigos do EPIFISMA e do IMECC: Luiz Fernando, Carpegiani, Felipo, Miller, Michael, Evandro e todos os demais, pelo apoio e companheirismo.

Aos amigos da UNIFEI: Denis, Maicon, Rodrigo e todos os demais, pelo apoio e companheirismo.

Ao Dr. Gerson Yoshinari Jr. pelas conversas sobre câncer.

À Secretaria de Pós-Graduação, nas pessoas da Tânia, Eliana, Ednaldo e Luciana, pelos diversos auxílios prestrados ao longo do tempo.

À CAPES pelos 19 meses de bolsa.

*"Não há termos, não há palavras,*
*nenhum som que deles se ouça,*
*contudo, por toda a terra espalha-se a sua voz,*
*e até os confis do mundo a sua linguagem."*
*Sl 19*

# Resumo

Esta tese trata de modelos matemáticos para descrever o surgimento e tratamento de tumores avasculares. Os modelos são baseados em sistemas de equações diferenciais ordinárias. Primeiramente, propomos um modelo para descrever o surgimento do câncer como um processo multi-passo, envolvendo transições entre células normais, células pré-malignas, e células tumorais, e considerando instabilidade genética como um fator que aumenta a taxa de mutações. O modelo prevê que a agressividade das células tumorais abre espaço para a sobrevivência das células menos adaptadas. Simulações numéricas mostram que o tempo para o tumor alcançar um tamanho detectável varia de cinco a oitenta anos, em razão de alterações mínimas nos parâmetros. Em seguida, estudamos um caso particular do primeiro modelo de um ponto de vista da teoria da Resiliência Ecológica. Os resultados ilustram como o surgimento e o tratamento efetivo do câncer podem ser vistos como a alternância entre dois estados de equilíbrio estáveis antagônicos. Neste contexto, alterações genéticas em uma escala de tempo lenta podem levar à destruição ou perda de estabilidade de um destes estados, tornando impossível tanto a cura ou o surgimento da doença. Na etapa seguinte, estudamos um modelo para quimioterapia metronômica em tumores avasculares, e mostramos como este tipo de tratamento pode levar à cura do paciente. Uma condição relacionando a toxicidade do tratamento aos parâmetros do modelo surge naturalmente e sua interpretação indica que a terapia metronômica tem baixa toxicidade quando administrada em tumores de crescimento lento, tumores com alta agressividade e competitividade por recursos, ou tumores com alta capacidade de suporte. Na última etapa, consideramos tratamentos não-autônomos visando comparar diversos regimes de dosagem em busca de protocolos ótimos. Mostramos como a utilização de uma abordagem simples para parametrizar a função que descreve o tratamento implica em facilidades tanto para a aplicação de métodos de otimização, quanto para a elaboração de critérios de otimalidade que englobem diversas características, como toxicidade, risco de recidiva, tempo de recuperação, e limitações na dosagem de droga.

**Palavras-chave**: Câncer. Carcinogenese. Quimioterapia. Equações diferenciais ordinárias. Dinâmica não-linear.

# Abstract

This thesis studies mathematical models describing the onset and treatment of avascular tumors. The models are based on systems of ordinary differential equations. Initially, we propose a model to the onset of cancer as a multi-step process, involving transitions among normal cells, pre-malignant cells and tumor cells. The model considers genetic instability as a factor that enhances the mutation rates. Results predict that aggressiveness of tumor cells opens space to survival of less adapted cells. Numerical simulations show that the time for the tumor attains a detectable size ranges from five to eighty years, depending on minimal changes in parameters. Next, we study a particular case of the first model, from the point of view of Ecological Resilience. Results illustrate how the onset and the effective treatment of cancer may be seen as the switching between two alternative stable states. In this context, genetic alterations in a slow time-scale may cause the destruction or the loss of stability of one of these states, what makes impossible either the cure or the beginning of the disease. In the next stage, we study a model for metronomic chemotherapy in an avascular tumor, and we show how this treatment may lead to cure. A condition regarding toxicity and related to parameters arises naturally. Its interpretation indicates that metronomic chemotherapy has lower toxicity when administered in slow-growing tumors, tumors with high aggressiveness or competitiveness, and tumors with a high support capacity. In last, we consider non-autonomous treatments in order to compare different dosage regimes seeking for an optimal protocol. We show how the use of a simple approach for parameterizing the function which describes the treatment implies in advantages both for applying optimization methods as well as for formulating optimality criteria encompassing diverse features such as toxicity, relapse risk, recovery time and drug dosage.

**Keywords**: Cancer. Carcinogenesis. Chemotherapy. Ordinary differential equations. Non-linear dynamics.

# Sumário

# 1 Introdução

Muitas são as estatísticas existentes a respeito do câncer e sua crescente incidência na população mundial, sobre o grande número de mortes causadas por ele, os elevados gastos governamentais com tratamento de pacientes e investimentos em pesquisa (1). Assim, é de suma importância estudar e conhecer a fundo as causas de seu surgimento, os seus mecanismos de desenvolvimento, e os diversos tipos e estratégias de tratamento e de diagnóstico.

A Biomatemática é uma área de pesquisa que vem se firmando e atraindo cada vez mais pesquisadores nas últimas décadas (2). Em linhas gerais, ela trata de descrever problemas e fenômenos biológicos utilizando a matemática como linguagem básica e, resolvendo os problemas matemáticos resultantes, devolver à biologia algum novo entendimento sobre o fenômeno, levando ao direcionamento de testes e experimentos que validem tais conclusões. Assim, por estar situada na interface entre Matemática e Biologia, é uma área dinâmica, em constante mudança e crescimento. Se, por um lado, a necessidade de se descrever problemas biológicos numa linguagem matemática tem impulsionado o desenvolvimento e aprimoramento de métodos e teorias matemáticas, por outro lado, as várias conclusões matemáticas a respeito destes fenômenos tem levado biólogos, médicos e ecólogos a um melhor entendimento dos fenômenos naturais. Por isto, a Matemática tem sido chamada “o novo microscópio da Biologia”, enquanto esta tem sido chamada “a nova Física da Matemática” (3).

A “Oncologia Matemática” é o ramo da Biomatemática que diz respeito ao câncer. A modelagem matemática tem sido usada já há um bom tempo como ferramenta para auxiliar nesta luta contra o câncer (4, 5, 6, 7, 8, 9, 10, 11, 12, 13, 14, 15). Devido a complexidade desta doença e ao enorme número de fatores envolvidos, o auxílio da matemática pode ser muito proveitoso ao entendimento dos diversos aspectos relacionados a ela. De fato, se os modelos matemáticos conseguirem capturar alguns mecanismos essenciais envolvidos, os resultados das predições e simulações destes modelos podem ser confrontados com resultados clínicos e experimentais, ora corroborando hipóteses pré-existentes, ora lançando luz ou novos questionamentos sobre determinados aspectos (16, 17). Ainda, e principalmente, os modelos podem ser também uma primeira baliza e fonte de predições para testes experimentais e protocolos de tratamento, com a vantagem de poderem ser repetidos inúmeras vezes, sem possíveis danos a saúde dos pacientes e sem o alto custo financeiro decorrente dos experimentos em laboratório e testes clínicos.

Nesta tese, propomos e analisamos modelos matemáticos de Equações Diferenciais Ordinárias para descrever a fase inicial e o tratamento de um tumor sólido

avascular.

No Capítulo 2, consideramos a fase inicial da doença, estudando um modelo para crescimento de um tumor a partir do surgimento de uma população de células pré-malignas que adquirem mutações específicas e posteriormente se tornam células tumorais. Aspectos como instabilidade genética são considerados para formular as taxas de transição entre as populações de células.

No Capítulo 3, abordamos o crescimento e tratamento de câncer de um ponto de vista de Ecologia Teórica. Mais especificamente, examaminamos as consequências da aplicação de conceitos de Resiliência Ecológica a um modelo simples para crescimento tumoral. Neste contexto, o surgimento e tratamento da doença podem ser vistos de maneira geral como a alternância entre dois estados de equilíbrio, e aspectos relacionados a bacias de atração se tornam cruciais para o entendimento desta alternância.

No Capítulo 4, apresentamos um modelo para tratamento de um tumor sólido avascular por quimioterapia metronômica. O modelo é analisado em detalhes, com uso da Teoria de Sistemas Competitivos. A interpretação destes resultados matemáticos fornece critérios para avaliação da toxicidade da quimioterapia metronômica em diferentes tipos de tumor.

No Capítulo 5, modificamos o modelo anterior para considerar diversos regimes de tratamento quimioterápico. A forma utilizada para modelar o tratamento permite a aplicação de métodos de otimização em dimensão finita para comparar diferentes estratégias de tratamento e buscar o que seria um protocolo ótimo segundo algum critério estabelecido. Além disso, mostramos como diferentes efeitos de cada tratamento podem ser quantificados de forma a comporem uma função objetivo que englobe diversas características que deseja-se otimizar.

No Capítulo 6, apresentamos as conclusões desta tese e indicamos perspectivas futuras para continuação desta pesquisa. Os Capítulos 2 a 5 foram escritos em formato de artigo, em inglês, para publicação em periódicos internacionais. As demais partes da tese estão escritas em português.

# 2 Modeling dynamics for oncogenesis encompassing mutations and genetic instability

*Abstract.* Tumorigenesis has been described as a multistep process, where each step is associated with a genetic alteration, in the direction to progressively transform a normal cell and its descendants into a malignant tumor. In this work, a mathematical model is proposed for cancer onset and development, considering three populations: normal, premalignant, and cancer cells. The model takes in account three hallmarks of cancer (self-sufficiency on growth signals, insensibility to anti-growth signals, and evading apoptosis) and includes genetic instability as an enabling characteristic. Mathematical analysis was performed in detail. Results indicate that apoptosis and tissue repair system are the first barriers against tumor progression. One of these mechanisms must be corrupted for cancer to develop from a single mutant cell. Further, aggressive tumors have an extra protection against the tissue repair system and elevations in the apoptotic rate. Results also show that the presence of aggressive cancer cells opens way to survival of less adapted premalignant cells. Numerical simulations were performed with parameter values based on real data of breast cancer, and the necessary time taken for cancer to reach a detectable size from a single mutant cell was estimated with respect to some parameters. We find that the rates of apoptosis and mutations have a large influence on the pace of tumor progression and on cancer occurrence within a clinically detectable time.

*Keywords*: Multi-step tumorigenesis; Avascular tumour growth; Stability; Bifurcations.

## 2.1 Introduction

Cancer is a complex disease that has more than a hundred different types and can occur in almost all tissues in the body. Although each type of cancer has unique characteristics, the mechanisms that lead to its development are similar and share a few cellular and molecular characteristics. In this way, one can say that almost all cancer types obey certain universal rules (18, 19, 20).

Cancer begins when a mutation occurs in a cell and leaves it to escape one of the mechanisms that regulate the process of growth, division and death. The mutant cell becomes deaf to the proliferation control imposed to normal cells at the tissue, and divides in a frequency higher than the normal one. In fact, only one mutation is not enough to originate a malignant tumor, because the organism and the own cells have mechanisms that lead the mutant cells to die, thus preserving the system integrity. It is necessary

that, over the generations, the descendants of this mutant cell accumulate other very specific mutations that allow them to surpass the various barriers imposed by the organism against uncontrolled growth. Thus, tumorigenesis is a multistep process, where each step is associated with a genetic change, in the direction of progressive transformation of a normal cell and its descendants into a malignant tumor (21, 18, 19). It is worth to note that some clinical analyses revealed lesions that would be cells in intermediary stages during the process of cancer formation (22). Other experiments also comproved that all cells in a tumor descend from only one common ancestral (23). For a detailed description of the biology of cancer, we refer to the book (20).

Hanahan and Weinberg (18, 19) proposed that all the genetic alterations and the various cancer cellular genotypes can be grouped and conceptually described in eight acquired capabilities, essential alterations in the cellular physiology, which were denominated the *Hallmarks of Cancer*. They are: *self-sufficiency in growth signals*; *insensitivity to anti-growth signals*; *evading apoptosis*; *limitless replicative potential*; *sustained angiogenesis*; *tissue invasion and metastasis*; *reprogramming energy metabolism*; *evading immune destruction*. They also included two enabling characteristics, which represent the means that enable populations of premalignant cells to reach the above hallmarks: *genetic instability*; and *tumor-promoting inflammation*.

Several works have developed mathematical models in the context of carcinogenesis and evolution of cancer through its different stages, using different modeling approaches such as ODE models (24, 25, 26, 27, 28, 29, 30, 31), PDE models (32, 33, 34, 35, 36, 37), discrete models (38, 39), and computational models (cellular automata, agent-based, and boolean network models) (40, 41, 42, 43, 44). A review can be found in (45).

From the point of view of model formulation, the model presented here is more similar to those in (24), (25), (26) and (32), which consider each mutation (hallmark acquisition) as a transition between compartments. Spencer et. al (24) developed an ODE model to analyze how the interplay among angiogenesis, apoptosis, genetic instability, and abnormal growth gives rise to different kinetics in the development of cancer. They parametrized the model with values based on breast cancer, and identified particular ordering of mutations under which cancer develops faster. The same group adapted this model in a cellular automata model and included the hallmark of *limitless replicative potential* by considering a division counter for each cell, based on telomere length (40). The group of Gentry also developed ODE models (25, 26) that incorporate the sequential acquisition of mutations as transitions between compartments. In order to simulate the cancer stem cell hypothesis (46, 47), they also considered tissue hierarchy, by considering three cell types: stem, progenitor and mature cells. In a more recent work (26), they included the mechanisms of chemical signaling and interaction with the niche to control

stem cell self-renew, like the effect of mature cells on the proliferation and division of stem cells. Their model was parametrized with values based on the hematopoietic system. They find that the order in which mutations occur have a significant influence on the pace of tumorigenesis and on tumor final composition. Also, they analyzed the impact of disrupting the feedback mechanisms that maintain system homeostasis through the control that mature cells exert on stem cells. If this mechanism remains intact, a tumor can grow but attains a stationary size, while, if this regulation is lost, then cancer is easily initiated and grows exponentially. The model of Enderling *et al.* (32) considered the development of breast cancer as a step-wise process that involves the loss of function of two tumor suppressor genes by breast stem cells. They also included a spatial dynamics (random motion and haptotaxis) for cancer cells. The model predicted that genetic instability or a high number of breast stem cells are necessary conditions in order to a tumor rises within a clinically observable time, i.e. within 30 years after puberty. They also found that the likelihood of a tumor arising in a breast is increased when a first mutation in stem cells occurs very early so that it forms a field of non-normal cells that later will give rise to a tumor.

This work presents and analyzes a mathematical model to the onset of cancer at an initial, avascular stage, with the following three characteristics: *self-sufficiency in growth signals*; *insensitivity to antigrowth signals*; and *evading apoptosis*. We also consider in the formulation of the model the enabling characteristic *genetic instability*. The model is based on a system of three nonlinear ordinary differential equations, describing three cell populations: normal, premalignant and cancer cells.

A fundamental difference of the model presented in this work from previous ones lies in the terms describing the transition between cell compartments. All models considered linear transitions between the pools. Additionally, based on the relations of cause and effect between genetic instability and tumor progression, we adopt different transition terms here: a pulse transition from normal to precancer cells, and a nonlinear transition from precancer to cancer.

Our goal is to perform qualitative and quantitative extensive analyses in the parameter space, and compare the outcomes predicted by the model in different parameter ranges. With these analyses, we expect to elucidate the individual role of each physiological change (uncontrolled growth, evading apoptosis) and of genetic instability in the process of tumorigenesis, but also the combined effect of these factors. The mathematical results are applied to breast cancer. As will be seen, small changes in nonlinear parameters that are difficult, if not impossible, to estimate, give rise to very distinct qualitative and also quantitative behaviors. Thus, this comprehensive and detailed analysis exhausts all different possibilities predicted by the model, what sheds some light on the discussion and deepens the biological implications. The paper is organized as follows. Section 2.2 deals

with the mathematical modeling. In Section 2.3 we present the mathematical analysis of the model. To a better reading, some mathematical results are only stated and their proofs are presented in Appendix 2.A. In Section 2.4, we present numerical simulations of the model with parameter values based on literature data. In Section 2.5, we discuss the biological implications of both analytical and numerical analysis. Finally, in Section 2.6, the conclusions are presented.

## 2.2 Mathematical modeling

The model we propose considers three distinct cell populations: $N(t)$ represents the normal cells at the tissue; $G(t)$ represents premalignant cells exhibiting a first hallmark corresponding to self-sufficiency in growth signals; and $A(t)$ stands for cancer cells, with the hallmarks self-sufficiency in growth signals and evading apoptosis. Due to the similarity between the hallmarks of self-sufficiency in growth signals and insensitivity to anti-growth signals, we consider both as a single characteristic acquired by cells $G$ and $A$.

We start by presenting the full model describing the dynamics of these populations, then we present the model hypothesis and parameters, and finally we perform simplifications and obtain a final model which accentuates the characteristics we are interested. The model equations are

$$\frac{dN}{dt} = r_N - \mu_N N - \beta_1 NA - \beta_4 NG - G_0\delta(t-t_0), \tag{2.1a}$$

$$\frac{dG}{dt} = r_G G\left(1-\frac{G}{K_G}\right) - (\mu_G+\epsilon_G)G - \beta_2 NG - \beta_5 AG + G_0\delta(t-t_0) - \frac{\sigma G^2}{\xi+G}, \tag{2.1b}$$

$$\frac{dA}{dt} = r_A A\left(1-\frac{A}{K_A}\right) - (\mu_A+\epsilon_A)A - \beta_3 NA - \beta_6 AG + \frac{\sigma G^2}{\xi+G}. \tag{2.1c}$$

The hypothesis behind this model are the following.

Parameter $r_N$ represents the total constant reproduction of normal cells, and $\mu_N$ is their natural mortality. We use this constant flux vital dynamics for normal cells, and not a density-dependent one, like logistic growth, generally assumed by other models (48, 49, 50, 51), because the production of new normal cells does not depend directly on the total number of living normal cells, but is an intrinsic property of the tissue, described here by the term $r_N$. In fact, in a normal tissue, the imperative dynamics is not the cells intraspecific competition by nutrients, but the maintenance of a homeostatic state, through the natural replenishment of old and dead cells (52). Here the homeostatic state in absence of mutations ($G = 0 = A$ and $G_0 = 0$) is given by $r_N/\mu_N$. Further, due to the limitation in the number of divisions that a cell can pass, this cellular replacement many times depends on special cells, like stem cells or progenitor cells, localized in specific regions of the tissue,

that provide new cells with a large life span (53, 52). It is easy to anticipate that this choice of a constant flux implicates that there will be no trivial equilibrium with $N = 0$, i.e., normal cells can never be extinct, on the contrary of other models that consider the logistic growth for normal cells. We believe that this is not a problem, but, on the contrary, it is a realistic outcome. In fact, roughly speaking, what makes cancer dangerous is not the fact that it kills all cells in the organ, but the fact that it reaches dangerous size that disrupt the well functioning of the tissue, which ends up with a lower level of its initial number of healthy cells (20). Finally, we note that a constant flux term was already taken by other well-know models to describe the growth of normal cells, specifically, the growth of immune cells (54, 55).

On the other hand, precancer and cancer cells, due to the self-sufficiency in growth signals, are at proliferative state and keep their own growth program, independent of tissue's structure, like an embrionary tissue in growth phase (56, 57). Thus, in this case, a density dependent growth is considered. Since the model refers to the onset of cancer and its establishment at an avascular stage, where there are constrains in nutrients and oxygen that preclude the tumor growth beyond a maximum size, a saturating growth term must be used. We opt for the logistic growth due to its simplicity. Thus, $r_G$ and $r_A$ are the per capita growth rates of populations $G$ and $A$, and $K_G$ and $K_A$ are their carrying capacity. In a future work, we intend to include angiogenisis and the tumor growth beyond this limit (58).

Parameters $\mu_G$ and $\mu_A$ are the natural mortality rates of populations, while parameters $\epsilon_G$ and $\epsilon_A$ represent the extra mortality rates of populations $G$ and $A$ due to apoptosis, since mutations they present are recognized by their internal apoptotic program (59, 60). As $A$ cells have evaded apoptosis or diminished it, $\epsilon_A$ is thought to be less than $\epsilon_G$ and can be zero.

Parameters $\beta_i$, with $i = 1, \ldots, 6$, represent the interactions between the three cell populations. While in general the terms with $\beta_i$ can be thought as representing the interspecific competition by space and nutrients, here, they also comprise other effects and interactions. For instance, parameters $\beta_2$ and $\beta_3$ embrace the response of the tissue repair system, activated by normal cells in the presence of mutant populations (61). On the other hand, $\beta_1$ and $\beta_4$ describe the damage imposed by mutant cells against normal cells, not only by depletion of nutrients or space, but also by introducing changes in the local micro-environment that disrupt the homeostasis of the tissue, like increasing the local acidity due the abnormal metabolism of mutant cells (62, 63). Parameters $\beta_5$ and $\beta_6$ describe the negative effects caused by population $G$ on $A$, and vice-versa.

We now consider the transition from normal cells to premalignant cells, and from these to cancer cells. These transitions can occur through mutations or activation of oncogenes (19). In most mathematical models in this context (24, 26, 32), they are modeled

by linear terms like $pN$ or $qG$, where $p$ and $q$ represent the probabilities of occurrence of mutations/activation of oncogenes, per cell per division, that turns on the corresponding hallmarks. These probabilities are of order of $10^{-8}$ to $10^{-6}$ (64, 65, 24), but not always constant (66, 67, 68). Indeed, as tumor progression proceeds, the genomes of tumor cells often become increasingly unstable, and the rate at which mutations are acquired during each cell generation increases and may exceed the rate at which Darwinian selection can eliminate the less-fit sub-clones of cells. Thus, a linear probability rate oversimplifies the reality of cancer and does not capture this departure from the genome's highly stable state when tumor proceeds ((20), Sec. 11.7 and Chap. 12; (66, 67, 68)). This step-wise process occurs differently in each phase of tumor development.

The first successful transition of a normal cell to a mutant cell is probabilistic ((20), Chap. 11). Once this viable transition from $N$ to $G$ occurs, the first precancer cell will proliferate soon due to its accelerated growth program. It acts as a spark to activate cancer and we are interested in analyzing whether or not its progeny will be able to survive enough to reach the next transition stage, from $G$ to $A$. Also, as the initial proliferation of these cells will be high, the entering of other normal cells in this pool can be neglected. Therefore, we model the first effective transition from $N$ to $G$ by a Dirac Delta term

$$\pm G_0 \delta(t - t_0),$$

representing that $G_0$ normal cells passed to population $G$ at time $t_0$, with the possibility to have $G_0 = 1$ cell.

After the onset of these precancer cells, their viable mutation is propagated trough cell generations, and there is an increase of genetic instability, so they will be subject to continuous transition from $G$ to $A$. We also note that there is biological evidence that some of the same mutations that increase cell proliferation are also responsible for enchanced genetic instability (67, 68). Here, it is exactly the case of premalignant cells $G$, which have achieved high proliferative rates. This fact jointly with the effect of increased genetic instability as tumor progresses justifies the continuous transition from $G$ to $A$. In order to capture this threshold effect, instead of considering a linear transition, $qG$, with a constant per capita probability $q$, we model the transition from $G$ to $A$ by

$$\pm \frac{\delta G^2}{G + \xi},$$

with a nonlinear per capita mutation rate given by $\delta G/(G + \xi)$. This per capita probability is small when there are few cells, increases as the number of cells increases, and saturates to the level $\delta$ when the number of these cells surpass the threshold described by $\xi$.

Thus, while other models consider linear flow between all cell compartments (24, 26, 32), here, based on the role and causes of genetic instability, the first transition is reduced merely to a pulse, and the second one is a nonlinear flow that approaches a linear one, at a high rate, only when there is a large number of cells.

Now, we perform some simplifications in the model. Because of the control imposed to abnormal cells, premaligant cells $G$ probably will be eliminated soon if they do not acquire the hallmark of evading apoptosis, by triggering the activation of the pool of cancer cells. Thus, we are interested in the appearing of $G$ cells as an intermediary stage in the process of tumor formation, and, then, the values of interest in the dynamics of $G$ are relatively low, so that the negative effect caused by them on normal and cancer cells can be neglected, and also the negative effect suffered by them due to the interaction with cancer cells. Thus we disregard the interaction terms $-\beta_4 NG$ in (2.1a), $-\beta_5 AG$ in (2.1b) and $-\beta_6 AG$ in (2.1c). By the same reasons, we also disregard the saturation term $-r_G G^2/K_G$. It is a simplifying hypothesis on the dynamics of $G$ cells, but it allows us to perform a more detailed mathematical analysis that focuses in the slow dynamics of cancer cells $A$. If in some conclusions and simulations we observe that $G \to \infty$, it will be understood that population $G$ has survived and reached a stationary state far from $G = 0$, which is what would happen if the logistic term was included. The term $-\beta_2 NG$ in (2.1b) cannot be disregarded because it encompasses the tissue response to precancer cells, which may occur at the very beginning of tumor formation. On the contrary to $G$ cells, $A$ cells constitute the final step in this avascular phase of cancer, and therefore the terms $-\beta_1 NA$ in (2.1a) and $-\beta_3 NA$ and $-r_A A^2/K_A$ in (2.1c) must be included for.

With these remarks, we obtain a simplified version of system (2.2) that accentuates the characteristics we want to examine. Translating the time axis to set the time of first mutation, $t_0$, to be $t = 0$, the model becomes

$$\frac{dN}{dt} = r_N - \mu_N N - \beta_1 NA, \tag{2.2a}$$

$$\frac{dG}{dt} = r_G G - \beta_2 NG - (\mu_G + \epsilon_G)G - \frac{\delta G^2}{\xi + G}, \tag{2.2b}$$

$$\frac{dA}{dt} = r_A A\left(1 - \frac{A}{K_A}\right) - \beta_3 NA - (\mu_A + \epsilon_A)A + \frac{\delta G^2}{\xi + G}, \tag{2.2c}$$

supplied with initial conditions

$$(N(0), G(0), A(0)) = (N_0 - G_0, G_0, 0).$$

## 2.3 Model Analysis

In this section, a mathematical analysis of system (2.2) is performed. The equilibrium points are obtained by setting derivatives in (2.2) equal to zero. The stability of each equilibrium depends on the eigenvalues of the Jacobian matrix of (2.2), $J(N, G, A)$, evaluated at the equilibrium. We obtain conditions about positiveness and stability for each equilibrium and discuss the results.

### 2.3.1 Trivial equilibrium

We start by analyzing the trivial equilibrium,

$$P_0 = \left(\frac{r_N}{\mu_N}, 0, 0\right).$$

Stability of $P_0$ is easily determined, since the eigenvalues of the Jacobian matrix $J(P_0)$ are

$$\lambda_1^{(0)} = -\mu_N, \;\; \lambda_2^{(0)} = \frac{r_N}{\mu_N}(\beta_3^{th} - \beta_3), \;\; \text{and} \;\; \lambda_3^{(0)} = \frac{r_N}{\mu_N}(\beta_2^{th} - \beta_2),$$

where

$$\beta_2^{th} = \frac{\mu_N}{r_N} l_G, \quad \text{with} \quad l_G = r_G - \mu_G - \epsilon_G, \;\; \text{and} \tag{2.3}$$

$$\beta_3^{th} = \frac{\mu_N}{r_N} l_A, \quad \text{with} \quad l_A = r_A - \mu_A - \epsilon_A. \tag{2.4}$$

Parameters $l_G$ and $l_A$ can be thought as the liquid reproduction rates of cells $G$ and $A$, respectively, and both will be assumed to be positive (otherwise cells $G$ and $A$ would be extinct naturally without interaction with normal cells). Thus, $P_0$ is stable if and only if,

$$\beta_2 > \beta_2^{th} = \frac{l_G}{N_0} \;\; \text{and} \;\; \beta_3 > \beta_3^{th} = \frac{l_A}{N_0},$$

where $N_0 = r_N/\mu_N$ is the total normal cells population at equilibrium in absence of cancer. It means that if the responses $\beta_3$ and $\beta_2$ of normal cells population to mutant cells $A$ and $G$ are high, then the tissue is able to eliminate the few mutant cells that arise. If the tissue repair system is not good enough, and one of the two conditions above is not satisfied, $P_0$ will be unstable, and the appearing of a few mutant cells, small disturbances of $P_0$, will break the tissue homeostatic state free of cancer and will lead to cancer progression with presence of one or two types of mutant cells. Further, larger values of the carrying capacity $N_0$ decrease the thresholds $\beta_i^{th}$, and thus increase the protection against cancer. On the other hand, larger values of reproduction rates $l_G$ and $l_A$ (achieved by evading apoptosis for instance) increase the thresholds, and thus, increase the risk of cancer onset.

### 2.3.2 Boundary equilibria

Now, we analyze the boundary equilibria corresponding to absence of precancer cells. Solving $dN/dt = 0 = dA/dt$ with $A \neq 0$, we obtain the solution

$$\bar{P} = (\bar{N}, 0, \bar{A}) = \left(\frac{r_N}{\mu_N + \beta_1 \bar{A}}, 0, \bar{A}\right),$$

where $\bar{A}$ is a root of the second degree polynomial

$$q(A) = aA^2 + bA + c, \tag{2.5}$$

with coefficients

$$a = \beta_1 \frac{r_A}{K_A} > 0, \qquad b = \mu_N \frac{r_A}{K_A} - \beta_1 l_A, \qquad c = r_N \beta_3 - l_A \mu_N. \tag{2.6}$$

This equilibrium point represents the establishment of tumor in absence of premalignant cells. We will denote the smaller root of $q(A)$ by $\bar{A}_1$ and the largest by $\bar{A}_2$. Thus, there can be up to two equilibrium points $\bar{P}$, denoted by $\bar{P}_i$, $i = 1, 2$.

#### 2.3.2.1 Existence

Let us determine conditions for $\bar{P}_1$ and $\bar{P}_2$ being positive. As $\bar{N}_i > 0$ if $\bar{A}_i > 0$, it is enough to obtain the conditions for the roots of $q(A)$ to be positive. We consider the signals of $b$ and $c$. They can be rewritten as

$$b = l_A \left(\beta_1^{th} - \beta_1\right), \qquad c = r_N \left(\beta_3 - \beta_3^{th}\right),$$

where

$$\beta_1^{th} = \frac{\mu_N r_A}{l_A K_A}. \tag{2.7}$$

Note that this threshold for tumor aggressiveness increases as the mortality $\mu_N$ of normal cells increases, and decreases as the effective carrying capacity of tumor cells $l_A K_A / r_A$ increases.

I) Suppose $\beta_3 > \beta_3^{th}$. Thus, $c > 0$. If $\beta_1 < \beta_1^{th}$, then $b > 0$. By the Descartes' Rule of Signs (69), no root $\bar{A}_i$ is positive, and no $\bar{P}_i$ is positive. If $\beta_1 > \beta_1^{th}$, then $b < 0$. We can have two or zero positive roots $\bar{A}_i$. We must analyze the sign of the discriminant $\Delta = b^2 - 4ac$, which is written in terms of the thresholds as

$$\Delta = l_A^2 \left(\beta_1^2 - (2\beta_1^{th} + 4\eta)\beta_1 + \left(\beta_1^{th}\right)^2\right), \tag{2.8}$$

where $\eta = r_A r_N (\beta_3 - \beta_3^{th}) / (K_A l_A^2) > 0$. Therefore, we must consider a second threshold, $\beta_{1,\Delta}^{th}$, given by the value of $\beta_1 > \beta_1^{th}$ for which $\Delta = 0$. Solving this equation, we obtain

$$\beta_{1,\Delta}^{th} = \beta_1^{th} + 2\eta + 2\sqrt{\eta(\beta_1^{th} + \eta)} > \beta_1^{th}. \tag{2.9}$$

If $\beta_1 < \beta_{1,\Delta}^{th}$, then $\Delta < 0$. Thus, no root $\bar{A}_i$ exists. Again there is no $\bar{P}_i$ positive, the same result corresponding to $\beta_1 < \beta_1^{th}$, and we can consider both as a single case. II) If $\beta_1 > \beta_{1,\Delta}^{th}$, then $\Delta > 0$, and the two roots $\bar{A}_i$ are positive. Equilibria $\bar{P}_1$ and $\bar{P}_2$ are positive. III) Suppose now that $\beta_3 < \beta_3^{th}$. Then, $c < 0$. Again by the Descartes' rule of signs, we conclude that $q(A)$ has exactly one positive root, which is $\bar{A}_2$. The value of $b$ does not matter. Only $\bar{P}_2$ is positive in this case. These three cases are summarized as follows:

I) If $\beta_3 > \beta_3^{th}$ and $\beta_1 < \beta_{1,\Delta}^{th}$, there is no positive boundary equilibrium.

II) If $\beta_3 > \beta_3^{th}$ and $\beta_1 > \beta_{1,\Delta}^{th}$, three are two positive boundary equilibria, $\bar{P}_1$ and $\bar{P}_2$.

III) If $\beta_3 < \beta_3^{th}$, $\bar{P}_2$ is the unique positive boundary equilibrium.

As these inequalities with $\beta_1$ and $\beta_3$ will appear frequently, from now on we refer to them as cases, or regions, I, II and III.

#### 2.3.2.2 Local Stability

Now, we analyze the linear stability of $\bar{P}_i$, $i = 1, 2$. The Jacobian matrix $J(\bar{N}, 0, \bar{A})$ is given by,

$$J(\bar{N}, 0, \bar{A}) = \begin{bmatrix} -\beta_1\bar{A} - \mu_N & 0 & -\beta_1\bar{N} \\ 0 & l_G - \beta_2\bar{N} & 0 \\ -\beta_3\bar{A} & 0 & l_A - 2\dfrac{r_A}{K_A}\bar{A} - \beta_3\bar{N} \end{bmatrix}. \tag{2.10}$$

The characteristic polynomial $p(\lambda)$ of $J(\bar{N}, 0, \bar{A})$ factors as

$$p(\lambda) = (l_G - \beta_2\bar{N} - \lambda)p_2(\lambda)$$

where $p_2(\lambda)$ is the characteristic polynomial of the submatrix $j(\bar{P})$,

$$j(\bar{P}) = \begin{bmatrix} -\beta_1\bar{A} - \mu_N & -\beta_1\bar{N} \\ -\beta_3\bar{A} & -\dfrac{r_A}{K_A}\bar{A} \end{bmatrix},$$

obtained from (2.10) using the fact that $\bar{N}$ and $\bar{A}$ satisfy

$$l_A - \frac{r_A}{K_A}\bar{A} - \beta_3\bar{N} = 0. \tag{2.11}$$

Thus, the eigenvalues $\lambda_1^{(i)}$ and $\lambda_2^{(i)}$ of $J(\bar{P}_i)$, $i = 1, 2$, are the eigenvalues of $j(\bar{P}_i)$. The third eigenvalue is $\lambda_3^{(i)} = l_G - \beta_2\bar{N}_i = \dfrac{r_N}{\mu_N + \beta_1\bar{A}_i}(\beta_{2,\lambda}^{th,i} - \beta_2)$, where

$$\beta_{2,\lambda}^{th,i} = \beta_2^{th} + \frac{l_G\beta_1\bar{A}_i}{r_N} > \beta_2^{th}. \tag{2.12}$$

Let us analyze the eigenvalues of $j(\bar{P})$. We see that whenever $\bar{P}$ is a positive equilibrium, the trace of $j(\bar{P})$ is negative. Thus, when $\bar{P}$ is positive, both eigenvalues of $j(\bar{P})$ will have a negative real part if $\det(j(\bar{P})) > 0$. Using equation (2.11) and expressions of $a$ and $b$ in (2.6), we obtain

$$\det(j(\bar{P})) = \bar{A}(2a\bar{A} + b). \tag{2.13}$$

As $\bar{A}_1$ is the smallest root of $q(A)$ and $\bar{A}_2$ is the largest, we have, whenever $\bar{P}_i$ is a positive equilibrium, $i = 1, 2$,

$$\det(j(\bar{P}_1)) = -\bar{A}_1\sqrt{\Delta} < 0, \qquad \text{and} \qquad \det(j(\bar{P}_2)) = \bar{A}_2\sqrt{\Delta} > 0,$$

where $\Delta$ is the discriminant given in (2.8). Therefore, we conclude that $\bar{P}_1$ will be unstable whenever it is positive, having one eigenvalue with positive real part if $\beta_2 > \beta_{2,\lambda}^{th,1}$, and two eigenvalues with a positive real part otherwise. For the point $\bar{P}_2$, if $\beta_2 > \beta_{2,\lambda}^{th,2}$, it will be stable whenever it is positive (cases II and III). Otherwise, $\bar{P}_2$ will be unstable whenever it is positive, having one positive eigenvalue.

#### 2.3.2.3 Asymptotic behavior of boundary subsystem $G = 0$

As $G$ cells work only as a trigger to cancer onset, it is expected that, in some cases, $G \to 0$ after a transient period of time. Thus, it is worth to study dynamical properties of system (2.2) restricted to the boundary $G = 0$ ($N \times A$ plane), which is invariant with respect to the flux. From analysis above, it is easy to see that equilibria on this plane are $P_0$, $\bar{P}_1$, and $\bar{P}_2$. Further, the first two eigenvalues, $\lambda_1^{(i)}$ and $\lambda_2^{(i)}$, of each Jacobian matrix $J(P_0)$, $J(\bar{P}_1)$ and $J(\bar{P}_2)$ dictate the stability of equilibria in this subsystem since they correspond to directions (eigenvectors) parallels to plane $N \times A$, while the third corresponds to a direction pointing outside this plane. Thus, the value of $\beta_2$ does not matter. Therefore, considering cases I, II and III above, we can summarize the following about the stability of positive equilibria in this subsystem. In case I, $P_0$ is stable. In case II, $P_0$ and $\bar{P}_2$ are stable, and $\bar{P}_1$ is a saddle point. In case III, $P_0$ is unstable and $\bar{P}_2$ is stable.

Let us characterize the global asymptotic behavior of this subsystem. We first show that it is dissipative. In fact, we have:

$$\frac{dN}{dt} = r_N - \mu_N N - \beta_1 NA \leqslant r_N - \mu_N N,$$

and

$$\frac{dA}{dt} = r_A A\left(1 - \frac{A}{K_A}\right) - \beta_3 NA - (\mu_A + \epsilon_A)A \leqslant l_A A\left(1 - \frac{r_A A}{l_A K_A}\right).$$

Therefore, by classical comparison principles (70), all solutions $(N(t), 0, A(t))$ starting at this plane remain restricted to region $B = \left[0, \frac{r_N}{\mu_N}\right] \times \{0\} \times \left[0, \frac{l_A}{r_A} K_A\right]$ when $t \to \infty$. Applying the Dulac Criterion with $u(N, A) = 1/NA$, we have

$$\nabla \cdot \left(\frac{1}{NA}\left(\frac{dN}{dt}, \frac{dA}{dt}\right)\right) = -\frac{r_A NA + K_A r_N}{K_A A N^2} < 0$$

for $(N, A) \in B$. Thus, subsystem $N \times A$ has no periodic orbits. By the Poincaré-Bendixson Theorem (71) we conclude that all trajectories converge to an equilibrium point. Joint with the previous results, we conclude that subsystem $N \times A$ has one of the three behaviors:

I) If $\beta_3 > \beta_3^{th}$ and $\beta_1 < \beta_{1,\Delta}^{th}$: $P_0$ is globally stable. Cancer is eliminated, whatever the initial conditions;

II) If $\beta_3 > \beta_3^{th}$ and $\beta_1 > \beta_{1,\Delta}^{th}$: $P_0$ and $\bar{P}_2$ are locally stable; $\bar{P}_1$ is a saddle point and its stable manifold is the separatrix between the basins of attraction of $P_0$ and $\bar{P}_2$. Cancer may develops or be eliminated. The outcome depends on the initial conditions.

III) If $\beta_3 < \beta_3^{th}$: $\bar{P}_2$ is globally stable. Cancer develops, whatever the initial conditions.

Figure 1 presents the phase portrait in each case. Figure 2 presents the bidimensional bifurcation diagram of $P_0$, $\bar{P}_1$ and $\bar{P}_2$ depending on $\beta_1$ and $\beta_3$, and regions I, II and III in the $\beta_3 \times \beta_1$ plane are presented.

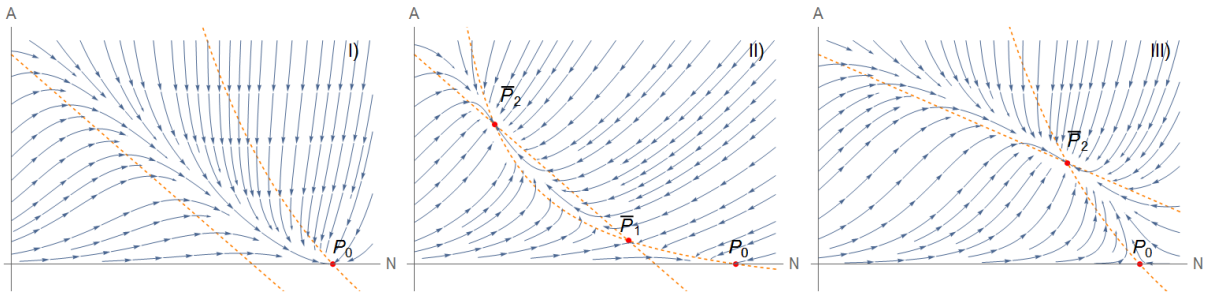


Figure 1 – Phase portraits of subystem $N \times A$ in cases $I$, $II$ e $III$. In case I), $P_0$ is globaly stable. In case II), the stable manifold of $\bar{P}_1$ divides the phase plane in basins of attraction of $P_0$ and $\bar{P}_2$. In case III), $\bar{P}_2$ is globally stable for initial conditions $A(0) > 0$.

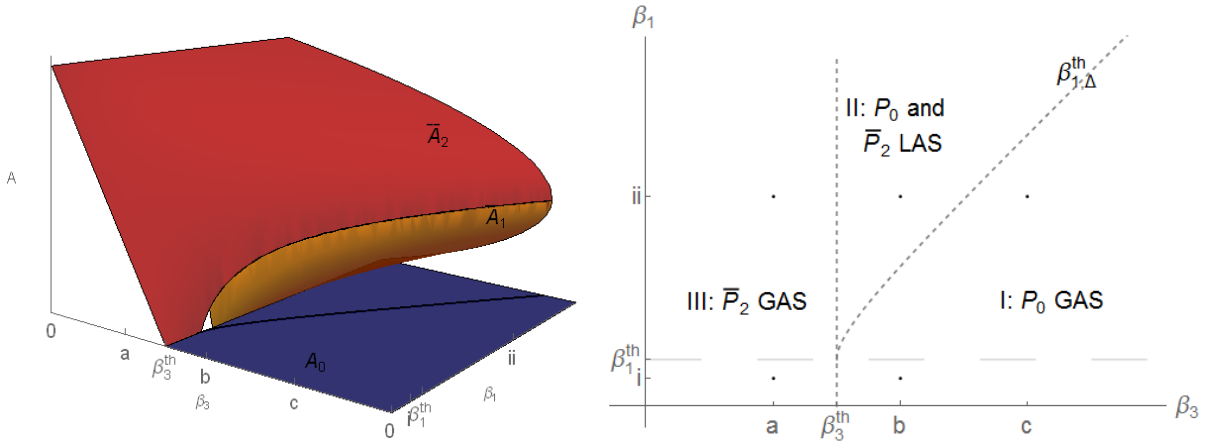


Figure 2 – Bidimensional bifurcation diagram depending on $\beta_1$ and $\beta_3$ (left) and regions I, II and III in the $\beta_3 \times \beta_1$ plane, together with equilibria behavior (right). When $\beta_3$ varies, it is observed the occurrence of a forward bifurcation if $\beta_1 < \beta_1^{th}$, and a backward bifurcation if $\beta_1 > \beta_1^{th}$, with the rising of a fold in region II.

#### 2.3.2.4 Discussion

Let us discuss the results above. By looking Figure 2, we see that the first necessary condition to have no cancer cells is $\beta_3 > \beta_3^{th}$, which was already discussed above in the analysis of $P_0$. However, this condition may not be sufficient, due the role played by tumor aggressiveness $\beta_1$. When the tumor is not very aggressive, $\beta_1 < \beta_1^{th}$, the above condition indeed is sufficient. In this case a simple forward bifurcation occurs between regions III and I when $\beta_3$ increases. On the other hand, when $\beta_1 > \beta_1^{th,\Delta}$, region II arises between regions I and III, presenting bistability between $P_0$ and $\bar{P}_2$, and a tumor may

grow even if $\beta_3 > \beta_3^{th}$, provided initial conditions are large enough. Now, a backward bifurcation occurs when $\beta_3$ varies. In order to guarantee that no cancer cells can survive, it is necessary that $\beta_3$ surpasses another threshold, the one defined by the curve $\beta_{1,\Delta}^{th}$, which is greater than $\beta_3^{th}$ and is increasing with $\beta_1$. Thus, we conclude that aggressive cancer cells have an extra chance of survival, but depend on extrinsic factors which increase their initial number. Further, from expression of $\beta_1^{th}$ in (2.7), we see that condition $\beta_1 < \beta_1^{th}$ is more likely to be satisfied in tumors which arise in rapidly regenerating tissues, and which have limited nutrients supply.

### 2.3.3 Internal Equilibria

Now, we deal with the mathematical analysis of the internal equilibrium points for system (2.2), which are given by

$$\tilde{P} = (\tilde{N}, \tilde{G}, \tilde{A}),$$

where

$$\tilde{N} = \frac{r_N}{(\mu_N + \beta_1 \tilde{A})}, \qquad \tilde{G} = \frac{\xi \left(l_G(\mu_N + \beta_1 \tilde{A}) - \beta_2 r_N\right)}{\beta_2 r_N - (l_G - \delta)(\mu_N + \beta_1 \tilde{A})}, \tag{2.14}$$

and $\tilde{A}$ is a root of the fourth degree polynomial equation

$$f(A) = g(A), \tag{2.15}$$

with

$$f(A) = \beta_1(l_G - \delta)\ A\ q(A)\,(A_M - A) \quad \text{and} \quad g(A) = \xi\ l_G^2\ \beta_1^2\ (A - A_m)^2\,. \tag{2.16}$$

Here, $q(A)$ is the second degree polynomial given in (2.5), and $A_m$ and $A_M$ are given by

$$A_m = \frac{r_N}{\beta_1 l_G}\left(\beta_2 - \beta_2^{th}\right),\ A_M = \frac{r_N}{\beta_1(l_G - \delta)}\left(\beta_2 - \beta_{2,\delta}^{th}\right),\ \text{with } \beta_{2,\delta}^{th} = \frac{\mu_N(l_G - \delta)}{r_N}, \tag{2.17}$$

where $\beta_2^{th} = \dfrac{\mu_N l_G}{r_N}$ is the threshold introduced in (2.3).

#### 2.3.3.1 Existence

As it is a fourth degree polynomial equation, (2.15) admits up to four roots, which will be labeled in the order $\tilde{A}_3 < \tilde{A}_4 < \tilde{A}_5 < \tilde{A}_6$. Thus, there can be up to four equilibrium points $\tilde{P}_i = (\tilde{N}_i, \tilde{G}_i, \tilde{A}_i)$, $i = 3, 4, 5, 6$. We analyzed the existence and positiveness of equilibria $\tilde{P}_i$ in the entire parameter space and the results are summarized in Figure 3. Proofs and additional details are left to Appendix 2.A. In order to obtain these conditions, the following thresholds were considered:

$$\beta_{2,\delta}^{th,i} = \beta_{2,\delta}^{th} + \frac{(l_G - \delta)\beta_1 \bar{A}_i}{r_N},\ i = 1, 2,\ \ \delta_1 = \frac{l_G \beta_1(\bar{A}_2 - \bar{A}_1)}{\mu_N + \beta_1 \bar{A}_2} \text{ and } \delta_2 = \frac{l_G \beta_1 \bar{A}_2}{\mu_N + \beta_1 \bar{A}_2}. \tag{2.18}$$

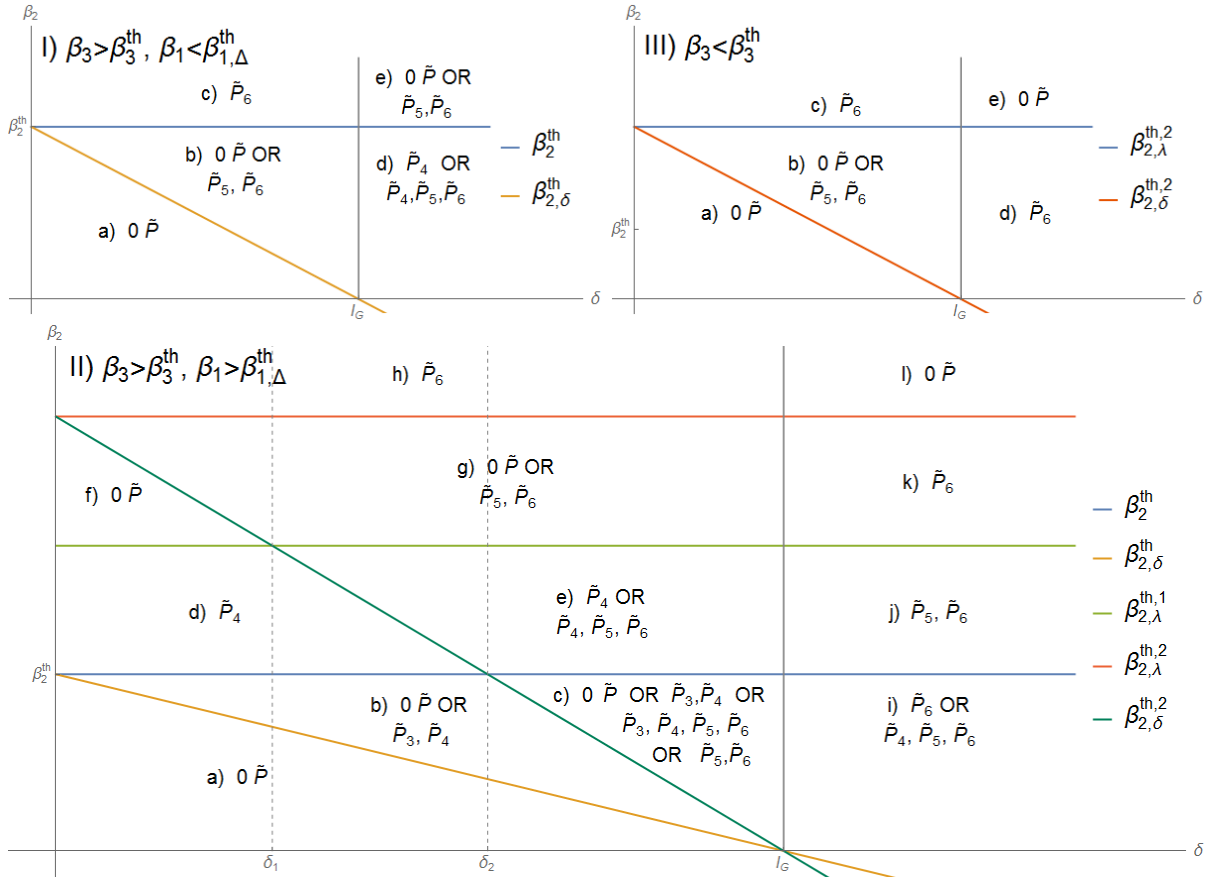


Figure 3 – Existence of positive equilibria $\tilde{P}_i$, $i = 3, 4, 5, 6$, depending on $\beta_2$ and $\delta$. On top left, we have the case I) $\beta_3 > \beta_3^{th}$ and $\beta_1 < \beta_{1,\Delta}^{th}$; on top right, case III) $\beta_3 < \beta_3^{th}$; on bottom, the case II) $\beta_3 > \beta_3^{th}$ and $\beta_1 > \beta_{1,\Delta}^{th}$. At regions where there is the word "OR", the existence depends also on other conditions. Details are in Appendix 2.A.

#### 2.3.3.2 Local Stability

Stability analysis of equilibria $\tilde{P}_i$, $i = 3, 4, 5, 6$, is dealt by studying the roots of the characteristic equation of $J(\tilde{P}_i)$,

$$\lambda^3 + a_1\lambda^2 + a_2\lambda + a_3 = 0,$$

whose coefficients are

$$\begin{aligned}
a_1 &= \beta_1\tilde{A} + \mu_N + \frac{\xi(l_G - \beta_2\tilde{N})}{\tilde{G} + \xi} - d,\\
a_2 &= -d\left(\frac{\xi(l_G - \beta_2\tilde{N})}{\tilde{G} + \xi} + \beta_1\tilde{A} + \mu_N\right) + \frac{\xi(l_G - \beta_2\tilde{N})}{\tilde{G} + \xi}\left(\beta_1\tilde{A} + \mu_N\right) - \beta_1\beta_3\tilde{N}\tilde{A},\\
a_3 &= -d\frac{\xi(l_G - \beta_2\tilde{N})}{\tilde{G} + \xi}\left(\beta_1\tilde{A} + \mu_N\right) - \beta_1\tilde{N}\frac{(l_G - \beta_2\tilde{N})}{\tilde{G} + \xi}\left(\beta_2\tilde{G}(\tilde{G} + 2\xi) - \beta_3\tilde{A}\xi\right),
\end{aligned}$$

where $\tilde{N}$, $\tilde{G}$ are given in (2.14), $\tilde{A}$ is a root of (2.15), and $d = (l_A - 2\frac{r_A}{K_A}\tilde{A} - \beta_3\tilde{N})$. The Routh-Hurwitz criteria (72) says that an equilibrium $\tilde{P}$ is stable if

$$a_1 > 0, \qquad a_3 > 0, \qquad \text{and} \qquad a_1a_2 - a_3 > 0. \tag{2.19}$$

These conditions were studied numerically, through bifurcation diagrams shown in Appendix 2.A. Results obtained are summarized in Figures 4 and 5, where the stability of each positive equilibrium $\tilde{P}_i$ in each region of parameter space is indicated. For further details and explanations see Appendix 2.A.

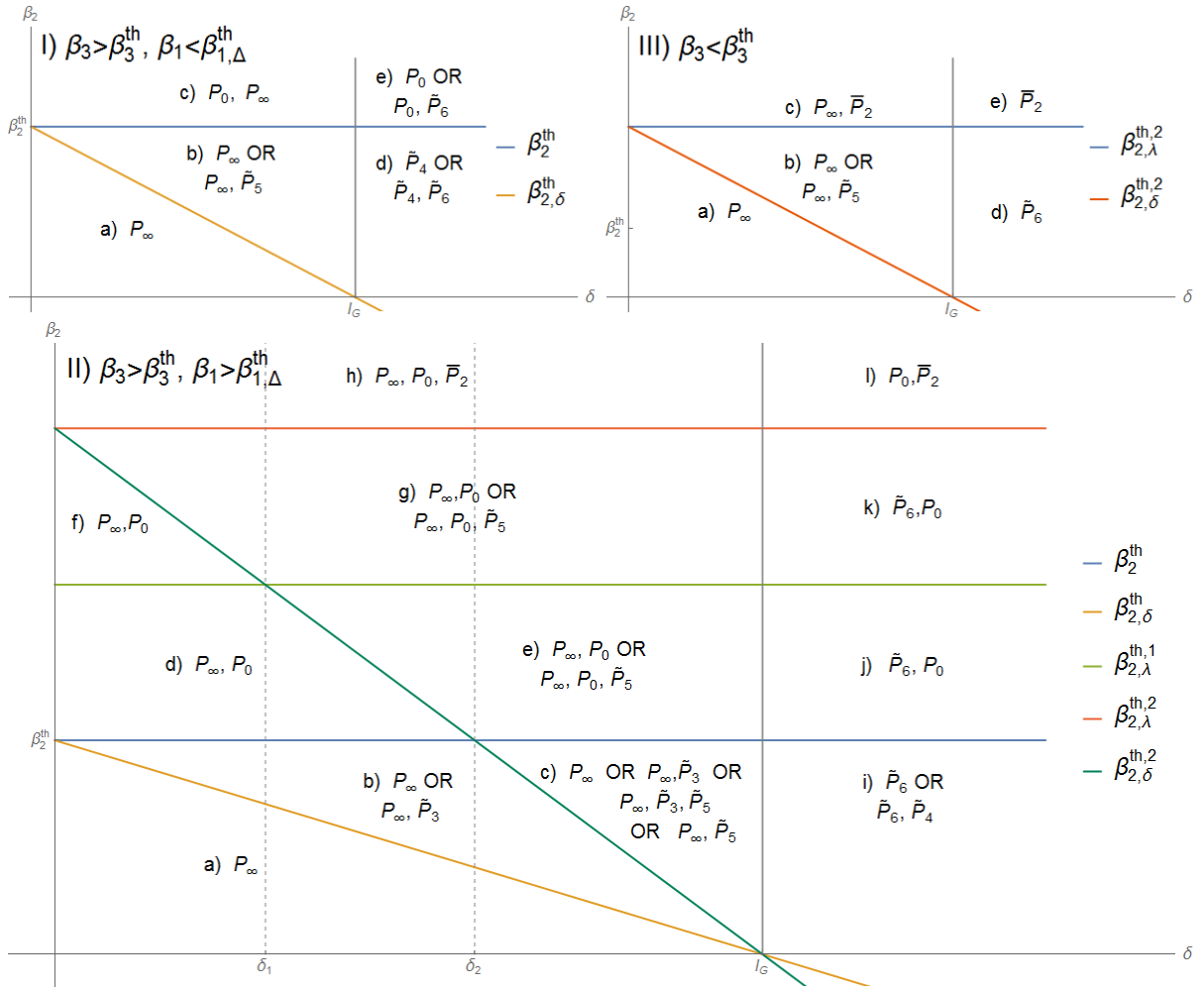


Figure 4 – This figure shows which equilibria are locally stable in each sub-region of parameter space. On top left, we have the case I) $\beta_3 > \beta_3^{th}$ and $\beta_1 < \beta_{1,\Delta}^{th}$; on top right, case III) $\beta_3 < \beta_3^{th}$; on bottom, the case II) $\beta_3 > \beta_3^{th}$ and $\beta_1 > \beta_{1,\Delta}^{th}$. At regions where there is the word "OR", the existence depends also on other conditions. Details are in Appendix 2.A. These results were obtained numerically as presented in Appendix 2.A.

Corresponding phase portraits to each case of Figure 5 were obtained in order to illustrate conclusions. Some of them are presented in Figure 6. In many cases it can be seen that some solutions converge to point at "infinity" such as $(N, G, A) = (N, \infty, \infty)$, which will be denoted by $P_\infty$. As commented before, $P_\infty$ represents the survival of $G$ cells at a quantity very far from $G = 0$, due to the lack of a logistic term in the dynamics of $G$.

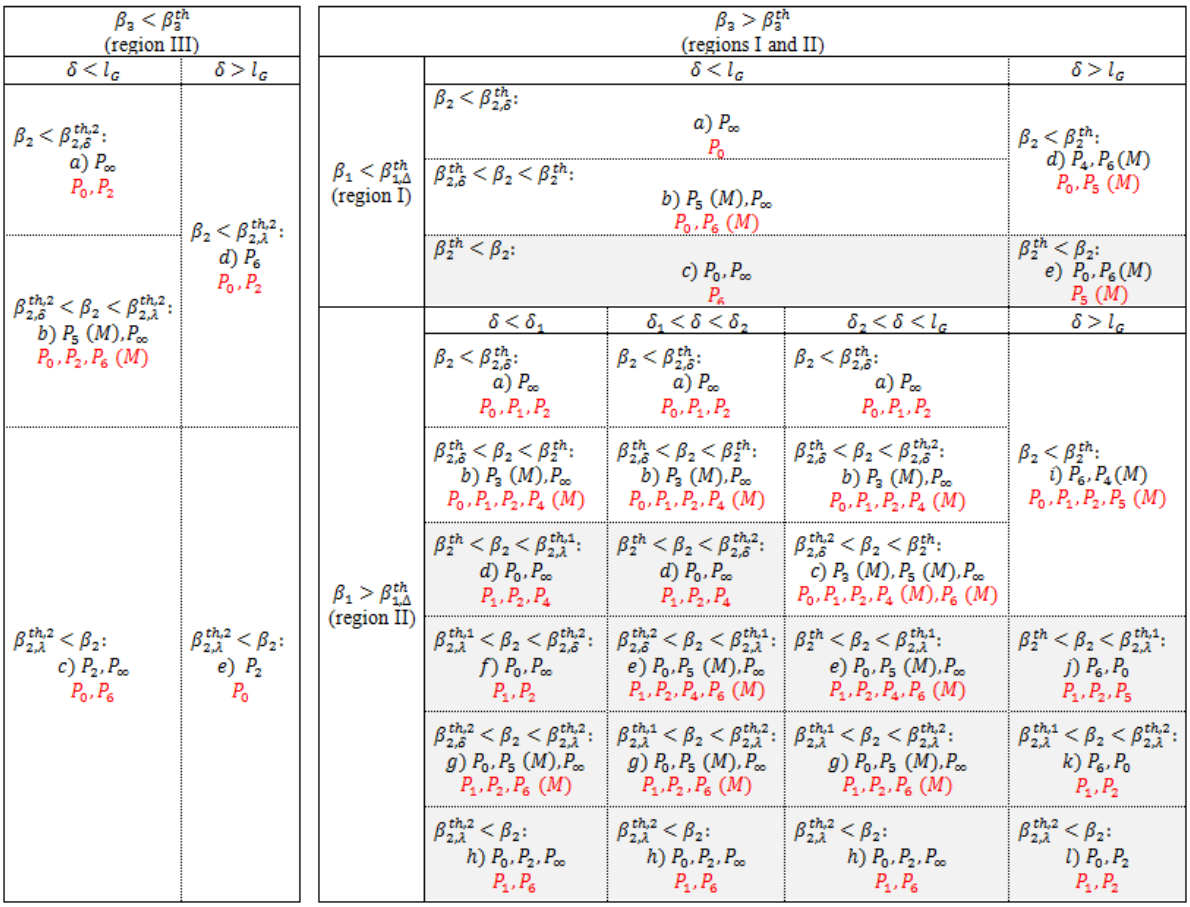


Figure 5 – This scheme shows which equilibrium points are positive in each region of parameters space. In each region where "(M)" appears after two points, a collision between these two points can occur depending on other parameters, and the points can be both positive or not. Stability of equilibria is also indicated: black for stable, and red for unstable. Highlighted cells represent regions of parameter space where $P_0$ is stable, i.e., cancer can be eliminated. All results for points $P_0$, $\bar{P}_1$ and $\bar{P}_2$, and those about positiveness of points $\tilde{P}_i$, $i = 3, 4, 5, 6$ were mathematically proved, while results about stability of $\tilde{P}_i$, $i = 3, 4, 5, 6$ and $P_\infty$ were obtained numerically. See Appendix 2.A for details.

We also see in Figures 5 and 6 that there are regions on parameters space where the phase space is divided into three basins of attraction, with the boundaries between them being the two-dimensional stable manifolds of saddle points.

Before discussing the qualitative results above, we numerically simulate system (2.2) with realistic parameters values to assess how some key parameters influence its quantitative behavior.

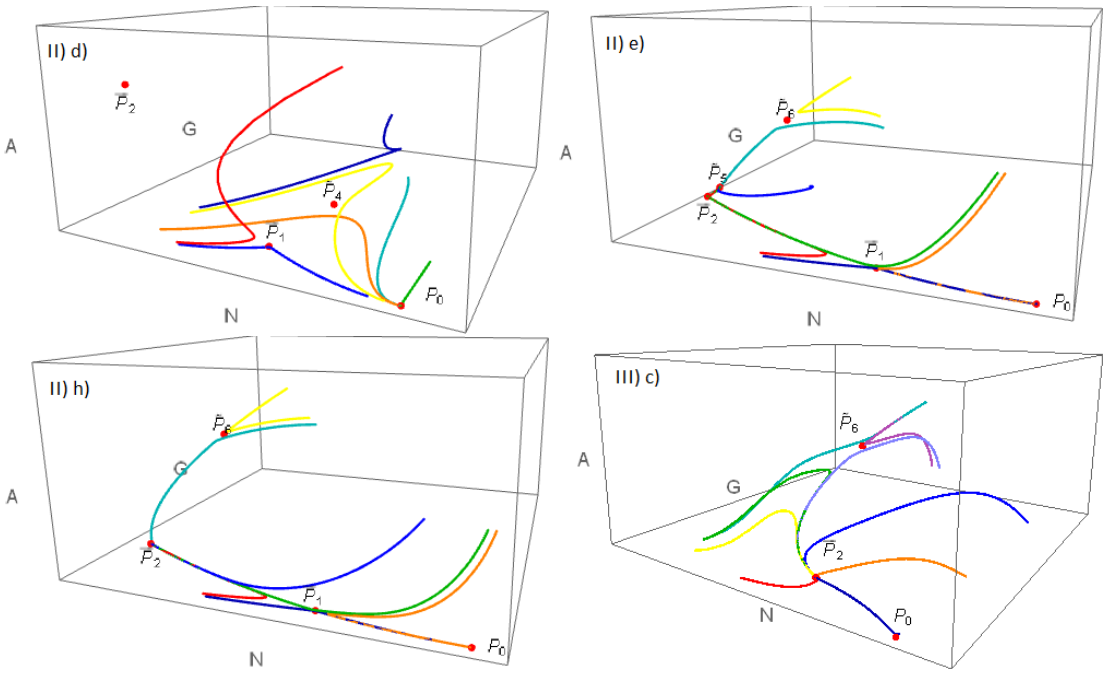


Figure 6 – Phase portraits of system (2.2) for parameters values corresponding to some cases of Figure 5. Case II)d): phase space is divided in the basins of attraction of $P_0$ and $P_\infty$. Region II) g): phase space is divided in the basins of attraction of $P_0$, $\tilde{P}_5$ and $P_\infty$. Case II)h): phase space is divided in the basins of attraction of $P_0$, $\bar{P}_2$ and $P_\infty$. Case III)c): phase space is divided in the basins of attraction of $\bar{P}_2$ and $P_\infty$.

## 2.4 Numerical Results

In this section, based on values found in the literature, we evaluate critical values of the parameters, and perform numerical simulations. Due to the available data in literature, we choose as an application of our model the breast cancer.

We assume that the lifetime of a normal cell is 100 days and that the number of normal cells in the breast cannot pass $N_0 = 10^8$ cells (24). Thus, we have $\mu_N = 1/100$ days$^{-1}$. In order to adjust the equilibrium of $N$ cells in the absence of cancer, given by $r_N/\mu_N$, to be $N_0 = 10^8$ cells, we consider $r_N = 10^6$ cells/day. For the mutated cells, we assume the same lifetime of normal cells, $\mu_G = \mu_A = 1/100$ days$^{-1}$. We assume that the induced intrinsic apoptosis in $G$ cells doubles its mortality rate, thus $\epsilon_G = 1/100$ days$^{-1}$. The ratio *birth rate / death rate* is 1 for a normal tissue, in order to maintain a homeostatic state. Following (24), we assume that the first mutation from $N$ to $G$ increases this ratio by a factor of five for a mutant cell. Thus, we have $r_G = 5/100$ days$^{-1}$. We suppose that the reproduction rate of $A$ cells is the same as $G$ cells, $r_A = 5/100$ days$^{-1}$. The difference between the order of the values of $r_N$ against $r_A$ or $r_G$ is due to the fact $r_N$ that is the total reproduction rate of $N$ cells, while $r_G$ and $r_A$ are the per capita growth rates of $G$ and $A$. For the apoptotic rate of $A$ cells, we use several values in the range $0 \leqslant \epsilon_A \leqslant \epsilon_G = 1/100$.

Without angiogenesis supplying blood, some early *in situ* carcinomas reach a size of $10^6$ cells (73). Thus, as we are considering the avascular phase of tumor growth, we would have $K_A = 10^6$. But as it is a conservative estimate, and in order to have the maximum number of cancer cells being 10% of the normal cells, we consider $K_A = 10^7$. In the literature, the probability of occurring a mutation in a gene during cell division is estimated to be $10^{-8}$ to $10^{-6}$ (64, 65). Also, it is assumed that approximately 100 genes are involved in a same physiological change that characterizes a hallmark, like evading apoptosis or self-sufficiency in growth signals. Thus, we consider the gene mutation probability to be $10^{-7}$ and multiply it by 100 in order to obtain the maximal mutation rate $\delta = 10^{-5}$. The value at which the effective mutation rate reaches half the value of $\delta$ is set to be $G = \xi = 10^3$ cells. The values of interacting parameters $\beta_1$, $\beta_2$ and $\beta_3$, in units of cell$^{-1}$day$^{-1}$, are unknown *a priori* but, by substituting the values of other parameters, it is possible to obtain at least the values for the thresholds to $\beta_1$, $\beta_2$ and $\beta_3$.

We re-scale the populations, by setting $\hat{N} = N/N_0$, $\hat{A} = A/N_0$, and $\hat{G} = G/N_0$. With this change of scale, the new equations are

$$\frac{d\hat{N}}{dt} = r\hat{}_N - \mu_N \hat{N} - \hat{\beta}_1 \hat{N}\hat{A}, \tag{2.20a}$$

$$\frac{d\hat{G}}{dt} = r_G \hat{G} - \hat{\beta}_2 \hat{N}\hat{G} - (\mu_G + \epsilon_G)\hat{G} - \delta \hat{G}\frac{\hat{G}}{\hat{\xi} + \hat{G}}, \tag{2.20b}$$

$$\frac{d\hat{A}}{dt} = r_A \hat{A}\left(1 - \frac{\hat{A}}{\hat{K_A}}\right) - \hat{\beta}_3 \hat{N}\hat{A} - (\mu_A + \epsilon_A)\hat{A} + \delta \hat{G}\frac{\hat{G}}{\hat{\xi} + \hat{G}}, \tag{2.20c}$$

where $r\hat{}_N = r_N/N_0$, $\hat{\xi} = \xi/N_0$, $\hat{K_A} = K_A/N_0$, and $\hat{\beta}_j = \beta_j N_0$, $j = 1, 2, 3$. The initial conditions are rewritten as

$$\hat{N}(0) = 1 - G_0/N_0, \qquad \hat{G}(0) = G_0/N_0, \qquad \hat{A}(0) = 0, \tag{2.21}$$

representing the mutation of $G_0$ normal cells to precancer cells at time $t = 0$, with $1 \leqslant G_0 \ll N_0$.

Dropping the hats as usual, we see that system (2.20) is the same system (2.2), but now with $N$, $G$ and $A$ being cell populations in units of $10^8$ cells. Re-scaled parameters are given by

$$\begin{gathered} r_N = 0.01, \quad \mu_N = \mu_G = \mu_A = \epsilon_G = 0.01, \quad r_G = r_A = 0.05, \\ K_A = 0.1, \quad \delta = 10^{-5}, \quad \xi = 10^{-5}, \quad \epsilon_A \in [0, 0.01]. \end{gathered} \tag{2.22}$$

As systems (2.20) and (2.2) are equivalent, the mathematical analysis devised in the preceding section is still valid. With the numerical values above, the thresholds $\beta_2^{th}$ and $\beta_3^{th}$ are given by

$$\beta_2^{th} = 0.03 \quad \text{and} \quad \beta_3^{th} = 0.04 - \epsilon_A. \tag{2.23}$$

As we want to observe the different behaviors when $\beta_i$, $i = 1, 2, 3$, are greater or lesser than these thresholds, we start with the following basal values for them:

$$\beta_1 = 0.035, \quad \beta_2 = 0.035, \quad \beta_3 = 0.035. \tag{2.24}$$

Next, we present some simulations of system (2.20). A 10th order implicit Runge-Kutta solver was used to perform them.

### The effect of apoptosis and tissue response

First we analyze the outcome of varying $\epsilon_A$ and $\beta_3$, with all other parameters fixed, assuming values in (2.22) and (2.24). We suppose that a single precancer cell arises at time $t = 0$, i.e., $G_0 = 1$.

Initially, we consider that apoptotic rate of cancer cells is 40% less than the rate of precancer cells, $\epsilon_A = 0.006$, what gives us the threshold $\beta_3^{th} = 0.034$. In the first simulation, the tissue response to cells $A$ and $G$ is the same, $\beta_3 = 0.035 > \beta_3^{th}$. In Figure 7)a) we see that mutant cells are eliminated. With these parameters values, we are in case I, where $P_0$ is locally stable. Diminishing the value of $\beta_3$ below the threshold $\beta_3^{th} = 0.034$, we pass to case III, where $P_0$ is unstable and cancer onset is possible. In Figure 7)b), we see the result with $\beta_3 = 0.033$. With this value, tumor cells survive and spend 85 years to reach the stationary population of $0.25 \times 10^6$ cells. Based on (74), we assume that cancer is detectable when attains a tumor mass of $10^6$ cells, weightening 1 mg, with a volume of 1 $mm^3$. Thus, in this simulation the final tumor volume is 0.25 $mm^3$, clinically undetectable. The final tumor volume and the time that tumor cells spend to reach this stationary value are very sensible with respect to $\beta_3$. Diminishing it to $\beta_3 = 0.029$ leads to a tumor which spends 18 years to reach the equilibrium population of $0.12 \times 10^7$ cells, with a detectable tumor volume of 1.2 $mm^3$, as can be seen in Figure 7)c). If we decrease $\beta_3$ even more, to $\beta_3 = 0.012$, the tumor reaches the equilibrium $0.47 \times 10^7$ cells, 4.7 $mm^3$, in 5 years. This result is shown in Figure 7)d).

The effect of diminishing the intrinsic apoptotic rate is similar. If we fix $\beta_3 = 0.035$, then condition $\beta_3 < \beta_3^{th}$ becomes $\epsilon_A < 0.005$. When $\epsilon_A = 0.006$, there is no cancer (Figure 7)a)). If cancer cells have its apoptotic rate reduced below the threshold, to $\epsilon_A = 0.004$, then cancer develops and spends 85 years to reach the stationary population of $0.25 \times 10^6$ cells. If $A$ cells completely evade apoptosis, $\epsilon_A = 0$, then, cancer spends only 18 years to reach the equilibrium population of $1.3 \times 10^6$ cells. Figures resulting from these simulations are very similar to those on Figure 7)b) and c), respectively, and are not shown here.

Now, we analyze how $\beta_3$ and $\epsilon_A$ modify the necessary time for cancer to attain a clinically detectable size. Simulations of system (2.20), with initial conditions (2.21),

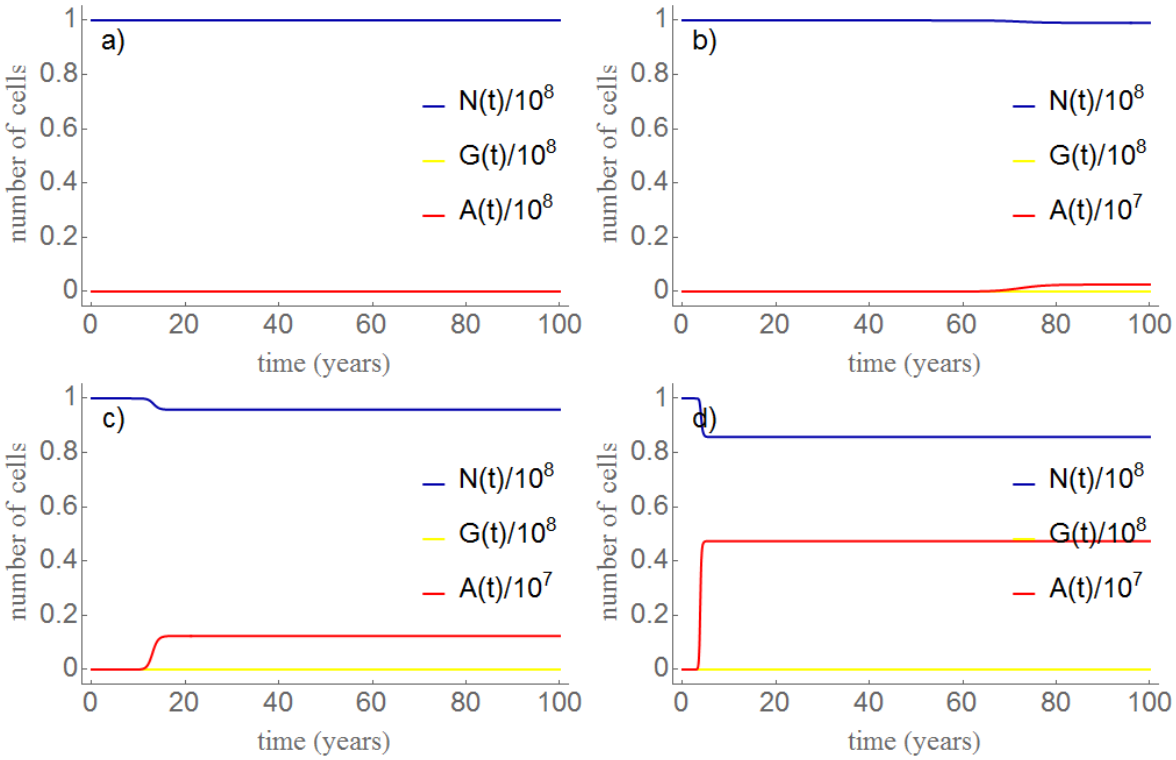


Figure 7 – Simulations of system (2.20) with $\epsilon_A = 0.010$ and different values of $\beta_3$: a) $\beta_3 = 0.035$; b) $\beta_3 = 0.029$; c) $\beta_3 = 0.025$; d) $\beta_3 = 0.012$. Initial conditions are (2.21) with $G_0 = 1$, and parameters values are given in (2.22) and (2.24).

$G_0 = 1$, and different values of $\epsilon_A$ and $\beta_3$ were performed. In each simulation, we seek for the first time at which cancer cells (either $A$ or $G$) reached the detectable size of $10^6$ cells. Results are shown in Figure 8. We see that diminishing both the tissue response and tumor intrinsic apoptotic rate lead to a smaller time for tumor development, which can vary from larger values, like 21 years, to small ones, like 2 years. Thus, besides predicting qualitatively that evading apoptosis allows cancer development, the model also agrees quantitatively with biological facts by showing that evading apoptosis increases the velocity of tumor progression. It is also worth noting that there are intervals of parameters $\beta_3$ and $\epsilon_A$ for which the tumor attains a maximum size smaller than the clinically detectable size. So the model also predicts the onset and establishment of cancer at non-detectable, avascular stage, but ready to suffer other mutations that allow angiogenesis and subsequent invasion and metastasis.

### The effect of genetic instability

Finally, we analyze the effect of genetic instability. Tissue exposure to carcinogenic factors increases the mutation rate of cells, or increases the initial number of premaligant cells.

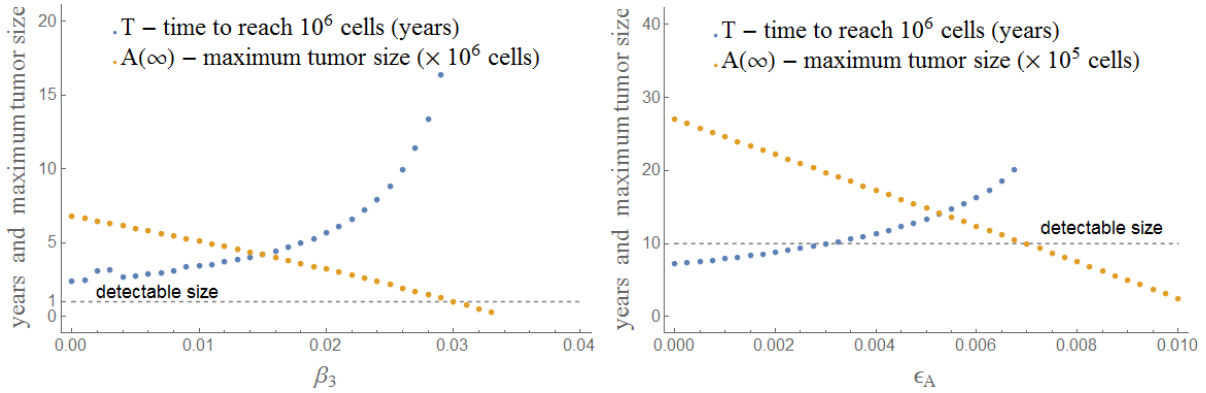


Figure 8 – Necessary time for cancer to reach detectable size ($10^6$ cells), beginning with a single mutant cell $G$. On the left, the effect of varying $\beta_3$ is shown (with $\epsilon_A = 0.006$ fixed): for values of $\beta_3$ near zero, cancer attains detectable size in only 2.5 years; as the tissue response is increased, this time grows up to 17 years; for $0.029 < \beta_3 < 0.034$, the maximum tumor size is below detectable size; for $\beta_3 > 0.034 = \beta_3^{th}$, cancer cells are eliminated ($P_0$ is stable). On the right, the effect of varying $\epsilon_A$ is assessed (with $\beta_3 = 0.029$ fixed): we see that the necessary time to reach a detectable size varies from 7 years (when $\epsilon_A = 0$) to 21 years (with $\epsilon_A = 0.007$); for $0.007 < \epsilon_A < 0.010$, the maximum tumor size is below detectable size; for $\epsilon_A > 0.010$ (not showed here), cancer cells are eliminated ($P_0$ is stable).

In Figure 9 (left), we see the results of changing the value of the maximum mutation rate, $\delta$. Parameters values are those in (2.22) and (2.24), with $\beta_3 = 0.0029$ and $\epsilon_A = 0.006$. If $\delta = 10^{-8}$, cancer attains a detectable size in 20 years. As $\log \delta$ increases, the time $T$ for cancer to reach the detectable size diminishes linearly according with $T = 10.05 - 1.26 \log \delta$. So, a 10 fold increase in the mutation rate diminishes the time $T$ by 1.26 years. At the standard value $\delta = 10^{-5}$ we have $T = 16.3$ years. When $\delta = 10^{-3}$, we have $T = 13.8$ years.

A similar behavior is observed when the initial number of mutant cells is changed. This behavior is illustrated in the plot of $T$ versus $\log_2 G_0$ in Figure 9 (right). The parameters values are those in (2.22) and (2.24), with $\beta_3 = 0.0029$, $\epsilon_A = 0.006$. When $G_0 = 1$, we have $T = 16.3$ years. As $G_0$ increases, $T$ decreases linearly with $\log_2 G_0$ according to equation $T = 16.30 - 0.74 \log_2 G_0$. Therefore, doubling the initial number of precancer cells leads to a reduction of 0.74 years, approximately 9 months, in the time taken for the tumor to reach $10^6$ cells.

## 2.5 Discussion

By looking qualitative results summarized on Figure 5 and numerical results from the previous Section, we now turn to discuss their biological implications.

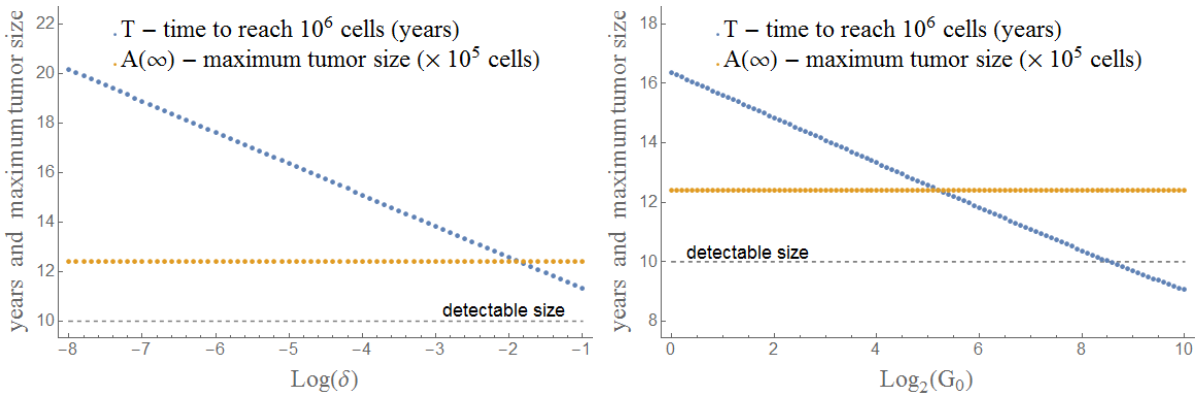


Figure 9 – Necessary time for cancer to reach the detectable size ($10^6$ cells), beginning with a $G_0$ mutant cells. On the right, the effect of varying $\delta$, with $G_0 = 1$ fixed. On the right, the effect of varying $G_0$, with $\delta = 10^{-5}$ fixed. Parameters values are indicated in the text.

### Cancer onset

First, we analyze these results from the point of view of cancer onset from very few mutant cells. We restrict our attention to specific regions of parameters space where tumor progression is possible. We must restrict to regions where $P_0$ is not stable, because the more biologically relevant initial conditions in this standpoint will be small disturbances from $P_0$. Since these are very small disturbances, they will return to $P_0$ if it is stable, and cancer will be eliminated.

If we disregard the mutation from $G$ to $A$ for a moment ($\delta = 0$), we have the following. When $\beta_2 < \beta_2^{th}$, then normal cells fail to prevent the growth of $G$ cells, because $G \to \infty$. In this case, there is no need for $G$ cells to acquire a second hallmark. On the other hand, if $\beta_2 > \beta_2^{th}$, normal cells are capable of preventing the growth of $G$ cells, and $G \to 0$. In this case, the hallmark of self-sufficiency in growth signals is not enough for the development of these mutant cells, and it is necessary that these cells acquire another hallmark that increases their survival possibility.

Thus, if we require that the mutation from $G$ to $A$ is a necessary step, then, the more biologically plausible regions are those where $\beta_2 > \beta_2^{th}$. Following these conditions, we observe that in regions I and II, when $\beta_3 > \beta_3^{th}$, there is no chance of cancer onset, since in all sub-regions, $P_0$ is locally stable if $\beta_2 > \beta_2^{th}$. Therefore, cancer onset is possible only in region III, with $\beta_3 < \beta_3^{th}$. This condition is equivalent to

$$\beta_3 + \frac{r_N}{\mu_N}\epsilon_A < \frac{r_N}{\mu_N}(r_A - \mu_A).$$

Therefore, if the repair system is not good enough or the intrinsic apoptotic rate of cancer cells is reduced, $P_0$ is unstable, and the tissue is not able to prevent tumor growth. The appearing of a few mutant cells, i.e., small disturbances of $P_0$, will break the tissue homeostatic state free of cancer and lead to the formation of a tumor with presence of

one or two types of mutant cells. Thus, the first barrier to tumor progression is broken by evading apoptosis (diminishing $\epsilon_A$) and/or the disruption of the repair system against cancer cells (diminishing $\beta_3$). The mutation from $G$ cells to $A$ cells represents the conditions of mutant cells to adapt, which requires evading apoptosis and/or acquiring more resistance to tissue response. These conclusions agree with the evidences that the probability of tumor progression is often enhanced in injured organs and tissues that display lost or diminished regenerative ability (75).

Even with the above conditions satisfied, apoptosis and tissue response are also barriers to tumor progression, from a quantitative point of view. In fact, as illustrated by numerical simulations in Figure 7, the time elapsed by the cancer cells to reach a stationary or detectable size vary from few to many years as these parameters increase. Further, as seen in Figure 8 if the above conditions are satisfied but very near the equality, tumor attains a undetectable size. Thus, it may be possible that a tumor starts to grow but the lifetime of a person is not enough to cancer achieve a harmless stage.

We now compare sub-cases in region III. In the subsystem $N \times A$, we have cancer progression, since $\bar{P}_2$ is globally stable in this subsystem. To understand what happens in the full system, we must consider two possibilities: $\delta < l_G$ and $\delta > l_G$, according to Figure 5.

The first one can be rewritten as $\delta + \epsilon_G < r_G - \mu_G$. Thus, the sum of mutation rate and additional apoptotic rate of $G$ is low, lesser than the net growth rate. In this scenario, we have the following. Case a): If $\beta_2 < \beta_{2,\delta}^{th,2}$ (which is possible even with $\beta_2 > \beta_2^{th}$ - see Figure 5), $P_\infty$ is globally stable and cancer grows in the tissue achieving a high number of cells. It happens because the presence of tumor cells $A$ resistant to the tissue response lead to a decrease in the quantity of $N$ cells. These cells, in a lesser number, do not make enough pressure to eliminate $G$ cells. Thus, while at an initial instant precancer cells $G$ work as a trigger to development of cancer cells $A$, at a subsequent instant, cancer cells $A$ open space in the tissue for the development of less adapted cells, which would not survive in the absence of the more adapted $A$ cells. This feedback implicates in a heterogeneous tumor, with distinct cell subpopulations. Case b): Increasing tissue aggressiveness against $G$ cells, if $\beta_{2,\delta}^{th} < \beta_2 < \beta_{2,\lambda}^{th}$, $\tilde{P}_5$ becomes stable. Thus, initial conditions near $P_0$ will converge to $\tilde{P}_5$. A heterogeneous tumor yet establishes in the tissue, but attains a steady state level less than the encountered in the previous case. Case c): increasing the tissue response, $\beta_2 > \beta_{2,\lambda}^{th}$, $\tilde{P}_5$ ceases to exist and $\bar{P}_2$ becomes stable. Thus, initial conditions near $P_0$ will converge to $\bar{P}_2$. Therefore, in this case, the tissue high aggressiveness against $G$ cells does not allow the survival of them, and the final tumor is not heterogeneous as in the previous case. However, the onset of precancer cells works at least as a trigger to tumor progression, since it enables $A$ cells, originated from $G$, to attain a positive stationary state.

The other possibility, $\delta + \epsilon_G > r_G - \mu_G$ is very similar to those of the previous

case. The difference is that the high apoptotic rate $\epsilon_G$ does not allow $G$ cells to attain high levels ($P_\infty$ is not stable).

Finally, we briefly discuss the possibility of cancer onset when $P_0$ is locally stable. In this case, mutant cells will be removed, unless another nontrivial equilibrium is stable and the initial number of mutant cells is large enough to drive the system outside the basin of attraction of $P_0$. This large number of initial mutations may be achieved through exposure to carcinogenic factors. A study of the quantitative behavior of this threshold for initial conditions is not performed in this work. However, in highlighted cells of case II in Figure 5, we note that eight different regimens of multistability (d,e,f,g,h,j,k,l) may arise depending on parameters. Three of them (e,g,h) exhibit three basins of attraction, the one of $P_0$, and two other corresponding to two different final tumor volumes. Thus, the model predicts that, in some cases, the amount of exposure to carcinogenic factors may have influence on the final tumor volume.

### Genetic instability

Let us depict the role of $G$ cells and their mutation to $A$ cells. We turn attention to region I of parameters space, where $A$ cells would be extinct if there would not be $G$ cells, since $P_0$ is globally stable in subsystem $N \times A$. However, in the full system, we see in Figure 5 that $P_0$ is not globally stable anymore. Under the more realistic condition $\beta_2 > \beta_2^{th}$ (discussed above), $P_0$ is only locally stable. Therefore, under high genome instability which increases initial conditions favorable for cancer cells, the constant transition from $G$ cells to $A$ cells may sustain the tumor progression in scenarios where $A$ cells would not survive alone.

Finally, results in Figure 9 show that changes in the mutation rate or the initial number of mutant cells have a large impact on the pace of tumor progression. These results illustrate the fact that the differences between a cancer patient and a healthy person may not be structural or qualitative differences between their intrinsic cellular systems, i.e., differences in parameters that lead to different regions on parameters space, where $P_0$ is stable and other where $P_0$ is unstable. On the contrary, the unique difference between these people would be only quantitative, in the sense that virtually both will have cancer some day, but after different times, due to the differences between the mutation rates or exposure to carcinogenic factors. From this point of view, genetic instability is the major factor that leads to tumor progression within a clinically observable time. These results agree with the fact that genetic instability is an enabling characteristic of cancer (19), and with results of (32), which predicts that normal mutation rates give rise to a tumor within a clinically observable time only if genetic instability is a driving force of the mutation pathway or if there is high number of breast stem cells and tumor suppressor genes.

## 2.6 Conclusion

An ordinary differential equation model considering normal, precancer and cancer cells was proposed to describe cancer onset and establishment at a normal tissue. The model incorporates in its hypothesis three hallmarks of cancer: self-sufficiency on growth signals, insensibility to anti-growth signals, and evading apoptosis. Transitions between compartments are modeled differently from previous works, by using Dirac Deltas and a continuous nonlinear flux in order to capture the effects of genetic instability as a factor that enhances the probabilities of mutations.

Dynamics of the boundary subsystem without precancer cells was globally characterized. This subsystem consisting only of normal and cancer cells is a simple system but presents an interesting behavior and captures well the possibility of tumor growth depending on parameters. It can be used as a basis to building more complex models by incorporating other phenomena. In a future work we will extend it by including angiogenesis and treatments like chemotherapy.

The full model was also studied in detail. The existence of nontrivial equilibria was characterized in the entire parameters space. Stability analysis of these equilibria was done numerically. From the point of view of cancer onset, the analysis of the model predicts that the first important barrier to cancer is the intrinsic apoptosis and the tissue repair system. Corruption of these systems revealed essential to cancer development from few mutant cells. The model also predicts that the presence of aggressive tumoral cells opens way to survival of less adapted cells which would not survive alone, leading to formation of a heterogeneous tumor. On the other hand, under high genome instability, the constant mutation from precancer cells to cancer cells may sustain the tumor growth in a scenario at which cancer cells would not persist in the absence of premalignant cells. Numerical simulations were performed with parameter values based on real data of breast cancer. The model predictions are similar, in quantitative and qualitative aspects, to biological observations. The necessary time for tumor progression and diagnosis were estimated with respect to some parameters of the model. This time may ranges from a few to eighty years, being very sensible to parameters like the intrinsic apoptotic rate of cancer cells, the mutation rate of premalignant cells, and the initial number of mutant cells. These parameters also have a major influence which determine whether the final tumor volume will be detectable or not.

## 2.A Mathematical analysis of nontrivial equilibria

In this Appendix, proofs and details concerning the existence and stability of nontrivial equilibria are presented.

### 2.A.1 Existence

The roots of (2.15) are the intersection points of graphs of $f(A)$ and $g(A)$ in (2.16). The roots of $f(A)$ are $A = 0, A_M, \bar{A}_1$ and $\bar{A}_2$ (where $\bar{A}_1 < \bar{A}_2$ are the roots of $q(A)$), and their relative positions determine the intervals where $f(A) > 0$. The polynomial $g(A)$ is always positive and has a double root $A = A_m$. If we know the relative positions of roots of $f$ and $g$, we can determine, through graphical analysis, the position of roots $\tilde{A}_i$, $i = 3, 4, 5, 6$, and then, know which of them give rise to a positive equilibrium $\tilde{P}_i$.

Notice that $\tilde{N} > 0$ whenever $\tilde{A} > 0$. Thus, from the expression of $\tilde{G}$ in (2.14), we obtain the following conditions for a equilibrium point $\tilde{P}_i$ be positive:

1. If $\delta < l_G$ and $\beta_2 < \beta_2^{th}$, then $\tilde{P}_i$ is positive if and only if, the root $\tilde{A}_i$ lies in the interval $I_1 = [0, A_M]$ (which is empty if $\beta_2 < \beta_{2,\delta}^{th}$).
2. If $\delta < l_G$ and $\beta_2 > \beta_2^{th}$, then $\tilde{P}_i$ is positive if and only if, the root $\tilde{A}_i$ lies in the interval $I_2 = [A_m, A_M]$.
3. If $\delta > l_G$ and $\beta_2 < \beta_2^{th}$, then $\tilde{P}_i$ is positive if and only if the root $\tilde{A}_i$ lies in the interval $I_3 = [0, \infty)$.
4. If $\delta > l_G$ and $\beta_2 > \beta_2^{th}$, then $\tilde{P}_i$ is positive if and only if, the root $\tilde{A}_i$ lies in the interval $I_4 = [A_m, \infty)$.

From definitions of $\beta_2^{th}$, $\beta_{2,\lambda}^{th,i}$, $A_m$, $A_M$ and $\beta_{2,\delta}^{th,i}$, in (2.3), (2.12), (2.17) and (2.18), we obtain the following relations

$$A_m > 0 \iff \beta_2 > \beta_2^{th}, \tag{2.25}$$

$$A_M > 0 \iff \beta_2 > \beta_{2,\delta}^{th} \text{ and } \delta < l_G, \tag{2.26}$$

$$\bar{A}_i < A_m \iff \beta_2 > \beta_{2,\lambda}^{th,i}, \qquad i = 1, 2, \tag{2.27}$$

$$\bar{A}_i < A_M \iff \beta_2 > \beta_{2,\delta}^{th,i} \text{ and } \delta < l_G, \qquad i = 1, 2. \tag{2.28}$$

Further, we have that

$$\begin{gathered} \lim_{A\to\pm\infty} f(A) = -\infty, \text{ if } \delta < l_G, \\ \lim_{A\to\pm\infty} f(A) = +\infty, \text{ if } \delta > l_G, \text{ and} \\ \lim_{A\to\pm\infty} |f(A)/g(A)| = +\infty. \end{gathered} \tag{2.29}$$

Also, from (2.18), notice that in case II, with $0 < \bar{A}_1 < \bar{A}_2$, we have

$$0 < \delta_1 < \delta_2 < l_G. \tag{2.30}$$

With relations (2.25-2.30), and considering each of the cases I, II and III which determine the existence of positive roots $\bar{A}_1$ and $\bar{A}_2$ for $q(A)$, we have all information about the roots of $f(A)$ and $g(A)$ and we can determine which root $\tilde{A}_i$, $i = 3, 4, 5, 6$, lies in the appropriate interval $I_j$. The thresholds for $\beta_2$ and $\delta$ in each case can be seen in Figure 3, as well a summary of the results. Some cases below are illustrated in Figure 10.

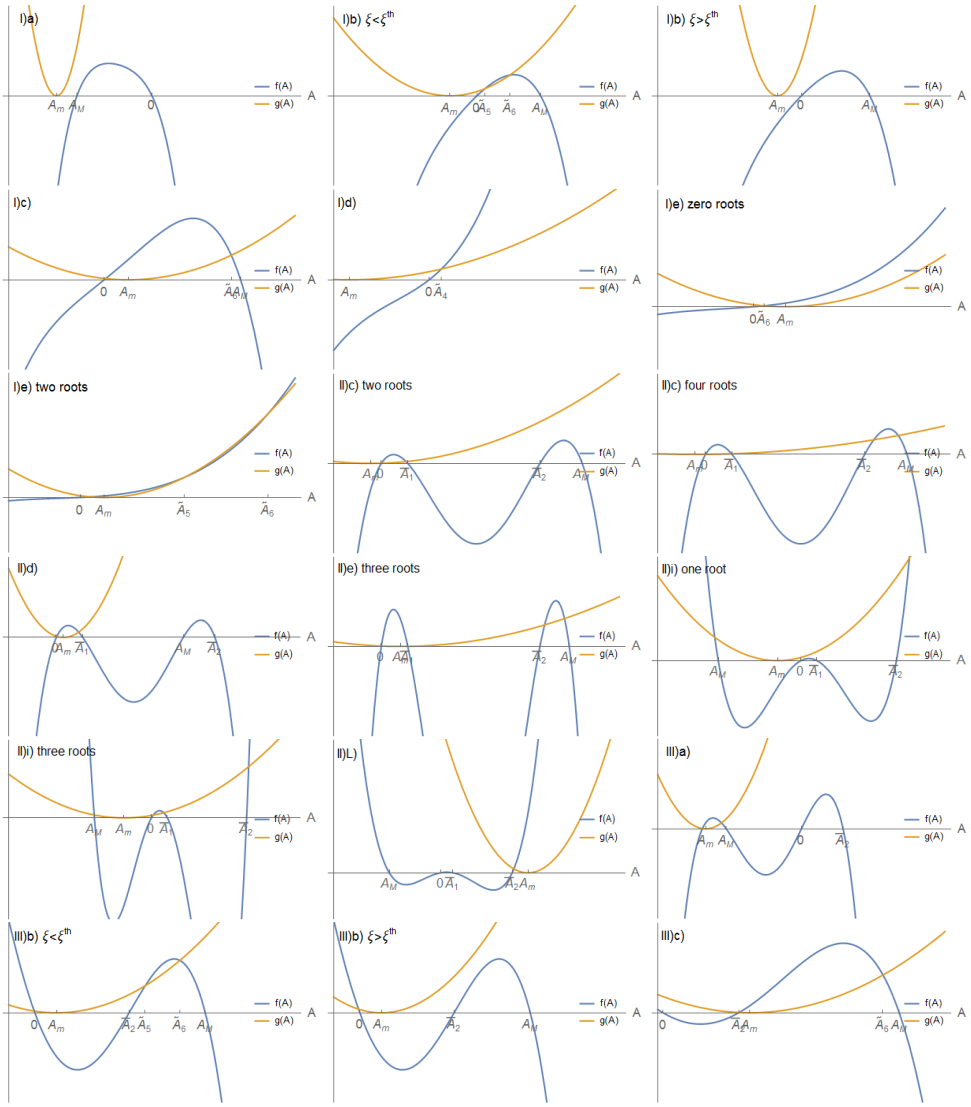


Figure 10 – Graphics of $f(A)$ and $g(A)$ in various subcases. The roots of equation (2.15) are the intersecting points of both graphs, and must occur at an appropriated interval $I_j$, in order to give origin to positive equilibria $\tilde{P}_i$. The roots of $f(A)$ are $A = 0, A_M, \bar{A}_1$ and $\bar{A}_2$ and their relative positions determine the intervals where $f(A) > 0$. The polynomial $g(A)$ is always positive and has a double root $A = A_m$.

1. If $\beta_3 > \beta_3^{th}$ and $\beta_1 < \beta_{1,\Delta}^{th}$, the roots $\bar{A}_i$, $i = 1, 2$, are complex or negative.

   For $\delta < l_G$, the thresholds for $\beta_2$ which are of interest are $0 < \beta_{2,\delta}^{th} < \beta_2^{th}$. We have:

a) If $\beta_2 < \beta_{2,\delta}^{th}$, the feasibility interval $I_1$ is empty. Thus, there is no positive equilibrium $\tilde{P}_i$.

b) If $\beta_{2,\delta}^{th} < \beta_2 < \beta_2^{th}$, then, from (2.25) and (2.26), we have $A_m < 0 < A_M$. The graphics of $f(A)$ and $g(A)$ may intersect zero or twice in the interval $I_1$. It depends on the value of $\xi$. For $\xi$ below a certain threshold $\xi^{th}$, the graphic of $g(A)$ intersects the curve of $f(A)$ twice. For $\xi > \xi^{th}$, the graphics do not intersect. The value of $\xi^{th}$ is the value of $\xi$ such that the graphics of $f$ and $g$ are tangent at a root $\tilde{A}$. Thus, $(\xi^{th}, \tilde{A})$ is a solution to the system

$$\begin{cases} f(A) = g(A) \\ f'(A) = g'(A) \end{cases} . \tag{2.31}$$

Thus, two equilibria, say $\tilde{P}_5$ and $\tilde{P}_5$, are both positive, or all equilibria are non-positive.

c) If $\beta_2 > \beta_2^{th}$, we have $0 < A_m < A_M$. The graphics of $f$ and $g$ intersect at $\tilde{A}_5 < A_m$ and at $\tilde{A}_6 \in I_2$. Therefore, $\tilde{P}_6$ is the unique positive equilibrium $\tilde{P}_i$.

For $\delta > l_G$, the thresholds for $\beta_2$ satisfy $\beta_{2,\delta}^{th} < 0 < \beta_2^{th}$. We have:

d) If $\beta_2 < \beta_2^{th}$, then $A_M < A_m < 0$. As $f$ is a fourth degree polynomial, while $g$ has degree two, from (2.29) we have that $f(A) > g(A)$ for $A$ sufficiently large. As $f(0) = 0 < g(0)$, there is at least one root $\tilde{A}_i$ in the interval $I_3 = [0, \infty)$. Other two roots can both lie in this interval, depending on other parameters, such as above. Therefore, equilibrium $\tilde{P}_4$ is positive, and $\tilde{P}_5$ and $\tilde{P}_6$ may be both positive.

e) If $\beta_2 > \beta_2^{th}$, then $A_M < 0 < A_m$. The graphics of $f$ and $g$ intersect at one root in the interval $(0, A_m)$, which do not result in a positive $\tilde{P}_i$. It is possible that the graphics intersect twice or zero in the interval $(A_m, \infty)$. Thus, no point $\tilde{P}_i$ is positive, or $\tilde{P}_5$ and $\tilde{P}_6$ are both positive.

2. If $\beta_3 > \beta_3^{th}$ and $\beta_1 > \beta_{1,\Delta}^{th}$, the roots $\bar{A}_1$ and $\bar{A}_2$ are positive, with $\bar{A}_1 < \bar{A}_2$.

   If $\delta < l_G$, we have:

   a) If $\beta_2 < \beta_{2,\delta}^{th}$, there is no positive $\tilde{P}_i$, since $I_1$ is empty.

   b) If $\beta_{2,\delta}^{th} < \beta_2 < \min\{\beta_2^{th}, \beta_{2,\delta}^{th,2}\}$, we have $A_m < 0 < \min\{\bar{A}_1, A_M\} < \max\{\bar{A}_1, A_M\} < \bar{A}_2$. Thus, $f(A)$ is positive only in the interval $I_2$ for values $A \in [0, \min\{\bar{A}_1, A_M\}]$. As $g(A) > 0$ for $A > A_m$, the graphics of $f$ and $g$ may intersect zero or twice in $I_2$, again depending on $\xi$. Therefore, either there are no positive equilibria $\tilde{P}_i$, or $\tilde{P}_3$ and $\tilde{P}_4$ are positive.

c) If $\beta_{2,\delta}^{th,2} < \beta_2 < \beta_2^{th}$, then $A_m < 0 < \bar{A}_1 < \bar{A}_2 < A_M$. The graphics of $f$ and $g$ may intersect zero or twice in the interval $[0, \bar{A}_1]$, and also zero or twice in the interval $[\bar{A}_2, A_M]$. Thus, the equilibria $\tilde{P}_3$ and $\tilde{P}_4$ may be both positive or not and the same happens with $\tilde{P}_5$ and $\tilde{P}_6$. Therefore, we may have zero, two or four positive equilibria $\tilde{P}_i$.

d) If $\beta_2^{th} < \beta_2 < \min\{\beta_{2,\lambda}^{th,1}, \beta_{2,\delta}^{th,2}\}$, then $0 < A_m < \min\{\bar{A}_1, A_M\} < \max\{\bar{A}_1, A_M\} < \bar{A}_2$. Thus, as $f(A)$ is positive only in the interval $I_2$ if $A \in [A_m, \min\{\bar{A}_1, A_M\}]$, and as $g(A_m) = 0$, the unique root in the interval $I_2$ is $\tilde{A}_4$, and only $\tilde{P}_4$ is positive.

e) If $\max\{\beta_2^{th}, \beta_{2,\delta}^{th,2}\} < \beta_2 < \beta_{2,\lambda}^{th,1}$, then $0 < A_m < \bar{A}_1 < \bar{A}_2 < A_M$. We have $f(A) > 0$ for $A \in (A_m, \bar{A}_1) \cup (\bar{A}_2, A_M)$. As $g(A_m) = 0$, the unique root in $(A_m, \bar{A}_1)$ is $\tilde{A}_4$. The roots $\tilde{A}_5$ and $\tilde{A}_6$ may both lie in $(\bar{A}_2, A_M)$, or both do not exist, depending on the value of $\xi$. Therefore, $\tilde{P}_4$ is positive and $\tilde{P}_5$ and $\tilde{P}_6$ may be both positive.

f) If $\beta_{2,\lambda}^{th,1} < \beta_2 < \beta_{2,\delta}^{th,2}$, then $0 < \bar{A}_1 < A_m < A_M < \bar{A}_2$. Therefore, $f(A) < 0$ in $I_2$, in such way no $\tilde{P}_i$ is positive, $i = 3, 4, 5, 6$.

g) If $\max\{\beta_{2,\delta}^{th,2}, \beta_{2,\lambda}^{th,1}\} < \beta_2 < \beta_{2,\lambda}^{th,2}$, then $0 < \bar{A}_1 < A_m < \bar{A}_2 < A_M$. At $I_2$, we have $f(A) > 0$ only if $A \in [\bar{A}_2, A_M]$. Thus, the graphics of $f$ and $g$ can intersect zero or twice (at $\tilde{A}_5$ and $\tilde{A}_6$) in the interval $I_2$. Therefore, only $\tilde{P}_5$ and $\tilde{P}_6$ may be positive.

h) If $\beta_2 > \beta_{2,\lambda}^{th,2}$, then $0 < \bar{A}_1 < \bar{A}_2 < A_m < A_M$. The graphics of $f$ and $g$ intersect exactly once in $I_2$, at $\tilde{A}_6$. Only $\tilde{P}_6$ is positive.

For $\delta > l_G$:

i) If $\beta_2 < \beta_2^{th}$, then $\min\{A_m, A_M\} < \max\{A_m, A_M\} < 0 < \bar{A}_1 < \bar{A}_2$. At the interval $I_3$, $f$ is positive when $0 < A < \bar{A}_1$ or $A > \bar{A}_2$. As $g(A_m) = 0$, from (2.29), there is a root $\tilde{A}_6 > \bar{A}_2$. At the interval $0 < A < \bar{A}_1$, the graphics can intersect zero or twice (at $\tilde{A}_4$ and $\tilde{A}_5$). Therefore, $\tilde{P}_6$ is positive and $\tilde{P}_4$ and $\tilde{P}_5$ may be positive.

j) If $\beta_2^{th} < \beta_2 < \beta_{2,\lambda}^{th,1}$, then $A_M < 0 < A_m < \bar{A}_1 < \bar{A}_2$. The graphics of $f$ and $g$ intersect twice, at $\tilde{A}_5 < \bar{A}_1$ and $\tilde{A}_6 > \bar{A}_2$. $\tilde{P}_5$ and $\tilde{P}_6$ are positive.

k) If $\beta_{2,\lambda}^{th,1} < \beta_2 < \beta_{2,\lambda}^{th,2}$, we have $A_M < 0 < \bar{A}_1 < A_m < \bar{A}_2$. The graphics intersect exactly once in the interval $I_4$, at $\tilde{A}_6 > \bar{A}_2$. Therefore, only $\tilde{P}_6$ is positive.

l) If $\beta_2 > \beta_{2,\lambda}^{th,2}$, we have $A_M < 0 < \bar{A}_1 < \bar{A}_2 < A_m$. Therefore, the four roots of $f(A)$ are positioned before $A_m$, in such way that $f$ is a strictly increasing function for $A > A_m$, because the three possible points where $f'(A) = 0$ lie between the roots of $f$. As $f(A_m) > 0 = g(A_m)$, the graphics can not intersect in the interval $I_4$. Therefore, no $\tilde{P}_i$ is positive.

3. If $\beta_3 < \beta_3^{th}$, then $\bar{A}_1 < 0 < \bar{A}_2$.

For $\delta < l_G$, we have:

a) If $\beta_2 < \beta_{2,\delta}^{th,2}$, there is no positive $\tilde{P}_i$. Indeed, if $\beta_2 < \beta_{2,\delta}^{th,2}$, we have $A_m < A_M < 0 < \bar{A}_2$, and the interval $I_1$ is empty. If $\beta_{2,\delta}^{th} < \beta_2 < \beta_{2,\delta}^{th,2}$, we have $A_1 < 0 < A_M < \bar{A}_2$, in such way that $f(A) < 0$ for $A \in [0, A_M]$. As $g(A) \geqslant 0$, there is no root $\tilde{A}_i$ in the intervals $I_1$ (for $\beta_2 < \beta_2^{th}$) and $I_2$ (for $\beta_2 > \beta_2^{th}$).

b) If $\beta_{2,\delta}^{th,2} < \beta_2 < \beta_{2,\lambda}^{th,2}$, then $A_1 < 0 < \bar{A}_2 < A_M$. Thus, $f(A) > 0$ in the interval $[\bar{A}_2, A_M]$. As $A_m < \bar{A}_2$, the graphics of $f(A)$ and $g(A)$ may intersect zero or twice in the interval $[\bar{A}_2, A_M] \subset I_j$, $j = 1, 2$. Therefore, there may be zero or two positive equilibria $\tilde{P}_i$, $\tilde{P}_5$ and $\tilde{P}_6$.

c) If $\beta_2 > \beta_{2,\lambda}^{th,2}$, then $A_1 < 0 < \bar{A}_2 < A_m < A_M$. Thus, there is exactly one root $\tilde{A}_i$ in the interval $I_2$. Thus, only $\tilde{P}_6$ is positive.

If $\delta > l_G$, we have:

d) If $\beta_2 < \beta_{2,\lambda}^{th,2}$, then $\min\{\bar{A}_1, A_M\} < \max\{\bar{A}_1, A_M\} < 0 < \bar{A}_2$, with $A_m < \bar{A}_2$. If $A > \max\{A_m, 0\}$, $f(A)$ is positive only if $A > \bar{A}_2$. Thus, there is only one root $\tilde{A}_i > \max\{A_m, 0\}$, which is $\tilde{A}_6$. Therefore, only $\tilde{P}_6$ is positive.

e) If $\beta_2 > \beta_{2,\lambda}^{th,2}$, we have $\min\{\bar{A}_1, A_M\} < \max\{\bar{A}_1, A_M\} < 0 < \bar{A}_2 < A_m$. The graphics of $f$ and $g$ can intersect zero or twice (at $\tilde{A}_5, \tilde{A}_6 > A_m$) in the interval $I_4$. Thus, or $\tilde{P}_5$ and $\tilde{P}_6$ are positive, or no $\tilde{P}_i$ is positive.

## 2.A.2 Stability

Now, we present numerical results concerning the stability of the nontrivial equilibria $\tilde{P}_i$, $i = 3, 4, 5, 6$. Conditions (2.19) were studied numerically. By varying $\beta_2$, bifurcation diagrams were obtained and stability of equilibria $\tilde{P}_i$ was inferred. In each of the cases I, II and III, we fixed $\delta$ in a determined region, according to Figure 3, and allowed $\beta_2$ to vary, obtaining the bifurcation diagrams for each value of $\delta$. In general, a bifurcation occurs when $\beta_2$ surpasses the thresholds that limit the subregions a), b), c), etc. The obtained diagrams are presented in Figures 11, 12 and 13, referring to cases I, II and III respectively. In the main graphic of each figure, the behavior of roots $\tilde{A}_i$ depending on $\beta_2$ is presented, together with the values of $A_m$ and $A_M$, which delimit the interval where the roots $\tilde{A}_i$ give origin to positive $\tilde{P}_i$ (see subsection 2.A.1 for details). Plotting is continuous, dashed, or dotted, according the corresponding equilibrium is stable, unstable, or not positive, respectively. Stability of points $\tilde{P}_i$ was determined by observing the smaller graphics, where coefficients $a_1$, $a_3$ e $a_1a_2 - a_3$ are plotted against $\beta_2$. The values $A_0 = 0$, $\bar{A}_1$ and $\bar{A}_2$, corresponding to equilibria $P_0$, $\bar{P}_1$ and $\bar{P}_2$, whose existence does not depend on $\beta_2$, but stability does, also are plotted in the main graphic.

Based on these diagrams, and corroborated by numerical simulations (not shown) and phase portraits like those of Figure 6, we conclude the following about the asymptotic behavior of system (these conclusions were obtained numerically for a discrete set of parameter values, and may be not valid for all parameter space, although they are valid in small open neighborhoods of these values):

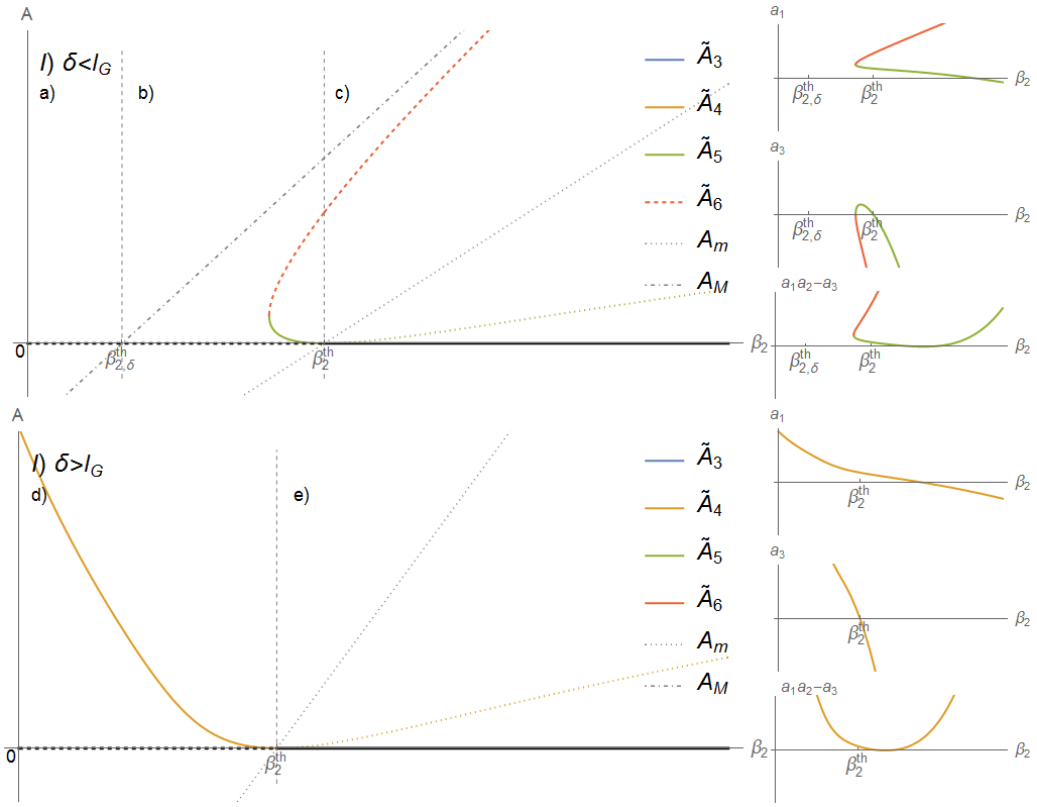


Figure 11 – Bifurcation diagram of equilibria $\tilde{P}_i$ depending on $\beta_2$, in case I.

I) If $\beta_3 > \beta_3^{th}$ and $\beta_1 < \beta_{1,\Delta}^{th}$, $P_0$ is locally stable, while $\bar{P}_1$ and $\bar{P}_2$ are not positive. Corresponding bifurcation diagrams are presented in Figure 11.

For $\delta < l_G$, we have:

a) If $\beta_2 < \beta_{2,\delta}^{th}$, there is no positive $\tilde{P}_i$, and $P_0$ is unstable. Numerical results indicate that all solutions tend to $P_\infty$.

b) If $\beta_{2,\delta}^{th} < \beta_2 < \beta_2^{th}$, $P_0$ is unstable, and $\tilde{P}_5$ and $\tilde{P}_6$ can be positive, depending on $\xi$. If they are, numerical simulations indicate that $\tilde{P}_5$ is stable and $\tilde{P}_6$ is unstable, separating solutions that converge to $\tilde{P}_5$ from those that tend to $P_\infty$.

c) If $\beta_2 > \beta_2^{th}$, $P_0$ and $\tilde{P}_6$ are the positive equilibria. $P_0$ is stable and $\tilde{P}_6$ is unstable, separating the basins of attraction of $P_0$ and $P_\infty$.

If $\delta > l_G$, according the bottom diagram on Figure 11, we have:

d) If $\beta_2 < \beta_2^{th}$, $P_0$ is unstable. $\tilde{P}_4$ is positive and stable. $\tilde{P}_5$ and $\tilde{P}_6$ can be both positive, depending on $\xi$. If they are not, numerical simulations indicate that all solutions converge to $\tilde{P}_4$. If $\tilde{P}_5$ and $\tilde{P}_6$ are positive (not shown in Figure 11), $\tilde{P}_5$ is unstable, separating the basins of attraction of $\tilde{P}_4$ and $\tilde{P}_6$, which are stable.

e) If $\beta_2 > \beta_2^{th}$, $\tilde{P}_4$ is no longer positive and $P_0$ becomes stable; a forward bifurcation occurs. $\tilde{P}_5$ and $\tilde{P}_6$ can be both positive, and the results are analogous to the previous case.

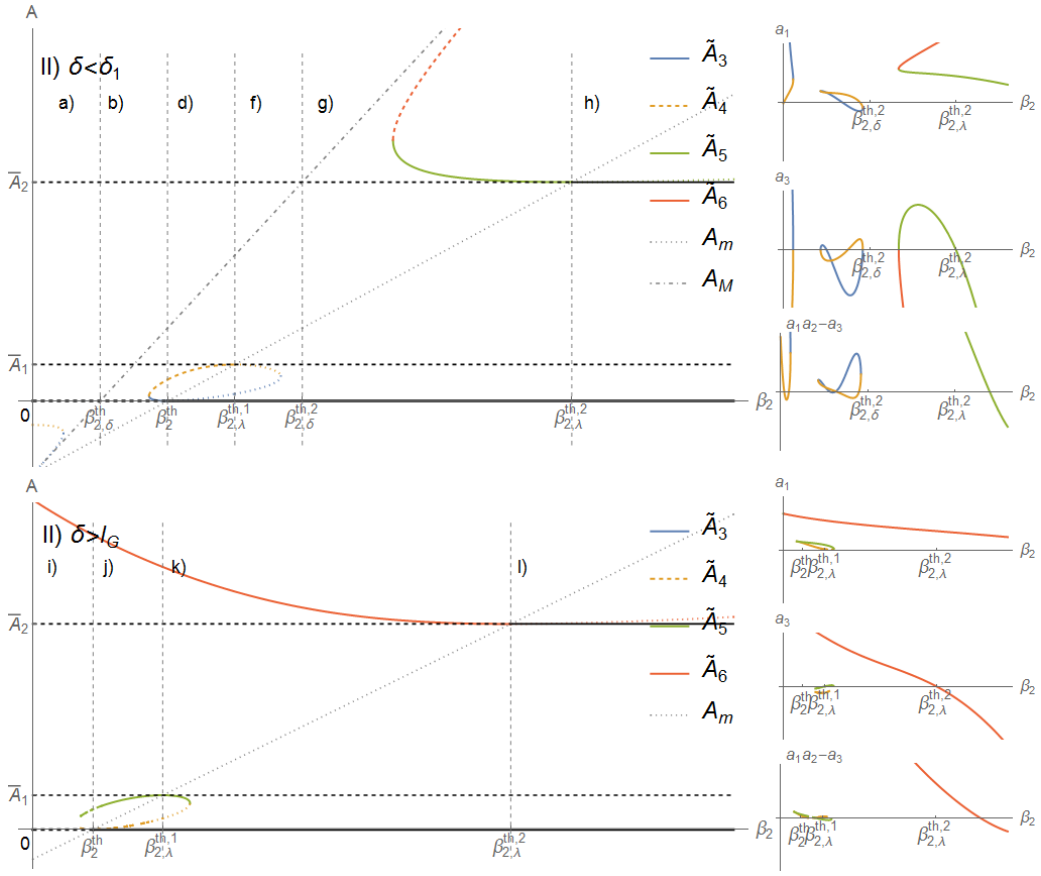


Figure 12 – Bifurcation diagram for equilibria $\tilde{P}_i$ depending on $\beta_2$, in case II.

II) If $\beta_3 > \beta_3^{th}$ and $\beta_1 > \beta_{1,\Delta}^{th}$, then $P_0$, $\bar{P}_1$ and $\bar{P}_2$ are positive. $\bar{P}_1$ is unstable. In order to analyze bifurcations with respect to $\beta_2$, we must consider four different intervals to parameter $\delta$, separated by $0 < \delta_1 < \delta_2 < l_G$ (see Figure 5). Corresponding bifurcation diagrams are presented in Figure 12.

For $\delta < \delta_1$, we have:

a) If $\beta_2 < \beta_{2,\delta}^{th}$, $P_0$ and $\bar{P}_2$ are unstable and there is no positive equilibrium $\tilde{P}_i$. All solutions go to $P_\infty$.

b) If $\beta_{2,\delta}^{th} < \beta_2 < \beta_2^{th}$, $P_0$ and $\bar{P}_2$ are unstable. Equilibria $\tilde{P}_3$ e $\tilde{P}_4$ can be positive (see Appendix 2.A for details). If it occurs, $\tilde{P}_3$ is stable and $\tilde{P}_4$ is unstable, separating the basins of attraction of $\tilde{P}_3$ and $P_\infty$.

d) If $\beta_2^{th} < \beta_2 < \beta_{2,\lambda}^{th,1}$, $P_0$ is stable and $\bar{P}_2$ is unstable. $\tilde{P}_4$ is positive and unstable, separating the basins of attraction of $P_0$ and $P_\infty$. The phase portrait of this case can be seen in Figure 6.

f) If $\beta_{2,\lambda}^{th,1} < \beta_2 < \beta_{2,\delta}^{th,2}$, $P_0$ is stable and $\bar{P}_2$ unstable. Equilibria $\tilde{P}_i$, $i = 3, 4, 5, 6$, are not positive. $\bar{P}_1$ separates the basins of attraction of $P_0$ and $P_\infty$.

g) If $\beta_{2,\delta}^{th,2} < \beta_2 < \beta_{2,\lambda}^{th,2}$, $P_0$ is stable and $\bar{P}_2$ is unstable. $\tilde{P}_5$ and $\tilde{P}_6$ can be positive. If it happens, $\tilde{P}_5$ is stable and $\tilde{P}_6$ is unstable, which separates the basins of attraction of $\tilde{P}_5$ and $P_\infty$. $\bar{P}_1$ separates the basins of attraction of $P_0$ and $\tilde{P}_5$ (or $P_0$ and $P_\infty$, when $\tilde{P}_5$ and $\tilde{P}_6$ are not positive). There can be three basins of attraction. The phase portrait of this case can be seen in Figure 6.

h) If $\beta_2 > \beta_{2,\lambda}^{th,2}$, $P_0$ and $\bar{P}_2$ are stable, and their basins of attraction are separated by $\bar{P}_1$. $\tilde{P}_6$ is positive and unstable, separating the basins of attraction of $\bar{P}_2$ and $P_\infty$. There are three basins of attraction. The phase portrait of this case can be seen in Figure 6.

If $\delta_1 < \delta < \delta_2$, transitions occur through regions a), b), d), e), g) and h), as can be seen in Figure 3. The corresponding bifurcation diagram is very similar to that of the previous case. The same happens in the interval $\delta_2 < \delta < l_G$, were transitions occur through regions a), b), c), e), g), and h). For sake of brevity, the detailed descriptions for these two cases are omitted, as well the bifurcation diagrams.

For $\delta > l_G$, we have:

i) If $\beta_2 < \beta_2^{th}$, $\tilde{P}_6$ is positive and stable. $\tilde{P}_4$ and $\tilde{P}_5$ can be both positive. If it happens, $\tilde{P}_4$ is stable, and $\tilde{P}_5$ unstable, separating the basins of attraction of $\tilde{P}_6$ and $\tilde{P}_4$. If they are not positive, all solutions converge to $\tilde{P}_6$.

j) If $\beta_2^{th} < \beta_2 < \beta_{2,\lambda}^{th,1}$, $\tilde{P}_6$ is positive and stable. $P_0$ is also stable. $\tilde{P}_5$ is positive and unstable, separating the basins of attraction of $P_0$ and $\tilde{P}_6$.

k) If $\beta_{2,\lambda}^{th,1} < \beta_2 < \beta_{2,\lambda}^{th,2}$, $\tilde{P}_6$ is positive and stable. $P_0$ also is stable. Their basins of attraction are separated by $\bar{P}_1$.

l) If $\beta_2 > \beta_{2,\lambda}^{th,2}$, $P_0$ and $\bar{P}_2$ are stable, and their basins of attraction are separated by $\bar{P}_1$.

III) If $\beta_3 < \beta_3^{th}$, $P_0$ and $\bar{P}_2$ are positive. $P_0$ is unstable. Corresponding bifurcation diagrams are presented in Figure 13.

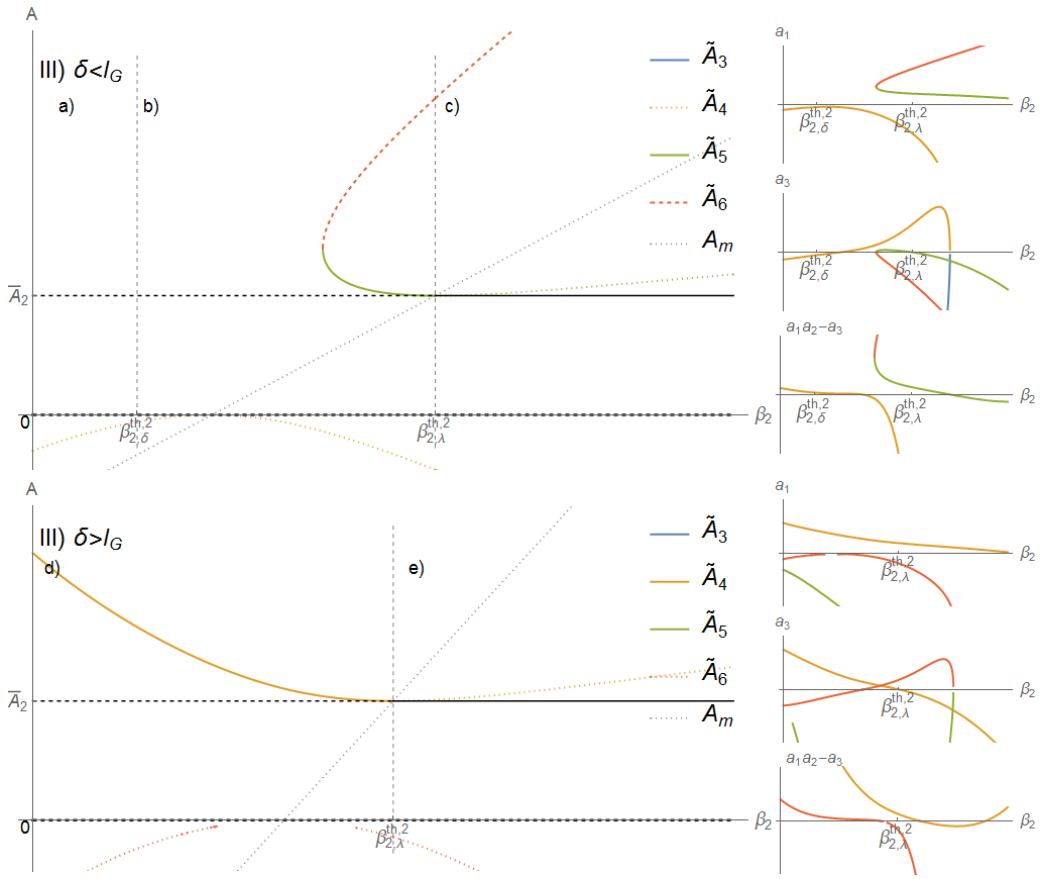


Figure 13 – Bifurcation diagram of equilibria $\tilde{P}_i$ depending on $\beta_2$, in case III.

For $\delta < l_G$, we have:

a) If $\beta_2 < \beta_{2,\delta}^{th,2}$, $\bar{P}_2$ is unstable and there is no positive $\tilde{P}_i$, $i = 3, 4, 5, 6$. All solutions converge to $P_\infty$.

b) If $\beta_{2,\delta}^{th,2} < \beta_2 < \beta_{2,\lambda}^{th,2}$, $\bar{P}_2$ is unstable and $\tilde{P}_5$ and $\tilde{P}_6$ can be both positive. If it happens, $\tilde{P}_5$ is stable and $\tilde{P}_6$ is unstable, separating the basins of attraction of $\tilde{P}_5$ and $P_\infty$.

c) If $\beta_2 > \beta_{2,\lambda}^{th,2}$, $\bar{P}_2$ is stable and $\tilde{P}_6$ is unstable, separating the basins of attraction of $\bar{P}_2$ and $P_\infty$. The phase portrait of this case can be seen in Figure 6.

For $\delta > l_G$, we have:

d) If $\beta_2 < \beta_{2,\lambda}^{th,2}$, $\bar{P}_2$ is unstable and $\tilde{P}_6$ is the unique positive equilibrium $\tilde{P}_i$, $i = 3, 4, 5, 6$, and it is stable.

e) If $\beta_2 > \beta_{2,\lambda}^{th,2}$, $\tilde{P}_6$ becomes negative and $\bar{P}_2$ becomes stable.

# 3 An ecological resilience perspective on cancer: insights from a toy model

*Abstract.* In this paper we propose an ecological resilience point of view on cancer, where tumor growth and treatment are seen as transitions between alternative stable states. This view is based on the analysis of a simple ODE model for the interactions between cancer and normal cells. The model presents two regimes for tumor growth. In the first, cancer arises due to three reasons: a partial corruption of the functions that avoid the growth of mutated cells, an aggressive phenotype of tumor cells and exposure to external carcinogenic factors. In this case, treatments may be effective if they drive the system to the basin of attraction of the cancer cure state. In the second and more dangerous regime, cancer arises because the repair system is intrinsically corrupted. In this case, the cure is not possible since the cancer cure state is no more stable, but tumor recurrence may be delayed if treatment is prolonged. In the second part of the paper we review three indicators of the resilience of a stable equilibrium, related with size and shape of its basin of attraction: latitute, precariousness and resistance. A novel method to calculate these indicators is proposed. This method is simpler and more efficient than those currently used, and may be easily applied to other population dynamics models. We apply this method to the model and investigate how these indicators behave with parameters changes. Results indicate that the cancer state has more resilience than the cure state.

*Keywords*: Tumor growth; Chemotherapy; Resilience; Basins of attraction; Regime shifts; Critical transitions.

## 3.1 Introduction

The ecological resilience perspective is an emerging approach for understanding the dynamics of social-ecological systems (76, 77, 78, 79, 80, 81). While the stability point of view emphasizes the equilibrium and the maintenance of present state, the resilience point of view focus on shifts between alternative basins of attraction, thresholds, uncertainty and unexpected disturbances. External forces or random events may cause state variable perturbations that drive a nonlinear system, which is initially near a stable state, to enter a undesirable basin of attraction. In this case, the resilience of the original steady state is related with the size and shape of its basin of attraction, and the capacity of the system to persist in this basin of attraction when subject to state variable perturbations. Three different indicators are established in the literature as measures of the resilience of a stable state with respect to state variable perturbations (82, 83): the *latitute* of an equilibrium

point, which is a measure of the volume of its basin of attraction; the *precariousness* of an equilibrium point, which is related with the minimal state space disturbance needed to drive the system outside its basin of attraction; and the *resistance* of an equilibrium point, which is a measure of the deepness of its basin of attraction.

On the other hand, changes in system parameters occur in a slow time scale, due to evolutionary forces acting on the system or by modifying the intensities of interactions and forces governing such system. In this case, parameters modify the resilience of the system with respect to state variable perturbations. Further, when parameters do change enough, the system may undergo several bifurcations and the phase portrait may change substantially. In this case, one can measure the resilience of the system with respect to parameters changes as the distance to the threshold values for which bifurcations occur. As a consequence of such bifurcations, an undesirable alternative stable state may be created, and its basin of attraction can be achieved by state variable perturbations, as commented above. A more dramatic outcome happens when parameters changes lead to loss of stability of the original steady state or even its disappearance. In this case, a regime shift occurs and the system moves to another state. Now, the question of reversibility takes place. Of first importance is the question whether it is possible or not to return the parameters to their original values. When parameters change due to evolutionary factors, it is more likely that this change can not be undone. Changes due to external forces can be undone more easily through the correct manipulation of those forces (if possible). However, even if the original values can by restored, the reversal to the original stable state may not be completely achieved if the system exhibits hysteresis.

In this paper we illustrate how these concepts of ecological resilience can be applied to cancer, a complex disease whose causes are far from being well understood and whose cure is far from being achieved. Indeed, despite the intense efforts that led the elucidation of many biochemical mechanisms developed by cancer cells to survive (19), there is a current debate on which are the major factors that allow the onset of cancer cells. While some arguee that alterations in intrinsic cellular processes are the main reasons that some tissues become cancerous (84), others defend the view that most cases of cancer result from extrinsic factors such environmental exposure to toxic chemicals and radiation (85). With respect to cancer treatment, although the development of new drugs and strategies to treat cancer in the last fifty years achieved good results in many cases, another large portion of cancer patients did not respond well to treatments, or presented tumor recurrence, indicating that there is still a long road in the fight against cancer (86, 17).

We propose a toy model for tumor growth and apply the above concepts to suggest a framework for viewing the arising of cancer and its effective treatment as critical transitions between two alternative stable states. In this framework, tumor growth and

tumor treatment depend ultimately on ecological resilience questions. Further, we briefly review the three resilience indicators commented above, propose a method to calculate these indicators and apply this method to the model. As far as we know, this novel method we propose is simpler and more efficient than those currently used, and can be applied to other population dynamics models to improve their analysis through this resilience perspective.

The paper is organized as follows. In Section 3.2 the model is presented. In Section 3.3 the analysis of the model is performed. In Section 3.4, the results are discussed in the ecological resilience perspective. In Section 3.5, the method to calculate resilience indicators is presented and applied to the model. Finally, conclusions are presented in Section 3.6.

## 3.2 A toy model for tumor growth

We present a toy model consisting of a system of ODEs describing tumor growth and its effect on normal tissue, together with the tissue response to tumor. Our goal is not to consider the several aspects of tumor growth and to reproduce quantitative behavior with very accuracy, but to use the model to give some insights about a resilience point of view on cancer. The model equations are given by

$$\frac{dN}{dt} = r_N - \mu_N N - \beta_1 NA, \tag{3.1a}$$

$$\frac{dA}{dt} = r_A A\left(1 - \frac{A}{K_A}\right) - \beta_3 NA - (\mu_A + \epsilon_A)A, \tag{3.1b}$$

where $N$ and $A$ stand for normal and tumor cells, respectively. This system is a limit case of a three-dimensional model for oncogenesis encompassing mutations and genetic instability (87).

Parameter $r_N$ represents the total constant reproduction of normal cells, and $\mu_N$ is their natural mortality. Thus, a constant flux for normal cells is considered in the vital dynamics, and not a density-dependent one, like the logistic growth generally assumed (48, 49, 50, 51). The reason for this choice is that at a normal and already formed tissue the imperative dynamics is not the cells intraspecific competition by nutrients, but the maintenance of a homeostatic state, through the natural replenishment of old and dead cells (52).

On the contrary, cancer cells have a certain independence on growth signals released by the tissue and keep their own growth program, like an embrionary tissue in growth phase (56, 57). Thus a density dependent growth is considered. Several growth laws could be used, such as the Gompertz, generalized logistic, Von Bertanlanfy and others (88). We choose the logistic growth due its simplicity, and a natural mortality $\mu_A$. An extra mortality rate $\epsilon_A$ due to apoptosis (60) is also included.

Several models for tumor growth consider the phenomena of tumor angiogenesis, i.e., the formation of new blood vessels to feed the tumor, in response to signals released by tumor cells (89, 58). In order to keep the model as simple as possible, we do not consider angiogenesis here.

Parameter $\beta_3$ encompasses, in the simplest way possible, all negative responses of the many cell types in normal tissue due to the presence of tumor cells. These interactions include the release of anti-growth and death signals by host cells (19), the immune-system response (90), competition by nutrients with tumor cells and so on. Similarly, parameter $\beta_1$ covers all mechanisms developed by tumor cells which damage the normal tissue, like increasing local acidity (63), supression of immune cells (91), release of death signals (19), and competition with normal cells.

System (3.1) is similar to the classical Lotka-Volterra model of competition (92), commonly used in models for tumor growth (48, 49, 50, 51) and biological invasions (93), but has a fundamental difference. The use of a constant flux instead a logistic growth to normal cells breaks the symmetry present in the classical Lotka-Volterra model, so that no equilibrium with $N = 0$ will exists. Thus, normal cells will never be extinct, on the contrary to the models that consider the logistic growth for normal cells. We believe that this is not a problem, but, on the contrary, is a realistic outcome. Indeed, roughly speaking, cancer 'wins' not by the fact that it kills all cells in the tissue, but by the fact that it reaches a dangerous size that disrupt the well functioning of the tissue and threaten the health of the individual. A constant flux term was already taken in other well-know models for cancer, specifically, to describe the growth of immune cells (54, 55, 94).

## 3.3 Analysis of the model

We now present the analysis of system (3.1). Biological implications are discussed in Section 3.4.

### 3.3.1 Equilibrium points

System (3.1) has a trivial equilibrium

$$P_0 = \left(\frac{r_N}{\mu_N}, 0\right),$$

and up to two nontrivial equilibria

$$P_i = (N_i, A_i) = \left(\frac{r_N}{\mu_N + \beta_1 A_i}, A_i\right), \ i = 1, 2.$$

Here, $A_1$ and $A_2$ are the roots of the second degree equation

$$aA^2 + bA + c = 0, \tag{3.2}$$

with coefficients

$$a = \frac{\beta_1 r_A}{K_A} > 0, \qquad b = l_A\left(\beta_1^{th} - \beta_1\right), \qquad c = r_N\left(\beta_3 - \beta_3^{th}\right).$$

where

$$\beta_1^{th} = \frac{\mu_N r_A}{l_A K_A}, \quad and \quad \beta_3^{th} = \frac{\mu_N}{r_N} l_A. \tag{3.3}$$

When $A_1$ and $A_2$ are real, we label them in the order $A_1 < A_2$. Conditions for having positive equilibria $P_1$ and $P_2$ are obtained by Descartes' Rule of Signs (69). Together with the trivial equilibrium $P_0$, the results are summarized as follows:

I) If $\beta_3 > \beta_3^{th}$ and $\beta_1 < \beta_{1,\Delta}^{th}$, the unique nonnegative equilibrium is the trivial equilibrium $P_0$.

II) If $\beta_3 > \beta_3^{th}$ and $\beta_1 > \beta_{1,\Delta}^{th}$, three nonnegative equilibria are $P_0$, $P_1$ and $P_2$.

III) If $\beta_3 < \beta_3^{th}$, the nonnegative equilibria are $P_0$ and $P_2$.

The threshold $\beta_{1,\Delta}^{th}$, defined for $\beta_3 > \beta_3^{th}$, is the value of $\beta_1 > \beta_1^{th}$ for which the discriminant $\Delta = b^2 - 4ac$ is zero, and is given by

$$\beta_{1,\Delta}^{th} = \beta_1^{th} + 2\eta + 2\sqrt{\eta(\beta_1^{th} + \eta)}, \tag{3.4}$$

where $\eta = r_A r_N(\beta_3 - \beta_3^{th})/(K_A l_A^2)$.

### 3.3.2 Local Stability

Stability of $P_0$ is easily determined. The eigenvalues of the Jacobian matrix of system (3.1) evaluated at $P_0$ are given by

$$\lambda_1 = -\mu_N, \quad \text{and} \quad \lambda_2 = \frac{r_N}{\mu_N}(\beta_3^{th} - \beta_3).$$

Thus, $P_0$ is locally asymptotically stable if $\beta_3 > \beta_3^{th}$, and is a saddle otherwise.

We now study the local stability of $P_i$, $i = 1, 2$. Using the fact that $N_i$ and $A_i$ satisfy

$$l_A - \frac{r_A}{K_A} A_i - \beta_3 N_i = 0, \tag{3.5}$$

we find that the Jacobian matrix of system (3.1) evaluated at $P_i$ is given by

$$j(P_i) = \begin{bmatrix} -\beta_1 A_i - \mu_N & -\dfrac{\beta_1}{\beta_3}(l_A - \dfrac{r_A}{K_A} A_i) \\ -\beta_3 A_i & -\dfrac{r_A}{K_A} A_i \end{bmatrix}.$$

Whenever $P_i$ is a positive equilibrium, the trace of $j(P_i)$ is negative. Thus, when $P_i$ is positive, both eigenvalues of $j(P_i)$ will have negative real part if $\det(j(P_i)) > 0$, and we

have opposite signs in the other case. Solving equation (3.2) for $A_i$, and calculating the determinant we obtain

$$\det(j(P_i)) = A_i(2aA_i + b).$$

As $A_1 < A_2$, we have, whenever $P_i$ is a positive equilibrium, $i = 1, 2$,

$$\det(j(P_1)) = -A_1\sqrt{\Delta} < 0, \qquad \text{and} \qquad \det(j(P_2)) = A_2\sqrt{\Delta} > 0,$$

where $\Delta$ is the discriminant of (3.2). Thus, $P_1$ will be a saddle point whenever it is positive (case II above), and $P_2$ will be stable whenever it is positive (cases II and III above).

### 3.3.3 Asymptotic behavior and global stability

Let us show the boundedness of trajectories of (3.1). By noting that

$$\frac{dN}{dt} \leqslant r_N - \mu_N N,$$

and

$$\frac{dA}{dt} \leqslant l_A A\left(1 - \frac{r_A}{l_A K_A}A\right),$$

we may apply classical comparison principles (70) and conclude that all solutions $(N(t), A(t))$ with non-negative initial values remain restricted in the box

$$B = \left[0, \frac{r_N}{\mu_N}\right] \times \left[0, \frac{l_A}{r_A}K_A\right] \tag{3.6}$$

when $t \to \infty$.

In order to rule out periodic orbits for system (3.1) we apply the Dulac Criterion (71) with $u(N, A) = 1/NA$, obtaining

$$\nabla \cdot \left(\frac{1}{NA}\left(\frac{dN}{dt}, \frac{dA}{dt}\right)\right) = -\frac{r_A NA + K_A r_N}{K_A A N^2} < 0$$

for $(N, A) \in B$. Thus, system (3.1) has no periodic orbits.

By the Poincaré-Bendixson Theorem we conclude that all trajectories converge to an equilibrium point (71). It implies that equilibria $P_0$ and $P_2$ are globally stable in cases I and III, respectively (in the latter, $P_2$ is globally stable for initial conditions $A(0) > 0$, since the $N$ axis is the stable manifold of $P_0$). In case II, the plane $N \times A$ is divided in the basins of attraction of $P_0$ and $P_2$. The stable manifold of $P_1$ is the separatrix between these basins. All these results are summarized in Theorem 3.1.

**Teorema 3.1.** *System (3.1) has the following behavior:*

*I) If $\beta_3 > \beta_3^{th}$ and $\beta_1 < \beta_{1,\Delta}^{th}$, then $P_0$ is globally stable.*

*II) If $\beta_3 > \beta_3^{th}$ and $\beta_1 > \beta_{1,\Delta}^{th}$, then $P_0$ and $P_2$ are locally stable. Equilibrium $P_1$ is a saddle point whose stable manifold is the separatrix between the basins of attraction of $P_0$ and $P_2$.*

*III) If $\beta_3 < \beta_3^{th}$, then $P_2$ is globally stable for initial conditions $A(0) > 0$.*

The division of the $\beta_1 \times \beta_3$ plane into regions I, II and III is showed in Figure 14.

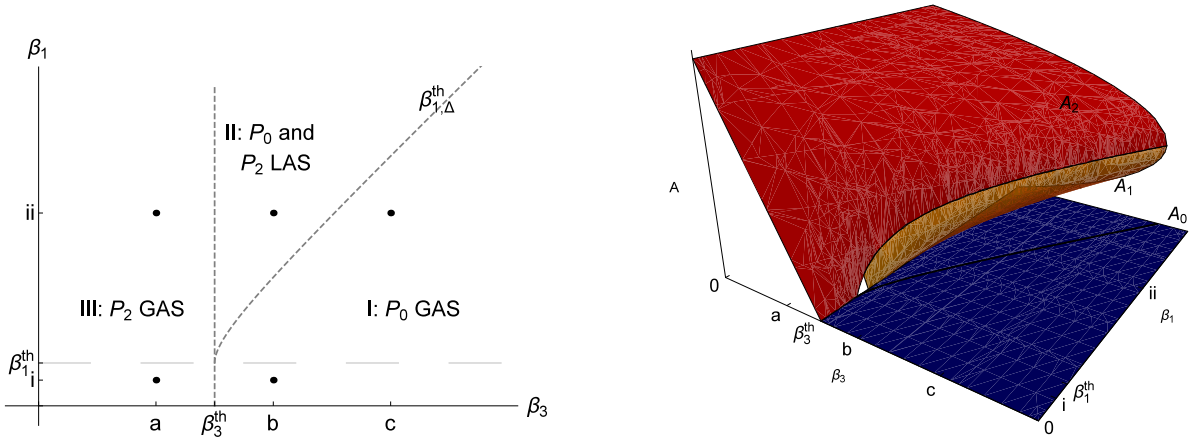


Figure 14 – Left: Regions I, II and III in the $\beta_3 \times \beta_1$ plane of parameters space, together with equilibria behavior. Right: bidimensional diagram of the $A$ coordinates of equilibria $P_2$ (red, stable), $P_1$ (orange, unstable) and $P_0$ (blue, stable for $\beta_3 > \beta_3^{th}$), when $\beta_3$ and $\beta_1$ vary.

### 3.3.4 Numerical simulations

We now present numerical simulations in order to stimulate discussions in next sections. Figure 15 shows simulations of system (3.1) in cases II and III. Parameters values were based on data from the literature, specially for breast cancer, according the procedure below. A summary of the parameter values is presented in Table 1.

We assume that the lifetime of a normal cell is 100 days, thus $\mu_N = 1/100$ days$^{-1}$. The number of normal cells in the breast cannot pass $N_0 = 10^8$ cells (24). Thus, in order to adjust the equilibrium $r_N/\mu_N$ of normal cells in the absence of cancer to be $10^8$ cells, we consider $r_N = 10^6$ cells/day. For cancer cells, we assume the same natural mortality, $\mu_A = 1/100$ days$^{-1}$. For the apoptotic rate of $A$ cells, we use $\epsilon_A = 1/100$ days$^{-1}$. The ratio *birth rate/death rate* is 1 for a normal tissue, in order to maintain a homeostatic state. Following (24), we assume that cancer cells have increased this ratio by a factor of five. Thus, we have $r_A = 5/100$ days$^{-1}$. In order to have the maximum number of cancer cells being 75% of the normal cells, we consider $K_A = 7.5 \times 10^7$. The values of

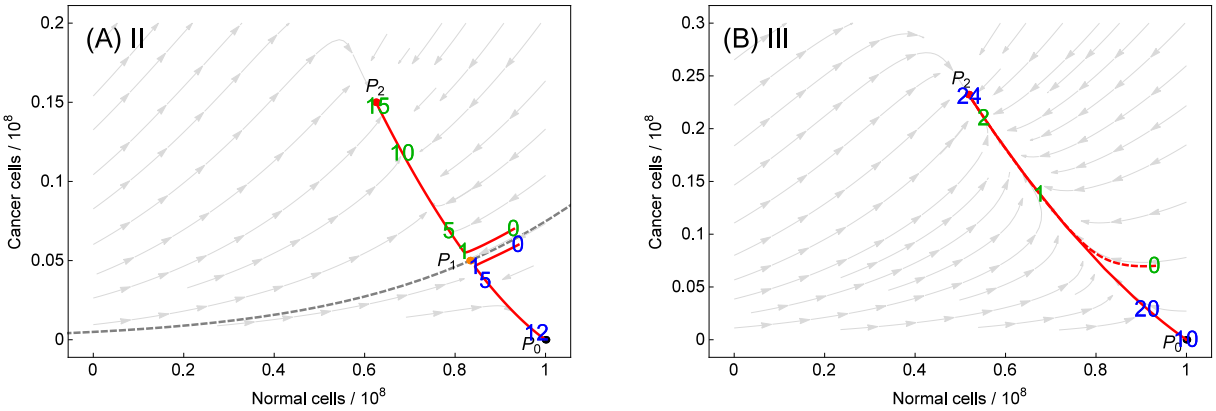


Figure 15 – Solutions os system (3.1) when parameters correspond to cases II (left) and III (right), using values in Table 1. Initial conditions are $N(0) = r_N/\mu_N - A_0$ and $A(0) = A_0$, representing that the tissue was initially at its homeostatic state when $A_0$ cells have become cancerous. The values of $A_0$ are: $A_0 = 0.06 \times 10^8$ and $A_0 = 0.07 \times 10^8$ (left); $A_0 = 1$ and $A_0 = 0.07 \times 10^8$ (right). In the left panel, the gray dotted curve represents the separatrix between the basins of attraction of $P_0$ and $P_2$. The green and blue numbers indicate the time (in years) corresponding to the trajectory.

Table 1 – Parameters description and values adopted in simulations.

| Parameter | Description | Value |
|---|---|---|
| $\mu_N$ | $1/\mu_N$ is the lifetime of a normal cell | 0.01 day$^{-1}$ |
| $r_N$ | total constant reproduction of normal cells | $10^6$ cell day$^{-1}$ |
| $r_A$ | tumor cells growth rate | 0.05 day$^{-1}$ |
| $K_A$ | tumor carrying capacity | $0.75 \times 10^8$ cells |
| $\mu_A$ | natural mortality rate of cancer cells | 0.01 day$^{-1}$ |
| $\epsilon_A$ | extra mortality rate of cancer cells | 0.01 day$^{-1}$ |
| $\beta_1$ | cancer cells aggressiveness | $0.40 \times 10^{-9}$ cell$^{-1}$day$^{-1}$ |
| $\beta_3^{II}$ | tissue response to cancer cells - case II | $0.28 \times 10^{-9}$ cell$^{-1}$day$^{-1}$ |
| $\beta_3^{III}$ | tissue response to cancer cells - case III | $0.32 \times 10^{-9}$ cell$^{-1}$day$^{-1}$ |

interacting parameters $\beta_1$ and $\beta_3$, in units of cell$^{-1}$day$^{-1}$, are unknown a priori but, by substituting the values of other parameters, we obtain the thresholds for $\beta_1$ and $\beta_3$: the threshold $\beta_3^{th}$ which separates cases II and III has the value $\beta_3^{th} = 0.30 \times 10^{-9}$. So, we assume two possible values for $\beta_3$: $\beta_3^{III} = 0.28 \times 10^{-9}$, and $\beta_3^{II} = 0.32 \times 10^{-9}$. Each of these values will originate a different behavior of subsystem NA (see Figure 14). If $\beta_3 = \beta_3^{III}$ we are in case III, for every value of $\beta_1$. If $\beta_3 = \beta_3^{II}$, we have $\beta_{1,\Delta}^{th} = 0.37 \times 10^{-9}$, so we assume $\beta_1 = 0.40 \times 10^{-9} > \beta_3^{II}$, which is reasonable since cancer cells are supposed to cause more damage to normal cells than the contrary. With these values we are in case II. In all numerical simulations in this paper, we use these parameter values, and $\beta_3 = \beta_3^{III}$ or $\beta_3 = \beta_3^{II}$, depending on the interest to simulate cases III or II.

## 3.4 An ecological resilience perspective on cancer

We now discuss the biological implications of the previous analysis. Our goal is to look to system (3.1) as being a simple cartoon, a toy model, of the underlying system governing tumor growth in a cancer patient and thus apply the perspective of ecological resilience to discuss the results above. Although this is a rough approximation, it may be instructive illustration on our understanding of cancer onset and cancer treatment. By cartoon or an approximation, we mean that the underlying system of cancer in real life, despite being very complex, may presents three qualitative distinct regimes, corresponding to regimes I, II and III of system (3.1). In this analogy, an equilibrium state corresponding to the presence of a tumor is not necessarily a static equilibrium, but a state of the system where a tumor is growing and developing. Let us discuss the differences between these regimes.

### 3.4.1 Cancer onset as a critical transition

Initially, we look to cancer onset as a critical transition. Let us first comment at the 'natural repair system of the patient', a mechanism which is operated at a variety of levels and by many agents. In the tissue level, it is operated by the immune system, trough lymphocytes and natural killers cells, for example (90). The presence of cancer cells at a given site stimulate the locomotion of immune system cells to that site in order to eliminate the cancer cells. In the cellular level, many cell components watch some parameters of the own cell and its neighbors, as the DNA integrity, the products of cellular metabolism, the concentration of growth factors, etc. When abnormal conditions are detected inside the cell, it kills itself through apoptosis (60). When abnormal conditions are detected on its neighbourhood, it releases death or inhibitor factors to control the undesired growth in its vicinity (19). We consider all these mechanisms as the natural barrier to cancer. In system (3.1), they are roughly described by the parameters $\beta_3$ and $\epsilon_A$. Greater the value of these parameters, better is the natural repair system. In our toy model (3.1), these are the parameters most subject to changes in a slow-time scale, through the multistep process of genetic alterations which transform the descendants of a normal cell in a malign tumor, where each genetic alteration confers some advantage for cancer cells (19). Parameter $\beta_1$ also is thought to be a varying parameter in this slow-time scale, since it encompasses the many types of negative interactions which cancer cells impose to the host tissue, specially due to changes in their metabolism which increase local acidity or lead to starvation of oxygen and nutrients for normal cells.

In the first regime (region I), we have a healthy person, since $P_0$ is globally stable. In this case, we have an efficient tissue response, since condition $\beta_3 > \beta_3^{th}$ can be

written as

$$\beta_3 + \epsilon_A \frac{\mu_N}{r_N} > \frac{\mu_N}{r_N}(r_A - \mu_A).$$

Further, we have a limited aggressiveness of cancer cells, $\beta_1 < \beta_{1,\Delta}^{th}$. This condition depends also on $\beta_3$, because $\beta_{1,\Delta}^{th}$ depends on $\beta_3$ (see Figure 14, left). Therefore, for a fixed $\beta_1$, condition $\beta_1 < \beta_{1,\Delta}^{th}$ is equivalent to $\beta_3 > \beta_{3,\Delta}^{th}$, where $\beta_{3,\Delta}^{th}$ is the inverse function of $\beta_{1,\Delta}^{th}$. Thus, for each level of aggressiveness of cancer cells, we have a second threshold that the tissue response must be above in order to completely eliminate the chance of cancer. More aggressive are the cancer cells, higher is this threshold. Thus, region I corresponds to parameters such that, although new mutant cells may arise all the time, they are not so much aggressive and the intrinsic repair system is capable to eliminate them.

In the second regime (region II), we have the possibility of having cancer, since $P_0$ and $P_2$ are both stable. Condition $\beta_3 > \beta_3^{th}$ implies that the tissue response is efficient, but condition $\beta_1 > \beta_{1,\Delta}^{th}$, which is equivalent to $\beta_3 < \beta_{3,\Delta}^{th}$, implies that the tissue response is not completely capable to face the aggressiveness of cancer cells. Thus, region II corresponds to a partially corrupted repair system due to the aggressiveness of cancer cells. In this region, the resilience of the cancer cure equilibrium $P_0$ plays an important role. The survival and installation of a tumor mass depends on an increased genetic instability and/or exposure to external carcinogenic factors, in such way the mutations from normal to cancer cells increase the initial conditions of cancer cells allow them to surpass the threshold separating the basins of attraction of $P_0$ and $P_2$; see simulation in Figure 15 left. Thus, the protection against cancer depends on the resilience of $P_0$. Therefore, it is important to analyze how the resilience of $P_0$ behave as key parameters are changed. In the next Section we develop this 'resilience analysis'. We refer to (87) for a model that comprises an intermediary pre-cancer population that continuously 'feed' the population $A$ with new individuals.

Finally, case III represents a dramatic corruption of the repair system, $\beta_3 < \beta_3^{th}$. Now, the cancer equilibrium $P_2$ is globally stable, and the onset and development of cancer is possible for any initial number of cancer cells. However, distinct quantitative behaviors may be observed, depending on the initial number of cancer cells. In Figure 15 we see that the time that the tumor reaches a detectable size (approximately $10^6$ cells (74)) is more than ten years if a single mutant cell arises. As the number of initial cancer cells increases, this time decreases.

Based on these discussions, we may look at the onset of cancer as a critical transition, involving changes in parameters and state-space disturbances. At a normal stage without disease, all people correspond to regime I. In this regime, although abnormal cells arise all the time, the intrinsic repair system is capable to eliminate them. Due to probabilistic mutations, exposure to carcinogens, or genetic propensity, parameters change in a slow time-scale, a transition from regime I to II or III happens. Transition to regime II

is more likely to occur first since parameters need to change less. If this transition occurs, the tissue is protected yet against small disturbances of the homeostatic state. Merely a high exposure to extrinsic factors is capable to drive the underlying system to cross the boundary of the basins; resilience is a key factor here. On the other hand, transition to regime III depends on a high decrease of $\beta_3$ and $\epsilon_A$, and it also may occur after an initial transition from regime I to II. When regime III is achieved, tumor growth is a matter of time, and exposure to extrinsic factors may accelerate this process.

In order to illustrate and analyze the different transitions which may occur, we present in Figure 16 bifurcation diagrams when $\beta_3$ and $\beta_1$ vary. When $\beta_3$ varies with $\beta_1$ fixed, two different cases occur (Figure 16, top panels). In the first case, the tumor is not much aggressive to normal cells, $\beta_1 < \beta_1^{th}$, and we have a transition between regimes I and III through a transcritical bifurcation. In the second case, the tumor is very aggressive, $\beta_1 > \beta_1^{th}$, and we have transitions from regimes I to II (saddle-node bifurcation) and from II to III (transcritical bifurcation). Before entering regime III, there is a previous and additional interval, $\beta_3^{th} < \beta_3 < \beta_{3,\Delta}^{th}$ that allows cancer onset depending on initial conditions (regime II). The comparison of cases (i) and (ii) contributes to the debate of whether intrinsic or extrinsic factors are the major responsible for cancer onset (85, 84). Due to the possibility of a direct transition from regime I to II in case (ii), we conclude that extrinsic factors appear to be the major cause of aggressive tumors (high $\beta_1$), but combined with small contribution of intrinsic factors (diminishing $\beta_3$). On the other hand, the possibility of direct transition from I to III in case (i) implicates that only non-aggressive tumors arise due to intrinsic factors only.

When $\beta_1$ varies while $\beta_3$ is kept constant, we have a different effect (Figure 16, bottom panels). In the case when the tissue response to tumor is low, $\beta_3 < \beta_3^{th}$, no bifurcation occurs and we remain in regime III for all $\beta_1$. In the second case, the tissue response is high, $\beta_3 > \beta_3^{th}$, and a transition between regimes I and II occurs through a saddle-node bifurcation. We remain in regime II for all values of $\beta_1 > \beta_{1,\Delta}^{th}$, and no transition to regime III occurs, on the contrary to case (b) when $\beta_3$ varies with a high aggressiveness of tumor. Comparison of diagrams (ii) and (b) lead to an interesting conclusion. While normal cells are able with their own characteristics (strong repair system) to guarantee tissue integrity against aggressive tumors, aggressive cancer cells, on the other hand, depend on genetic instability (initial conditions) when fighting aggressive normal cells. Thus, the first important barrier against cancer is the intrinsic response. If it is not corrupted, no cancer will arise. If it is only partially corrupted (regime II in case (b)), then cancer onset will depend entirely on the tissue being exposed to carcinogenic factors.

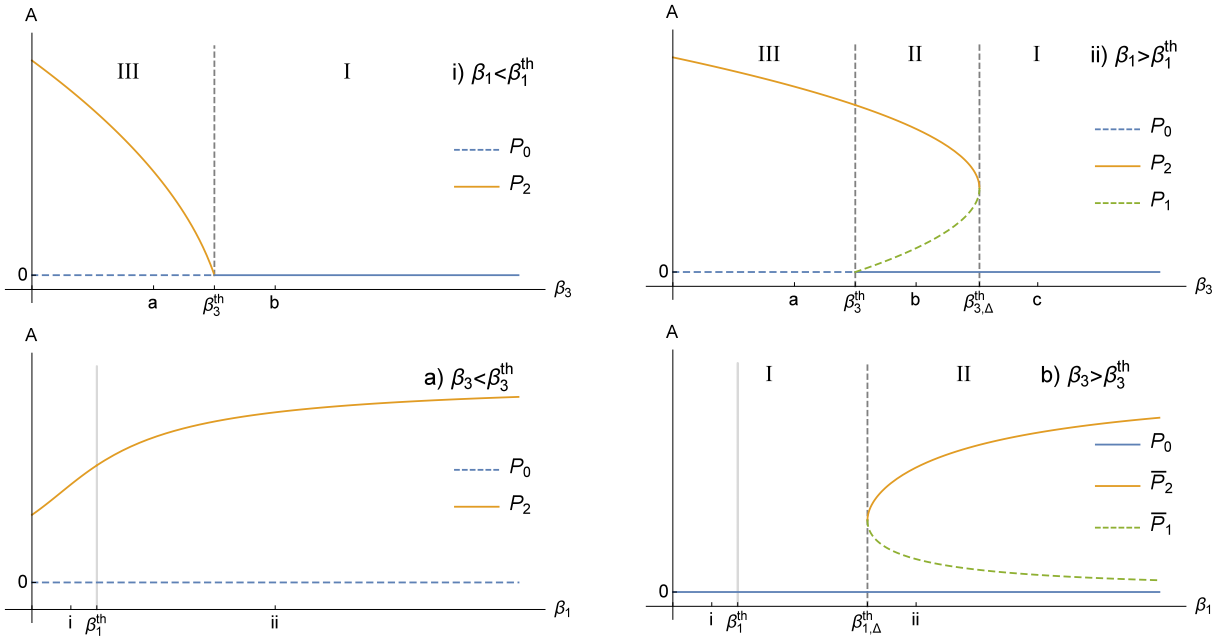


Figure 16 – Top: bifurcation diagrams of coordinate $A$ of equilibrium points when $\beta_3$ varies, with $\beta_1 < \beta_1^{th}$ (left), and $\beta_1 > \beta_1^{th}$ (right). Down: bifurcation diagrams when $\beta_1$ varies, with $\beta_3 < \beta_3^{th}$ (left), and $\beta_3 > \beta_3^{th}$ (right). Continuous plot corresponds to stable equilibrium, while dashed plot corresponds to unstable equilibrium. These diagrams are particular cases (horizontal sections i and ii and vertical sections a and b) of the bidimensional one, shown in Figure 14.

### 3.4.2 Cancer treatment as an attempt to allow a critical transition

Now, let us consider cancer treatment. We focus on application of chemotherapy due to its widely use, but some of the general results may be extend to other types of treatment, like radiotherapy or surgery. The simplest way to include chemotherapy in system (3.1) is to consider the following equations:

$$\frac{dN}{dt} = r_N - \mu_N N - \beta_1 NA - \alpha_N \gamma_N ND, \tag{3.7a}$$

$$\frac{dA}{dt} = r_A A\left(1 - \frac{A}{K_A}\right) - (\mu_A + \epsilon_A)A - \beta_3 NA - \alpha_A \gamma_A AD, \tag{3.7b}$$

$$\frac{dD}{dt} = v(t) - \gamma_N ND - \gamma_A AD - \tau D. \tag{3.7c}$$

Here, $D$ is the chemotherapeutic drug. It is administered according to a treatment function $v(t)$, and has a clearance rate $\tau$. The terms $\gamma_N ND$ and $\gamma_A AD$ describe drug absorption by normal and cancer cells, while the killing terms $\alpha_A \gamma_A AD$ and $\alpha_N \gamma_N ND$ follow the log-kill hypotheses (17). The treatment function can be described as a finite sum of Dirac Deltas,

$$v(t) = \sum_{i=1}^{n} \rho\delta(t - iT),$$

representing $n$ doses of $\rho$ mg of drug each, every $T$ days. Figure 17 shows simulations of the model with treatment, system (3.7), in cases II and III. In these simulations, we

assumed the values $\tau = 2.5$ day$^{-1}$, $\gamma_A = 0.3 \times 10^{-8}$ cell$^{-1}$day$^{-1}$, and $\alpha_A = 0.5 \times 10^8$ cell mg$^{-1}$. Since the chemotherapeutic agent is supposed to be more specific to cancer cells than normal cells, the values $\gamma_N = 0.6\gamma_A$ and $\alpha_N = 0.6\alpha_A$ were assumed for normal cells. The treatment parameters were $\rho = 10$ mg, $T = 7$ days, and $n = 4, 5, 6, 7$ doses.

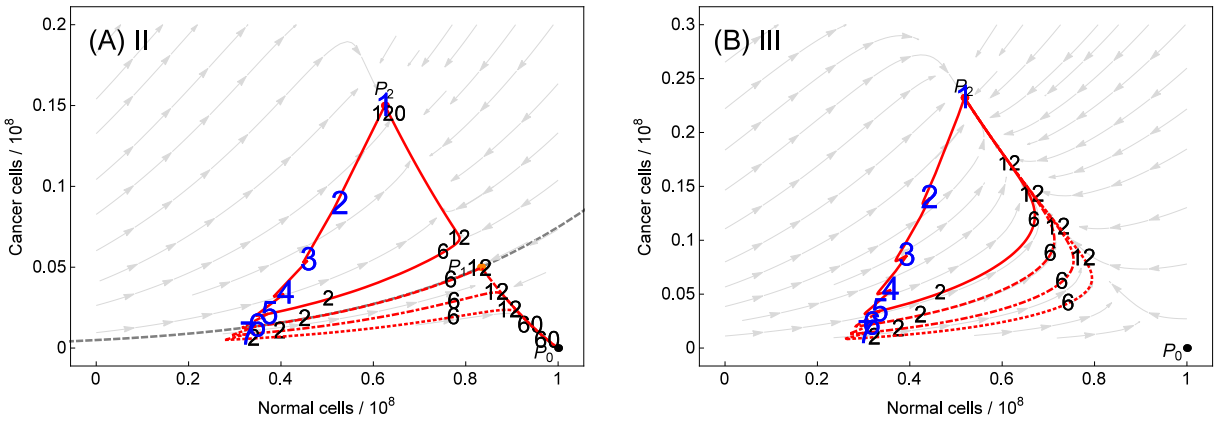


Figure 17 – Solutions of system (3.7) when parameters correspond to cases II (left) and III (right), with $n = 4, 5, 6, 7$ doses. The small black (large blue) numbers on phase portrait indicate the time in months (weeks) in which the solution was at each point. Initial conditions were $(A(0), N(0)) = P_2$, representing that the treatment was initiated only after the tumor reached the steady state $P_2$. In the left panel, the gray dotted curve represents the separatrix between the basins of attraction of $P_0$ and $P_2$.

More important than the form used to modeling the treatment $v(t)$, the general property is that all chemotherapeutic treatments cease after some time $t_f > 0$, i.e., $v(t) = 0$ for all $t > t_f$. Thus, $D(t) \leqslant -\tau D$ and so $D \to 0$ when $t \to \infty$. Therefore *all solutions of system* (3.7) *approach solutions of system* (3.1). This fact have an important consequence in our ecological perspective. In the real system underlying tumor growth, the treatment would have only the effect of moving the points on the state space, and do not altering the intrinsic dynamics. This important feature reveals that the possibility of cure, above all, concerns questions of stability and resilience. Figure 17 provides an illustration of this fact.

If tumor growth in a patient is described by some underlying dynamical system which does not have a cancer cure stable equilibrium, then a complete cure is not possible. This is what happens in case III, due to the weakness of the repair system, and it is illustrated in the right panel of Figure 18. After getting near this equilibrium through the treatment, the system moves back to the cancer equilibrium, even if it takes a long time. Thus, it is necessary a systemic change that alters the dynamics permanently. However, as also shown in Figure 17, even in this regime of instability of the cure equilibrium, treatment may lead to large time survival. Indeed, closer the system gets to the cure equilibrium,

longer it takes to tumor recurrence be observable. This fact is related with the large time necessary to pass through a saddle-point. In this case, an important feature will be the slope of the basin of attraction of the cancer equilibrium. A flat basin implicates in a large time to tumor recurrence.

On the other hand, even if the system has a cancer cure stable equilibrium, as in case II here, the treatment may be ineffective if the solution does not achieve the basin of attraction of the cure equilibrium. It is the case of simulation with $n = 4$ in case II, shown in Figure 17, left panel. In other words: a necessary condition to a treatment be effective is that the underlying system must have a stable cancer cure equilibrium; and the sufficient condition for the treatment be effective is that the treatment must move the trajectory to the basin of attraction of this equilibrium (simulations with $n = 5, 6, 7$ in case II). Once it has been reached, the treatment can stops, since the own patient repair system will eliminate the reminiscent cancer cells, and move the trajectory in direction to the cure equilibrium. Thus, the resilience of cancer equilibrium plays an important role: if this equilibrium has a large and deep basin, and is located at a large distance from the basin boundary, then more doses, or more intense doses, will be necessary in order to make the treatment be effective. Further, it also suggests a mechanism through which two individuals with similar diagnosis and treatments may have different fates: some of those treatments which end very near the separatrix (simulation with $n = 5$ in Figure 17, left) may become ineffective due tostochastic fluctuations which can drive the system to the cancer basin again, while other may continue effective due to very small fluctuations. This indicates that truly effective treatments should drive the system to a safe distance from the boundary of the basin. This rationale also agrees with the fact that treatments which consist of single surgery or radiotherapy may be reinforced if followed by adjuvant treatment in order to preclude tumor relapse (95).

## 3.5 Resilience Analysis

The ecological point of view on cancer discussed above is illustrated through the stability landscape in Figure 18. Of course, this view oversimplifies the reality of cancer, since there are many intermediary stages in the disease progression, but it provides at least a theoretical framework which sheds some light on the understanding of begin and the end of the disease. The better view of this landscape is that where it is not static, but a shaking landscape, due to the stochastic disturbances occurring all the time both on parameters and on state variables (96). Also, some features discussed above may not be correctly represented in Figure 18, where one can easily think that the escape from the cancer cure equilibrium in case III, a saddle point, will be as fast as a ball falls from the top of the hill, which is indeed false.

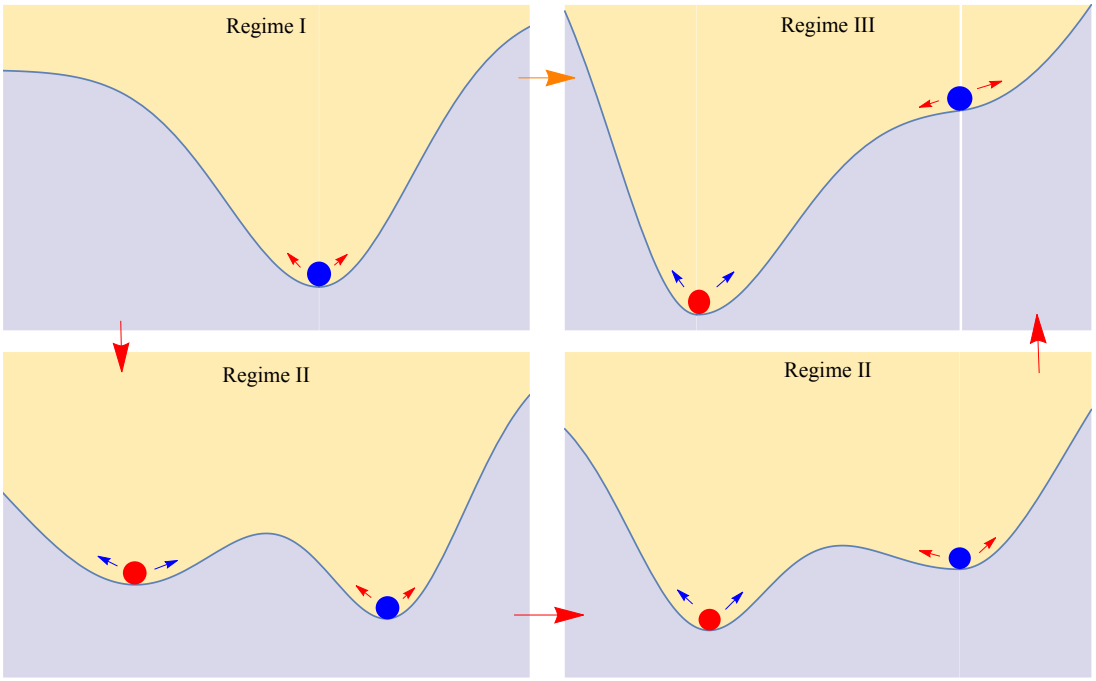


Figure 18 – An ecological view on cancer onset and treatment as the switching between two states, a cancer cure state (positions of blue balls) and a cancer state (positions of red balls). Perturbations on state variables are due to exposure to external carcinogenic factors and genetic instability (small red arrows), which favor the moving in the direction to the cancer state, or to chemotherapy, radiotherapy and surgery (small blue arrows), which move the system towards the cancer cure equilibrium. Perturbations in parameters (large arrows) lead to transitions between the three different regimes (I, II and III), create or destroy equilibria, or lead to changes of stability in these equilibria, what can makes impossible either the cure or the onset of cancer.

In the stability landscape in Figure 18, the creation of the cancer equilibrium and the loss of stability by the cancer cure equilibrium (large red and orange arrows) is achieved by the sequential acquiring of genetic alterations that improve the fitness of cancer cells (the hallmarks of cancer (19)), both by deregulating mechanisms of control or by creating mechanisms which favor cancer cell functions. The transition from I to III (large orange arrow) occurs only if tumor aggressiveness is low. Destruction of cancer equilibrium and creation of stability of the cancer cure equilibrium (opposite directions of large red and orange arrows) may be achieved by restoring the control systems (immunostimulation for example) or by limiting cancer cells functions (through anti-angiogenic treatments for example, which decrease the value of $K_A$ in theory). Finally, combination of small changes in parameters with perturbations on state variables also have a fundamental role, since the former can diminish the basin of attraction while the latter push the system to cross the basin boundary.

Let us analyze the effect of parameter changes on the resilience of stable equilibria of system (3.1), i.e., on size and shape of their basins of attraction. To perform

this analysis we briefly review the measurements which may be of importance when analyzing the resilience of an equilibrium (83, 81, 82, 80). As far as we know, very few papers have dealt with this kind of analysis for population dynamics models (83, 92, 93), although it is not an uncommon approach for systems modeling power grids (80). Recently, Mitra *et al.* applied these measures to the nonlinear pendulum, the daisy-world model, and to an one-dimensional model of desertification in Amazon forest (83). As far as we know, the methods provided here to calculate these measures are novel and more efficient than the currently used ones.

### 3.5.1 The latitude $L(P)$ of an equilibrium point

The *latitude* of an equilibrium point corresponds to the volume of the basin of attraction. It measures the resilience of that equilibrium with respect to state-space perturbations. Larger the latitude of an equilibrium, smaller is the chance that external or probabilistic events will drive the system outside the basin of attraction. For two dimensional systems, the latitude corresponds to the area of the basin of attraction. However, as it may happens that the basin of attraction has infinite area, it may be the case to consider its area inside a relevant bounded region. In the case of system (3.1), all trajectories remain in the box $B$ given in (3.6). This box could be this bounded region of interest. However, biological relevant perturbations of $P_2 = (N_2, A_2)$ will diminish the value of both coordinates, and relevant perturbations of $P_0 = (r_N/\mu_N, 0)$ will diminish the first coordinate and increase the second. Thus, we consider the smallest box $C$ which contains $P_0$ and $P_2$ as our bounded region of interest. It is clear that

$$C = [0, r_N/\mu_N] \times [0, A_2].$$

Thus, if $A(P)$ denotes the basin of attraction of $P$, then the latitude of $P$ in our case is defined by

$$L(P) = \frac{\text{Area } (A(P) \cap C)}{\text{Area } (C)}. \tag{3.8}$$

We divide by the total area of $C$ to obtain a non-dimensional quantity normalized between 0 and 1. In the case when system presents bistability (region II of parameters space) it is clear that

$$L(P_0) + L(P_2) = 1.$$

Extreme cases are regions I and III. In region I, when $P_0$ is globally stable, we have

$$L(P_0) = 1, \; L(P_2) = 0,$$

In region III, when $P_2$ is globally stable,

$$L(P_0) = 0, \; L(P_2) = 1.$$

We present a simple and efficient method to calculate $L(P)$ for two dimensional systems. It consists of two steps. The first step is to obtain the terms of a series expansion for a parametric representation of the stable manifold of saddle point in a two-dimensional system. The second step involves the use of Green's Theorem to transform the area of the basin of attraction in a line integral calculated along the stable manifold approximated in the first step. As far as we know it is a novel method and more efficient than those used in general, which consist in integrating the system in many points of the phase space, assigning each point to some basin of attraction, and then approximating the area. Throughout this section, we use the notation $\mathbb{R}^2 = \{X = (N, A);\ N, A \in \mathbb{R}\}$.

### Summary of first step

Let $X^*$ be a saddle point of the two-dimensional system

$$X' = F(X),\ X \in \mathbb{R}^2,$$

where $F$ is a $C^1$ vector field. In the vicinity of $X^*$, this system can be re-written as

$$X' = J(X - X^*) + G(X),$$

where $G(X) = O(||X - X^*||^2)$ and $J = F'(X^*)$ is the Jacobian matrix evaluated at $X^*$. Let $J = MKM^{-1}$ its Jordan decomposition, with $k_{11} < 0 < k_{22}$ (which are real since $X^*$ is a saddle-point). With the change of coordinates

$$U = M^{-1}(X - X^*),$$

the previous system becomes

$$U' = KU + R(U),$$

where $R(U) = M^{-1}G(X^* + MU) = O(||U||^2)$. This system can be written in coordinates $U = (u, v)$ as

$$u' = f(u, v),$$
$$v' = g(u, v).$$

The origin is a saddle point for this system. Its stable manifold is tangent to $v = 0$, and is locally the graph of a function $v = p(u)$. Substituting it into $v' = g(u, v)$ we obtain a nonlinear ODE for $p(u)$:

$$p'(u)f(u, p(u)) = g(u, p(u)).$$

Although this ODE cannot be solved in general, we can write a series expansion

$$p(u) = c_2u^2 + c_3u^3 + \cdots$$

and solve term by term, obtaining the coefficients $c_j$ recursively. For large $k$, the truncated polynomial $p_k(u) = c_2u^2 + \cdots + c_ku^k$ provides a good approximation of the stable manifold near the origin. Backing to the original coordinates,

$$s_k(u) = X^* + M\,(u, p_k(u))^T$$

is a parametric approximation of the stable manifold of $X^*$, for small $||u||$.

Summary of the second step

Now we explain how to calculate

$$L(P) = \frac{\text{Area } (A(P) \cap C)}{\text{Area } (C)} = \frac{\iint_{A(P)\cap C} dAdN}{\iint_C dAdN}. \tag{3.9}$$

The infinitesimal area element is denoted by $dAdN$. The integral in the denominator is easy to calculate in general; in our case $C$ is a rectangle. The difficult lies in calculating the integral in the numerator. However, it can be easily calculated by using the approximation of the stable manifold obtained in the first part and the Green's Theorem. Indeed, the boundary of the region $R = A(P) \cap C$ is formed by four curves, $\partial R = S \cup L_1 \cup L_2 \cup L_3$, where $S$ is the part of the stable manifold of $P_1$ which is contained in $C$, and $L_i$, $i = 1, 2, 3$, are line segments contained in the boundary of $C$. By Greens' Theorem, the integral can be written as

$$\iint_{A(P)\cap C} dAdN = \oint_{\partial R} NdA = \int_S NdA + \sum_{i=1}^{3} \int_{L_i} NdA,$$

with the correct orientation defined for these curves. The summation terms are easily computed, and a good approximation for the integral in $S$ is given by using the parametric approximation obtained in the first step. With this approach, we have a very good approximation of $L(P_i)$, $i = 1, 2$.

Let us comment on the applicability of this method. First of all, the method works when the boundary of the basin is formed by invariant manifolds of saddle points (97). If many saddle points lie in the boundary, then the first step needs to be applied to each point. Second, the bounded region $C$ must be such that this area is easily calculated. These first two requirements are very general (97). The last and most restrictive condition is that, for each saddle point on the boundary, the local approximation obtained in the first step must be a good approximation in all points inside $C$. The method fails when this requirement is not satisfied. In our case, for parameters values in Table 1, the approximation for the stable manifold of $P_1$ with 25 terms was obtained in a few seconds by *Mathematica*©, and provided a very good approximation for points inside $C$. The boundary of the basin in Figures 15, 17 and 19 was plotted with this approximation.

### 3.5.2 The precariousness $Pr(P)$ of an equilibrium point

Another important measure is the *precariousness* of an equilibrium point. Roughly speaking, it is defined as the the minimum perturbation required to drive the system to another basin of attraction. As a basin of attraction of interest may be large but the equilibrium may be located near the boundary, the precariousness is an important measure. It can be defined as

$$Pr(P) = \inf\{\text{dist}(P, X),\ X \in \partial A(P)\},$$

where $\partial U$ stands for the boundary of the set $U$, and $\text{dist}(X, Y)$ is the Euclidean distance. However, it may happens that perturbations of relevance may not occur in the direction where this minimum distance is achieved. Thus, one can consider

$$Pr(P) = \inf\{\text{dist}(P, X),\ X \in \partial A(P) \cap Z(P)\},$$

where $Z(P)$ is a specified set containing the relevant directions for perturbations from $P$. For system (3.1), all relevant perturbations of $P_2$ will diminish both coordinates. Thus we define

$$Pr(P_2) = \inf\{\text{dist}(P_2, X),\ X \in \partial A(P_2) \cap Z(P_2)\}, \quad Z(P_2) = [0, N_2] \times [0, A_2]. \tag{3.10}$$

Let us now consider which are the relevant perturbations of $P_0$. As new cancer cells may arise in the tissue, we may consider perturbations which increase the value of $A$. Thus, it would be the case to consider a single direction, $\vec{v}_1 = (0, 1)$. However, as cancer cells arise during mitosis, roughly speaking, the number of normal cells diminish by one when a cancer cell arise. Thus, it would be the case to consider the direction given by $\vec{v}_2 = (-1, 1)$. Therefore, we consider all directions between $\vec{v}_1$ and $\vec{v}_2$, what give us the set

$$Z(P_0) = \{(N, A) \in \mathbb{R}^2_+,\ N + A \geqslant r_N/\mu_N\}.$$

Thus, the precariousness of $P_0$ is given by

$$Pr(P_0) = \inf\{\text{dist}(P_0, X),\ X \in \partial A(P_0) \cap Z(P_0)\}. \tag{3.11}$$

An illustration of regions $Z(P_1)$ and $Z(P_2)$ can be seen in Figure 19.

In extreme cases I and III we do not have bistability, and $Pr(P)$ must be defined appropriately. In case III, when $P_2$ is globally stable, we define $Pr(P_2)$ as the tumor volume, $Pr(P_2) = A_2$, meaning that the removal of the entire tumor leads the system outside the basin of attraction of $P_2$. Indeed, this removal leads the system to the $N$-axis, which is the invariant manifold of $P_0$. Analogously, in case I, when $P_0$ is globally stable, we define $Pr(P_0) = N_0$. However, in this case the $A$-axis is not invariant, and another choice would be $Pr(P_0) = \infty$.

The result obtained in the first step of the previous section can be used to calculate the precariousness of an equilibrium straightforwardly. In our case, let be $s_k(u) = (s_k^1(u), s_k^2(u))$ the approximation for the stable manifold of $P_1$ obtained in that step. To calculate $Pr(P_0)$, for instance, we first must find the interval $I_0$ of values of $u$ such that $s_k(u) \in Z(P_0)$. By the definition of $Z(P_0)$, this can be done solving equations

$$s_k^{(1)}(u) = r_N/\mu_N$$

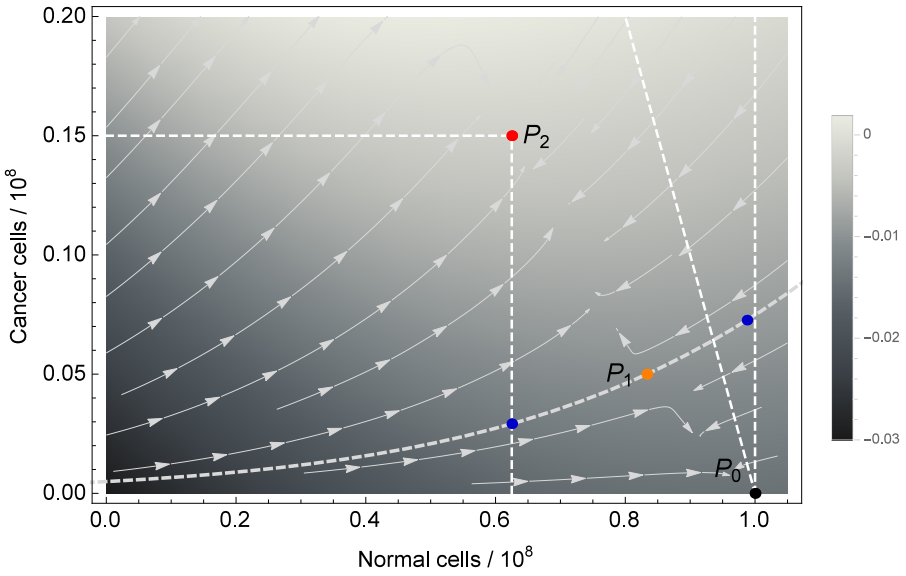


Figure 19 – Phase portrait of system (3.1). $Z(P_2)$ is the box with $P_2$ in one of the vertices. $Z(P_0)$ is the triangular region with $P_0$ in its vertices. The blue points are the nearest points of $P_0$ and $P_2$ inside regions $Z(P_0)$ and $Z(P_2)$ respectively. The intensity of color on background correspond to the value of the local resistance $R(N, A)$ defined in sub-section 3.5.3.

and

$$s_k^{(1)}(u) + s_k^{(2)}(u) = r_N/\mu_N$$

for $u$. The solutions are the extrema of interval $I_0$. With this, $Pr(P_0)$ is obtained by solving the minimization problem

$$\begin{aligned} \min \quad & ||s_n(u) - P_0|| \\ & u \in I_0 \end{aligned}$$

which can be easily solved. The precariousness of $P_2$ is calculated in an analogous way.

### 3.5.3 The resistance $R(P)$ of an equilibrium point

Finally, the third important measure concerning resilience of an equilibrium is termed as the *resistance* of this equilibrium. It refers to "the ease or difficulty of changing the system, related to the topology of the basin - deep basins of attraction indicate that greater forces or perturbations are required to change the current state of the system away from the attractor" (82). Thus, a resistant system will overcome perturbations rapidly, while a system with small resistance can be driven to a basin transition through a series of small perturbations that are not absorbed enough. This description concerns exactly the illustration provided by Figure 17. There, if $P_2$ was more resistant, more chemotherapeutic doses, or more intense doses, would be necessary to drive the system to the basin of attraction of $P_0$.

The task of characterizing the sizes and frequencies of perturbations that a basin of attraction can absorb is currently a research area (81). Recently, Mitra and others (83) proposed an approach to measure the resistance of a point in state-space to local pertubations using local Lyapunov expoents (98). Consider a $n$-dimensional system

$$X' = F(X),$$

where $F$ is a $C^1$ vector field. The *instantaneous Jacobian matrix at* $X$ is defined as

$$J_{dt}(X) = I_{n\times n} + J(X)dt$$

where $J(X)$ is the Jacobian at $X$ and $dt$ is a infinitesimal time. Let $\sigma_i(X)$, $i = 1, \cdots, n$ the square roots of the eigenvalues of the right Cauchy-Green tensor $J_{dt}(X)^T J_{dt}(X)$. The $\sigma_i(X)$'s are also the singular values of $J_{dt}(X)$. They measure the instantaneous stretching of the neighborhood of the trajectory at $X$. The $n$ local Lyapunov exponents evaluated at the state $X$ are defined as

$$\lambda_i(X) = \frac{1}{dt}\ln\left(\sigma_i(X)\right),\ \ i = 1, \cdots, n.$$

and measure the rate of stretching at $X$. Therefore, the local resistance $R(N, A)$ at the state $X = (N, A)$ may be defined as

$$R(X) = -\max\{\lambda_1(X),\ \lambda_2(X)\}, \tag{3.12}$$

where $\lambda_i$ are the local Lyapunov exponents. Thus, the resistance of an equilibrium point can be measured as

$$Res(P) = \frac{\iint_{A(P)\cap C} R(N, A)\, dNdA}{\iint_C R(N, A)\, dNdA}. \tag{3.13}$$

The division by the total resistance on $C$ is made to obtain a non-dimensional quantity normalized between 0 and 1.

For system (3.1), analytical expressions for $\lambda_i(X)$, $i = 1, 2$, at state $X = (N, A)$ can be calculated in *Mathematica*©. The density plot of $R(N, A)$ is showed in Figure 19. With these expressions, we can calculate integrals in (3.13). The unique concern is with respect to the region of integration in the first integral, $A(P) \cap C$. However, this integral can be calculated using the approximations for the stable manifold of $P_1$ obtained in the first step of 3.5.1.

### 3.5.4 Application of resilience analysis to system (3.1)

We analyze the behavior of above measures when parameters of system (3.1) vary. Figure 20 shows the results when $\beta_3$ varies while other parameters are kept constant, with $\beta_1 > \beta_1^{th}$, which corresponds to bifurcation diagram (ii) in Figure 16 (center), where a transition I-II-III is observed. Results when other parameters vary are similar (not shown here).

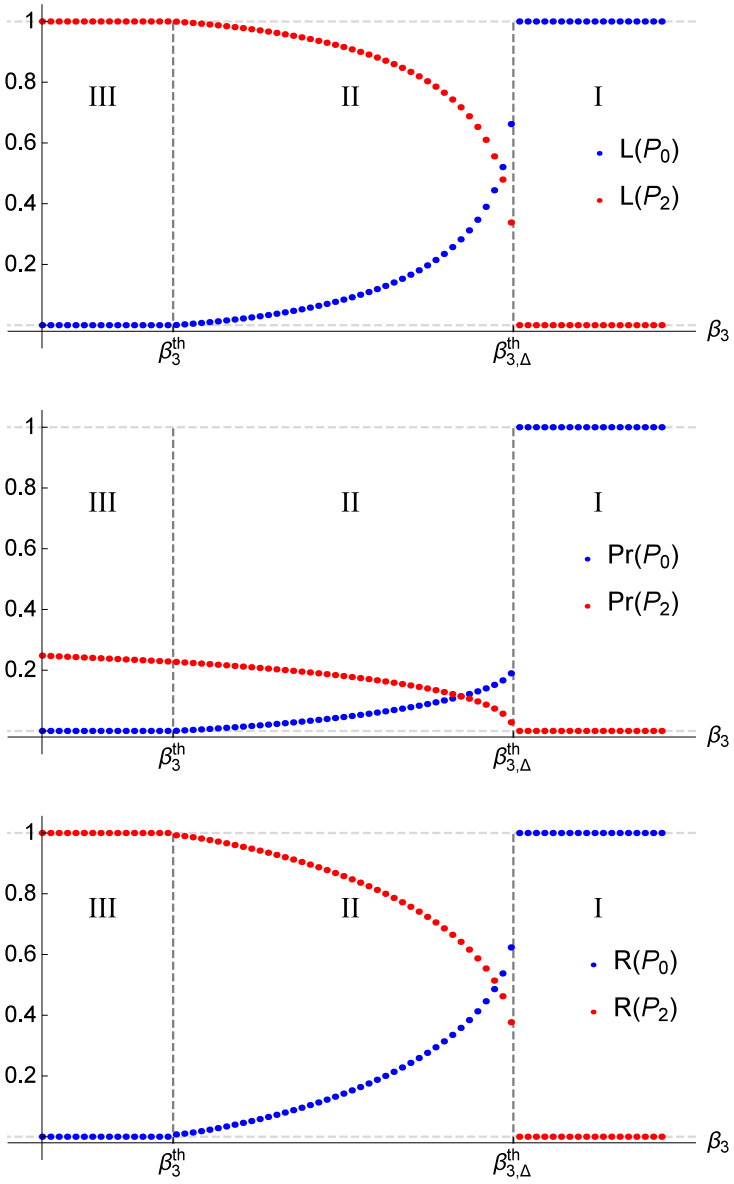


Figure 20 – Values of $L(P_i)$ (top), $Pr(P_i)$ (center) and $Res(P_i)$ (bottom), $i = 0, 2$, as $\beta_3$ varies, with $\beta_1 > \beta_1^{th}$, which corresponds to the bifurcation diagram (ii) in Figure 16 (top, right). As $\beta_3$ varies, we observe transitions between regimes III, II and I.

To discuss these results, we first consider the point of view of cancer onset and analyze the resilience measures of $P_0$. In region I, $P_0$ is globally stable and all these measures are equal to the unity. When $\beta_3$ becomes lesser than $\beta_{3,\Delta}^{th}$ and enters region II, equilibrium $P_0$ is no longer globally stable, and its resilience measures undergo an abrupt jump and decay rapid in a small strip near $\beta_{3,\Delta}^{th}$. The most notorious jump occurs with $Pr(P_0)$. For values in the midpoint between the two thresholds separating region II from regions I and III, the values of $Pr(P_0)$ and $L(P_0)$ are very small. These features are due to the up-concave shape of the graphs of $L(P_0)$, $Pr(P_0)$ and $Res(P_0)$, and indicate that in the bistable regime the healthy state $P_0$ is threaten by small disturbances which may

easily drive the system to the basin of attraction of $P_2$.

On the other hand, let us consider the point of view of treatment, and discuss the results concerning $P_2$. In regime III, this equilibrium is globally stable and $L(P_2)$, $Pr(P_2)$ and $Res(P_2)$ are equal to the unity. As $\beta_3$ becomes larger than $\beta_3^{th}$, these measures decay very slowly and are greater than the respective measures of $P_0$, until $\beta_3$ reaches the small strip near the next threshold, $\beta_{3,\Delta}^{th}$. Now, these features are due to the down-concave shape of the graphs, and implicate that $P_2$ is relatively protected against small perturbations.

By comparing these differences on the resilience measures of $P_0$ and $P_2$ we conclude that it is much more easy to drive the system outside the basin of attraction of the cure equilibrium $P_0$ when it loses its global stability, than driving the system out the basin of attraction of the cancer equilibrium $P_2$ when it reaches the bistable regime, unless the parameters get very near the next bifurcation threshold at which $P_2$ loses its stability. In other words, our analysis reveal that, in the bistable regime, although these are different phenomena, it is more likely to mutations or exposure to carcinogenic factors drive cancer onset than chemotherapy, surgery or radiotherapy lead to tumor regression.

## 3.6 Conclusion

In this paper, an ecological resilience framework to think of cancer as the alternance between two states is presented. This framework is based on the analysis of a simple ODE model for tumor growth considering the interaction with the host tissue. Despite the simplicity of the model, the approach adopted here gives interesting theoretical insights that shed some light on several relevant issues concerning cancer onset and treatment, and may help to improve the way we view cancer.

The model exhibits three regimes. These regimes are used to illustrate three different possibilities which may occur in clinical cases in general. The first regime corresponds to a healthy person where cancer onset is not possible since the cancer cure state is globally stable. The second regime corresponds to a person which can develop cancer if exposed to external carcinogenic factors, due to a partially corrupted repair system and/or a high aggressive phenotype of tumor cells. This regime presents bistability between the cancer and the cancer cure states. The third regime corresponds to a person in which cancer will arise due to intrinsic factors, i.e., the total corruption of repair systems. In this regime, the cancer state is globally stable.

Based on the general property that treatments are finite and, therefore, do not change the global dynamics in the phase space, we discuss the possibility of cure, which concerns stability and resilience questions above all. In the bistable regime the cure is possible if the treatment is able to drive the system to the basin of attraction of the cure

equilibrium. Tumor recurrence in this case is associated with treatments which are unable to cross the separatrix between the basins, or which do not end at a safe distance from the separatrix. In the third regime, the cure is not possible at all, since the repair system is intrinsically weak, but tumor recurrence may be delayed if the treatment is prolonged, because the system takes a long time to pass around the cure equilibrium, which is a saddle point. However, toxicity is not assessed in this model.

Besides perturbations on state variables, a view in the switching between these three regimes due to parameters changes in a slow time scale is discussed and the roles of the most important parameters in these transitions are assessed. Results indicate that only aggressive tumors may arise if intrinsic repair systems are not totally corrupted. However, in this scenario, these aggressive tumors also depends on external carcinogenic factors for arising.

Finally, we review the use of three different measures to assess the resilience of a stable equilibrium. We propose simple and efficient methods to calculate these measures. After applying this analysis to the model we conclude that in the bistable regime the cancer equilibrium has much more resilience than the healthy equilibrium, with respect to state variable perturbations as parameters changes.

This paper contributes to the current understanding on cancer by raising some issues in an ecological view, and also demonstrates how a 'resilience analysis' may be applied to population dynamics models in order to improve the understanding of nonlinear phenomena.

# 4 Minimal model for metronomic chemotherapy in avascular tumors: global dynamics and medical implications

*Abstract*. In the last years, a new era in the fight against cancer has began. An important example of new treatment strategy is metronomic chemotherapy, which consists in the frequent application of low doses of cytotoxic agents, with few or no interruptions. In this paper, we propose an ODE model for metronomic chemotherapy in avascular tumors, considering populations of normal and cancer cells, together with drug concentration, and taking in account the drug deactivation by cancer and normal cells, an interaction generally disregarded by other models. By using tools of competitive systems theory, a global analysis of this system is performed in the entire parameters space. Thresholds to the drug infusion rate are obtained for the system has a cancer cure equilibrium globally stable. The inclusion of normal cells allow us to measure the toxicity of a given treatment, and a condition is obtained which gives a way to compare the toxicities of metronomic chemotherapy in diverse tumor types. The results indicate that metronomic chemotherapy has a low toxicity in slow-growing tumors, highly competitive tumors and tumors with large carrying capacity.

*Keywords*: Cancer treatment; Toxicity; Global stability; Bifurcations; Competitive systems.

## 4.1 Introduction

In the last five decades of fight against cancer, the treatment which has prevailed was conventional chemotherapy (86). In this kind of treatment, citotoxic agents aiming to target proliferative cancer cells are administered according to the logic that "the more is better", i.e., the doses are the highest possible, in the very limit of a toxicity that does not threaten the patients life, and they are administered as a single or few number of doses, with long time intervals between them to allow the recovery of patients. This dosage regimen is named Maximum Tolerated Dose (MTD) (99). Despite the intense efforts, such as the development of a number of different chemotherapeutic agents and the performing of many clinical trails, a large number of patients are not cured or have a small survival rate (100, 1). One reason to these disappointing results is that in many times tumor cells have developed, or already had, resistance to the chemotherapeutics (acquired and intrinsic resistances). Further, the side effects of conventional chemotherapy, besides limiting the dosage and efficacy of these treatments, have a high price to the health of the patient,

since the cytotoxic activity of such drugs also harms other rapidly regenerating tissues in the human body, like hair-follicle cells, gut mucosa and bone marrow. Finally, currently there is no consensus of what would be the optimal protocol, i.e., the dose intensities and intervals which would give the best response with the lowest toxicity, and many clinical trials are done aiming to improve these outcomes (86, 101).

Therefore, new approaches are necessary, both with respect to treatment strategies (changing the standard protocols), as well as to new therapeutic targets (anti-angiogenic treatments, imunostimulation, and oncolytic virus therapy). Indeed, in the last years, a new era in the fight against cancer already has began and many strategies and therapeutic targets have come as an alternative to traditional chemotherapy, fueled mainly by biochemical deciphering of molecular and cellular interactions involved in the tumor microenvironment (1). In the near future, one can expect that personalized treatments based on individual factors of each patient, by combining several medicines and targets, will come into action (17, 1).

A relatively new therapy is known as metronomic chemotherapy (102, 86, 101). Motivated by the challenge to circumvent acquired drug resistance, and taking advantage of cytotoxic effects of conventional chemotherapeutics, Kerbel suggested in 1991 that low doses of these drugs could have a potential anti-angiogenic effect, because many of those endothelial cells that form the tumor vasculature are immature and are in constant proliferative state (103). Thus, the therapeutic target would become tumor vasculature instead tumor cells. Due to the genetic stability of normal endothelial cells, in contrast with the high genetic instability of cancer cells, this treatment would not face drug resistance. Besides, it would bring almost none side effect, since the low doses would harm only the immature tumor vasculature, because the other endothelial cells on the body are mature and do not proliferate like the immature ones (103).

A few years later, experiments with mouse showed that tumors which exhibited drug resistance when conventional MTD treatment was administered, responded well to low and frequent doses. These and many other studies have been changing the paradigm that MTD is the best way of chemotherapy administration (101). Thus, the new therapies would not preclude the use of standard chemotherapeutics, but change the way we dose it. In 2000, Hanahan *et al.* created the term "metronomic therapy", which refers to the frequent application of low doses of chemotherapeutics, with small or none intervals between applications (102). In the past decade, phase II clinical trails have shown the efficacy and low toxicity of metronomic chemotherapy with different drugs in diverse tumor types, specially in refractory tumors or those which relapsed after conventional treatments. Combinations like MTD treatments followed by metronomic chemotherapy also improved the overall results in some types of cancer (101).

The rationales behind the good outcomes of metronomic therapy against MTD

therapies are largely based on interactions in the tumor microenviroment (101). First, as commented above, it has anti-angiogenic effects. Standard high doses of conventional chemotherapy kill the tumor immature vasculature, but the long breaks necessary to allow the patient to recover are also large enough to this vasculature repair itself and return to feed the tumor. Thus this effect is achieved only at low (which are enough to kill the dividing endothelial cells) and frequent doses. Moreover, by targeting these cells, metronomic therapy is also able to destroy drug-resistant cancer cells by starvation of nutrients or induction of hypoxia. Second, an increasing body of researches has shown that metronomic therapy has also important immuno-stimulatory properties. While the phenomena of tumor escape from immune-surveillance have been described as an emerging hallmark of cancer (19), recent studies have demonstrated that certain drugs administered in a metronomic schedule were able to restore immuno-surveilance through the inhibition of $T_{REG}$ cells, which in many cancers are responsible for inhibition of anti-tumor immune response.

Several papers have been dealing with mathematical modeling of traditional or metronomic chemotherapy (104, 105, 106, 107, 108, 109, 110, 111, 112, 113, 114, 115, 116). Many other papers deal with the task of obtaining the best treatment protocols, mainly based on application of optimal control theory (117, 118, 119, 120, 121, 122, 123, 50, 124, 125, 126, 127). Other works focus on drug resistance, by considering structured populations of tumor cells (128, 129).

In this paper we propose a minimal model for the effect of metronomic chemotherapy on cancer cells and host tissue. Our goal is to perform a detailed mathematical analysis and thus assess the role of each parameter in the dynamical behavior of the system and analyze the biological implications. We seek for biological conditions from which different outcomes may emerge, i.e., when metronomic therapy is able to eradicate the tumor, and when it leads only to tumor dormancy. Another question is how much the host tissue is affected by the toxicity of chemotherapeutics, and which are the critical parameters that control this toxicity. As our model does not focus on a specific cancer, these global results allow us to compare, from a theoretical point of view, the effectiveness and toxicity of metronomic chemotherapy on diverse tumor types, since the qualitative differences between various tumor types would correspond to different parameter values on parameter space.

Some models cited above explicitly consider the effects of chemotherapy in the tumor microenvironment, like tumor-immune response, angiogenic signaling, acid-mediated invasion, stem-cell sub-populations, etc. As commented before, some of these interactions are very important and connected with the efficacy of metronomic therapy. However, aiming to obtain the simplest possible model for which a detailed description of the parameter space can be obtained, we consider that the drug acts directly on cancer

cells and normal cells. As we will comment in the Conclusion Section, a second stage in this work can be the inclusion of dynamical equations for tumor mature and immature vasculature, immune cells like $T_{REG}$ and killer or effector cells, and their coupling with equations for the drug, cancer cells and normal cells.

The paper is structured as follows. In Section 4.2 the mathematical model and its hypotheses are presented. In Section 4.3, a summary of the mathematical results is presented. In Section 4.4, the biological implications are discussed. In Section 4.5, we give the final conclusions and discuss possible future directions. In Appendix 4.A we present the proofs and mathematical details.

## 4.2 Mathematical modeling

A model we propose considers the interactions among normal cells, cancer cells, and chemotherapeutic agent in a tissue of the human body. The model equations are the following:

$$\frac{dN}{dt} = r_N - \mu_N N - \beta_1 NA - \alpha_N \gamma_N DN, \tag{4.1a}$$

$$\frac{dA}{dt} = r_A A\left(1 - \frac{A}{K_A}\right) - \beta_3 NA - (\mu_A + \epsilon_A)A - \alpha_A \gamma_A DA, \tag{4.1b}$$

$$\frac{dD}{dt} = \nu - \gamma_A DA - \gamma_N DN - \tau D. \tag{4.1c}$$

Here $N$, $A$ and $D$ represent, respectively, the number of normal and cancer cells, and drug concentration. The hypotheses that led to these equations and the meaning of each parameter are discussed below.

A variety of growth laws can be used to describe cancer growth, such as Gompertzian, Malthusian, generalized logistic, etc., since they present a good agreement with real data of distinct tumor types (88). But, due its simplicity and analytical tractability, we consider a logistic growth to cancer cells, with a per capita growth rate $r_A$ and carrying support $K_A$. Cancer cells present a natural mortality rate $\mu_A$, and also an extra mortality rate $\epsilon_A$ due to apoptosis induced to control undesirable growth of mutant cells (59).

On the other hand, for normal cells, a distinct growth law consisting of a constant total reproduction rate $r_N$ is considered, together with a natural per capita mortality $\mu_N$. The reasons for that are the different characters of the growth of the normal cells at a certain tissue, compared with cancer cells. While the growth of cancer cells is similar to an embryonic tissue, with a small initial number of cells which can develop or not depending on a series of factors, the creation of new normal cells at a mature tissue is intended to replenish the old ones, in order to maintain a homeostatic state, which, in this model, is given by $r_N/\mu_N$. Furthermore, in general, this replenishment is performed by a few precursor cells, like stem cells, in a manner that the growth rate of normal cells is not

directly connected with the total cell population, as in the logistic case, but is a intrinsic property of the tissue.

The interaction between cancer and normal cells is given by terms $-\beta_1 NA$ and $-\beta_3 NA$. While these terms are commonly described as the competition between these cells, here, we adopt a point of view that they encompass, in a simplified fashion, a lot of other interaction phenomena between these cells. For example, the term $-\beta_1 NA$, besides accounting for the killing of normal cells by the lack of nutrients and oxygen gathered by cancer cells, can also describes the acid mediated killing of normal cells, due the acidity produced by the metabolism of cancer cells (63). On the other hand, the term $-\beta_3 NA$ can encompass phenomena such as the effect of death and inhibitor factors released by normal cells, and the immune response of the tissue to mutant cells, which is activated by the detection of cancer cells, and which is performed by lymphocytes and other cells. Thus, in this model, the normal cells population is thought of as a pool of many types of cells, which operate in conjunction to maintain the tissue integrity and normal functioning. In this manner, we will refer to $\beta_1$ as the aggressiveness of cancer cells, and $\beta_3$ as the tissue response to cancer cells.

Now, the hypotheses that lead to equation (4.1c) describing the drug pharmacokinetics and pharmacodynamics are presented. The drug has a clearance rate $\tau$. The drug absorption and deactivation rates by normal and cancer cells is described by mass action law terms with rates $\gamma_N$ and $\gamma_A$. Following the linear log-kill hypothesis (17), we suppose that the quantities of absorbed drug by normal and cancer cells, $\gamma_N ND$ and $\gamma_A AD$, kill these cells with rates $\alpha_N$ and $\alpha_A$, respectively. Finally, the parameter $\nu$ represents a constant infusion rate, and approximates a metronomic dosage, i.e., an almost continuous and long-term administration of the drug. Although many models of cancer treatment do not consider drug absorption and deactivation explicitly, we believe that it is an important fact to consider, since this phenomena contributes to decrease drug concentration as the time pass by.

## 4.3 Main Results

In this section, we state the results of mathematical analysis of system (4.1).

### 4.3.1 Subsystem without drug

Initially, in order to better understanding the effect of chemotherapy on system (4.1), it is important to analyze the behavior of this system without the drug, i.e., equations (4.1a-4.1b) with $D = 0$, which will be refereed as subsystem NA. This subsystem was analyzed in a previous paper (130, 87). Here we briefly present the results. Throughout

this paper, the parameter $l_A = r_A - \mu_A - \epsilon_A$ is assumed to be always positive, since cancer would die even with no interaction with normal cells if $l_A < 0$.

Subsystem NA, (4.1a-4.1b) with $D = 0$, has the following equilibrium points: the cancer cure equilibrium

$$P_0 = (N_0, A_0) = \left(\frac{r_N}{\mu_N}, 0\right), \tag{4.2}$$

and two cancer equilibria,

$$P_i = (N_i, A_i) = \left(\frac{r_N}{\mu_N + \beta_1 A_i}, A_i\right), \ i = 1, 2, \tag{4.3}$$

where $A_1 < A_2$ are the roots of a second degree polynomial equation in $A$

$$\beta_1 \frac{r_A}{K_A} A^2 + \left(\mu_N \frac{r_A}{K_A} - \beta_1 l_A\right) A + (r_N \beta_3 - l_A \mu_N) = 0. \tag{4.4}$$

This system exhibits one of the following three possible behaviors, depending on parameters:

1. If $\beta_3 > \beta_3^{th}$ and $\beta_1 < \beta_{1,\Delta}^{th}$: $P_1$ and $P_2$ are negative; $P_0$ is globally stable.
2. If $\beta_3 > \beta_3^{th}$ and $\beta_1 > \beta_{1,\Delta}^{th}$: $P_1$ and $P_2$ are positive; $P_0$ and $P_2$ are locally stable. The phase plane $NA$ is divided in two basins of attraction, and $P_1$ is the turning point dividing these basins.
3. If $\beta_3 < \beta_3^{th}$: $P_1$ is negative, and $P_2$ is positive and globally attracting for initial conditions with $A > 0$.

The thresholds which separate cases I, II and III are given by

$$\beta_3^{th} = \frac{\mu_N}{r_N} l_A, \qquad \beta_1^{th} = \frac{\mu_N r_A}{l_A K_A}, \qquad \text{and} \qquad \beta_{1,\Delta}^{th} = \beta_1^{th} + 2\eta + 2\sqrt{\eta(\beta_1^{th} + \eta)}, \tag{4.5}$$

where $\eta = \frac{r_A}{K_A} l_A^2 r_N (\beta_3 - \beta_3^{th})$. From now on, we will refer to these cases as I, II and III. The division of the parameter space $\beta_1 \times \beta_3$ into these three regions can be seen in Figure 21, together with representative phase portraits of subsystem NA in cases II and III.

These results implicate that there are three different regimens concerning tumor growth (130). The first region of parameter space corresponds to a healthy person where cancer onset is not possible. In the second, cancer can either develop or die, depending on initial conditions. In the third, a tumor will be formed from any initial number of cancer cells. From the point of view of treatment, it is needed only in cases II and III. Thus our analysis of system (4.1) will be restrict to these regions.

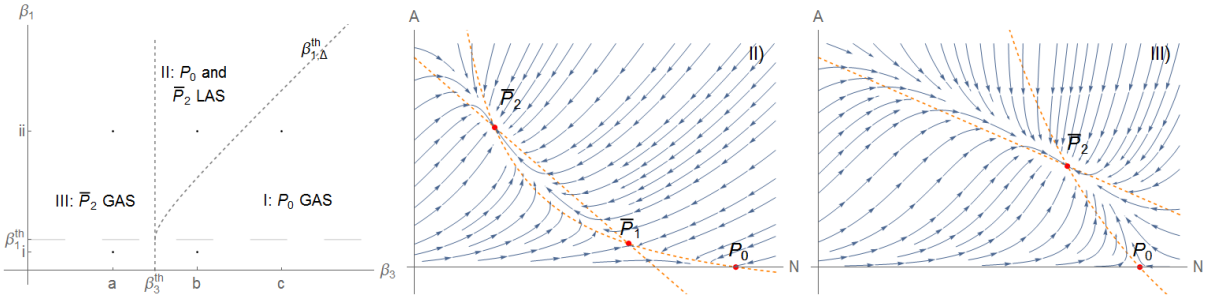


Figure 21 – Left: the plane $\beta_3 \times \beta_1$ divide into regions I, II and III. Center and right: the phase plane on cases II and III.

### 4.3.2 Trivial equilibrium

We now present the results of analysis of system (4.1). First, we analyze the trivial equilibrium and establishes conditions for its local stability and also global stability. It is easy to see that system (4.1) has an unique 'cancer cure equilibrium',

$$P_0^* = (N_0^*, 0, D_0^*) = \left(N_0^*, 0, \frac{\nu}{\gamma N_0^* + \tau}\right),$$

where $N = N_0^*$ is a root of the second degree equation

$$(r_N - \mu_N N)(\gamma_N N + \tau) = \alpha_N \gamma_N \nu N. \tag{4.6}$$

Graphing the two sides of (4.6), it is straightforward that it has one negative root, and one positive root inside the interval $[0, r_N/\mu_N]$. As $D_0^* > 0$ when $N_0^* > 0$, there is an unique biologically feasible cure equilibrium. We also note that the value of $N_0^*$ is decreasing with respect to $\nu$, and $N_0^*(\nu = 0) = N_0 = r_N/\mu_N$ and $N_0^*(\nu \to \infty) = 0$.

#### Local Stability

A straightforward calculation shows that two eigenvalues of the Jacobian matrix of system (4.1) evaluated at $P_0^*$, $\lambda_1$ and $\lambda_2$, corresponding to eigenvectors in the $ND$ plane, are the roots of

$$\lambda^2 + (N_0^* \gamma_N + \alpha_N \gamma_N D_0^* + \mu_N + \tau)\lambda + (\mu_N \gamma_N N_0^* + \tau \alpha_N \gamma_N D_0^* + \mu_N \tau) = 0.$$

Since all coefficients in this equation are positive, the Routh-Hurwitz criteria implies that $\lambda_1$ and $\lambda_2$ have negative real part. Thus, stability of $P_0^*$ depends only on the third eigenvalue, which corresponds to the $A$-direction, and is given by

$$\lambda_3 = l_A - \beta_3 N_0^* - \frac{\alpha_A \gamma_A \nu}{\gamma N_0^* + \tau}. \tag{4.7}$$

It is worth to note that in analysis of subsystem without drug, the condition to have the stability of the trivial equilibrium $P_0 = (N_0, 0)$ is

$$\beta_3 > \beta_3^{th} = \frac{l_A}{N_0}.$$

When we introduce drug, by the above expression for $\lambda_3$ we see that the cure equilibrium $P_0^*$ is stable if

$$\beta_3 > \frac{l_A}{N_0^*} - \frac{\alpha_A \gamma_A \nu}{N_0^*(\gamma N_0^* + \tau)}.$$

Thus, we see that the role of $\nu$ is to decrease the threshold $\beta_3^{th}$, enhancing the chances of $P_0^*$ being stable. However, as $N_0^*$ decreases with $\nu$, we see that increasing $\nu$ may also increase the new threshold. To fully understand this nonlinear interaction, we must analyze $\lambda_3$ in terms of $\nu$. Solving equation (4.6) explicitly for $N_0^*$ and replacing the result in (4.7), we obtain, after many algebra, that $\lambda_3$ can be written as

$$\lambda_3 = C_0 g(\nu) = C_0(a_g \nu^2 + b_g \nu + c_g), \tag{4.8}$$

where $C_0 > 0$. Details about these calculations and expressions for $C_0$, $a_g$, $b_g$ and $c_g$ are given in Appendix 4.A.1. Therefore, stability of $P_0^*$ depends whether the second degree polynomial $g(\nu)$ is negative. We denote by $\nu_1$ and $\nu_2$ the two roots of $g(\nu)$, and label them in the order $\nu_1 < \nu_2$ when they are real. In Appendix 4.A.1 we obtain that the leading coefficient $a_g$ is negative, and we show that $\nu_1$, $\nu_2$ and $P_0^*$ have the following behavior:

1. If $\beta_3 < \beta_3^{th}$ (region III) we have $\nu_1 < 0 < \nu_2$, and $P_0^*$ is locally stable if $\nu > \nu_2$.
2. If $\beta_3 > \beta_3^{th}$ (region II) and $\gamma_N > \gamma_N^{\#}$, then $0 < \nu_1 < \nu_2$, and $P_0^*$ is locally stable if $\nu < \nu_1$ or $\nu > \nu_2$.
3. If $\beta_3 > \beta_3^{th}$ (region II) and $\gamma_N < \gamma_N^{\#}$, then $\nu_1, \nu_2$ are complex conjugate or negative and $P_0^*$ is locally stable for all $\nu \geqslant 0$.

Expressions for $\nu_1$, $\nu_2$ and $\gamma_N^{\#}$ are given in Section 4.A. Figure 22 shows the surfaces $\nu_1$ and $\nu_2$ in parameter space $\gamma_N \times \beta_3 \times \nu$. In particular, if $\nu > \nu_2$, then $P_0^*$ is locally stable in cases II and III. Thus, $\nu_2$ is the minimal infusion rate for the constant treatment to be effective. However, $\nu > \nu_2$ does not guarantee that $P_0^*$ is globally stable, since nontrivial equilibria may exist and be stable.

#### 4.3.2.1 Global Stability

Now, we proof the following result concerning global stability of $P_0^*$.

**Teorema 4.1.** *If system (4.1) has no other non-negative equilibria, then $P_0^*$ is globally stable.*

*Proof.* Initially, we prove the boundedness of solutions of system (4.1). From (4.1a) we obtain $(dN/dt) \leqslant r_N - \mu_N N$. By comparison principles (131), it follows that $N(t) \leqslant r_N/\mu_N$ when $t \to \infty$. An analogous reasoning applied to (4.1b) and (4.1c) gives the upper bounds

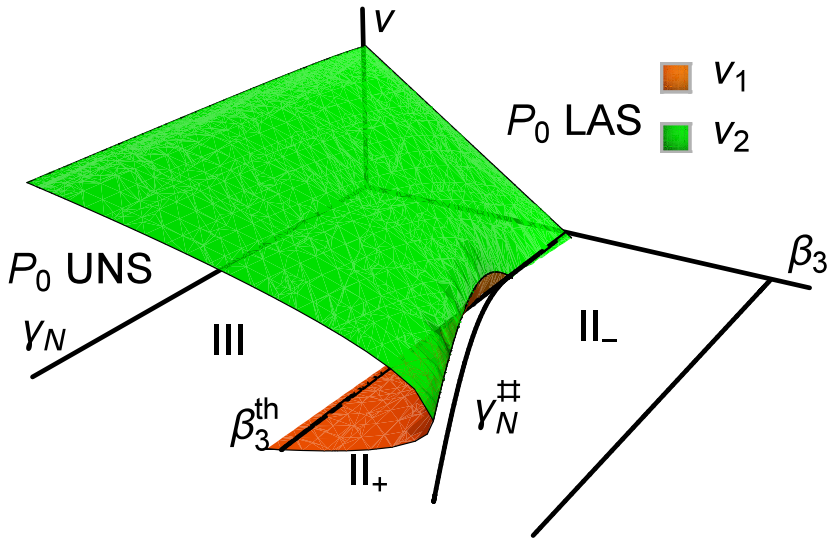


Figure 22 – Surfaces $\nu = \nu_1$ (orange) and $\nu = \nu_2$ (green) as functions of $\gamma_N$ and $\beta_3$. $P_0^*$ is locally stable outside the region delimited by $\nu_1$ and $\nu_2$, and is unstable inside this region.

$A(t) \leqslant (l_A K_A)/r_A$ and $D(t) \leqslant \nu/\tau$ when $t \to \infty$. Substitution of these bounds in (4.1a), give us

$$\frac{dN}{dt} \geqslant r_N - \mu_N N - \beta_1 \frac{l_A}{r_A} K_A N - \alpha_N \gamma_N \frac{\nu}{\tau} N$$

for large $t$. Again by comparison principles, we obtain, for large $t$,

$$N(t) \geqslant \frac{r_N}{\mu_N + \beta_1 \frac{l_A K_A}{r_A} + \alpha_N \gamma_N \frac{\nu}{\tau}}.$$

In the same way, using the upper bounds for $N(t)$ and $A(t)$ in (4.1c) implies

$$D(t) \geqslant \frac{\nu}{\tau + \gamma_N \frac{r_N}{\mu_N} + \gamma_A \frac{l_A K_A}{r_A}} \quad \text{for large } t.$$

Thus, all trajectories $(N, A, D)$ of system (4.1) remain in the box

$$Z = \left[ \frac{r_N}{\mu_N + \beta_1 \frac{l_A}{r_A} K_A + \alpha_N \gamma_N \frac{\nu}{\tau}}, \frac{r_N}{\mu_N} \right] \times \left[ 0, \frac{l_A}{r_A} K_A \right] \times \left[ \frac{\nu}{\tau + \gamma_N \frac{r_N}{\mu_N} + \gamma_A \frac{l_A}{r_A} K_A}, \frac{\nu}{\tau} \right] \tag{4.9}$$

for large $t$.

Now, we claim that the $\omega$-limit sets of all trajectories are equilibria or periodic orbits contained in $Z$. This statement follows from a straightforward application of the Poincaré-Bendixon Theorem for Competitive Systems in $\mathbb{R}^3$. Theorem 4.1, p. 41 of (132) states that a compact limit set of a competitive system in $\mathbb{R}^3$ that contain no equilibrium points is a periodic orbit. Since all off-diagonal entries of the Jacobian matrix of system (4.1) are non-positive for all points $(N, A, D)$ with non-negative coordinates, it follows that this system is competitive in $\mathbb{R}^3_+$ (see (132), p. 34), thus the result holds.

Therefore, to establishing global stability of $P_0^*$, it remains to show that system (4.1) has no nontrivial periodic orbits under the hypothesis that no other equilibrium is positive. Suppose, by contradiction, that system (4.1) has a nontrivial periodic orbit $\Gamma$. Then, $\Gamma \subset Z$. Suppose that $\Gamma$ touches the face $A = 0$ of $Z$. Since this face is invariant by system (4.1), $\Gamma$ would be entirely contained in this face. In this case, we know from index theory that there would be at least one equilibrium point in the region surrounded by $\Gamma$ (71). Since there are no other non-negative equilibria than $P_0^*$, and since $P_0^*$ is in the very edge of $Z$ and thus cannot be this equilibrium sorrounded by $\Gamma$, it follows that $\Gamma$ does not touches the face $A = 0$ of $Z$. Thus, if $W$ is the smallest box containing $\Gamma$, then $A > 0$ for all points $(N, A, D) \in W$ and $W \subset Z$. As system (4.1) is competitive in $\mathbb{R}^3_+$, it follows from Proposition 4.3, p. 44 of (132) that $W$ contains an equilibrium point. It is a contradiction, since $P_0^*$ is the unique positive equilibrium point and $P_0^* \notin W$. Thus, such a nontrivial periodic orbit $\Gamma$ cannot exists. Therefore, all trajectories must converge to an equilibrium point, which must be $P_0^*$. □

Note that we didn't have supposed that $\nu > \nu_2$, which is the condition for $P_0^*$ being locally stable. The unique hypothesis was that there were no other non-negative equilibria. Therefore, we can expect that $\nu > \nu_2$ is a necessary condition to have no other non-negative equilibria.

### 4.3.3 Nontrivial equilibria

We pass now to study the nontrivial equilibria of system (4.1). Calculations in Appendix 4.A.2 show that there are up to four nontrivial equilibria

$$P_i^* = (N_i^*, A_i^*, D_i^*) = \left( N_i^*, \frac{p(N_i^*)}{dN_i^*}, \frac{q(N_i^*)}{\alpha_A \gamma_A d N} \right), \ i = 1, 2, 3, 4, \tag{4.10}$$

where $N = N_i^*$ is a root of the fourth degree equation

$$q(N)r(N) = h(N), \tag{4.11}$$

and

$$p(N) = \kappa N(l_A - \beta_3 N) - (r_N - \mu_N N), \tag{4.12}$$

$$q(N) = \frac{r_A}{K_A}(r_N - \mu_N N) - \beta_1 N(l_A - \beta_3 N), \tag{4.13}$$

$$r(N) = dN(\gamma_N N + \tau) + \gamma_A p(N), \tag{4.14}$$

$$h(N) = \alpha_A \gamma_A \nu d^2 N^2, \tag{4.15}$$

$$d = \frac{r_A}{K_A}\frac{\alpha_N \gamma_N}{\alpha_A \gamma_A} - \beta_1. \tag{4.16}$$

Our analysis of these nontrivial equilibria is based on the fact that two nontrivial equilibria of system (4.1) are 'perturbations' of equilibria $P_1$ and $P_2$ of subsystem without

drug. To see this, note that when $\nu = 0$, we have $h(N) \equiv 0$, and then, the roots of (4.11) are the roots of $q(N)$ and $r(N)$. We claim that the roots of $q(N)$ are the $N$-coordinates of equilibria $P_i = (N_i, A_i)$, $i = 1, 2$, of subsystem without drug. In fact, remember that $A = A_i$ is a root of (4.4), and $N_i = r_N/(\mu_N + \beta_1 A_i)$. Writing $A_i$ in terms of $N_i$, $A_i = (r_N - \mu_N N_i)/\beta_1 N_i$, and substituting in (4.4), we obtain

$$\frac{r_N}{\beta_1 N_i^2} q(N_i) = 0, \ i = 1, 2. \tag{4.17}$$

Thus, the roots of $q(N)$ are $N_1$ and $N_2$. Now, substituting these roots in expressions of $A_i^*$ and $D_i^*$, we conclude that $A_i^* = A_i$ and $D_i^* = 0$, $i = 1, 2$, when $\nu = 0$. Therefore, when $\nu = 0$, two nontrivial equilibria $P_i^*$ coincide with the nontrivial equilibria of subsystem without drug. We label them as $P_1^* = P_1$ and $P_2^* = P_2$. As $\nu > 0$ increases, $h(N)$ increases while $q(N)r(N)$ is kept constant. Thus, the original roots move and possible enter or leave the feasibility interval or collide one with another. Therefore, our strategy was to track the behaviors of intersections of $q(N)r(N)$ and $h(N)$ as $\nu$ increases starting from $\nu = 0$. With this approach, we analyzed the existence of nontrivial equilibria $P_i^*$ in the entire parameter space. Details are given in Appendix 4.A.

We also analyzed the stability of these equilibria. Under the hypothesis that a Hopf bifurcation does not occurs with $P_2^*$, we characterized the number of nontrivial equilibria and their stability in the entire parameter space. Extensive numerical analysis have shown that this behavior is general and we believe that indeed no Hopf bifurcation occurs, although we were unable to prove it. Results are presented in next subsection.

### 4.3.4 Global analysis

The results of analysis of system (4.1) reveal that the three regimes of parameters presented by subsystem without drug (regions I, II and III) are somehow reproduced also in the parameter space of system (4.1): there are three regions in parameter space, which we call A, B and C, with the following behavior. In region A, we have no nontrivial equilibrium and $P_0^*$ is globally stable. In region B, the positive nontrivial equilibrium are $P_1^*$ and $P_2^*$; $P_0^*$ and $P_2^*$ are locally stable and their basins of attraction are separated by the two-dimensional invariant manifold of $P_1^*$. In region C, the unique positive nontrivial equilibrium is $P_2^*$, and it is globally stable.

Representative phase portraits of system (4.1) in each of cases A, B and C, are presented in Figure 23. We observe the occurrence of two distinct time scales. In a fast time scale, the value of $D$ changes rapidly, while $N$ and $A$ remain almost constant, and the solutions approach the surface defined by $dD/dt = 0$ (green surface). After $D$ attaining this quasi steady-state value, solutions move on this surface and converge to equilibrium on a slow time scale.

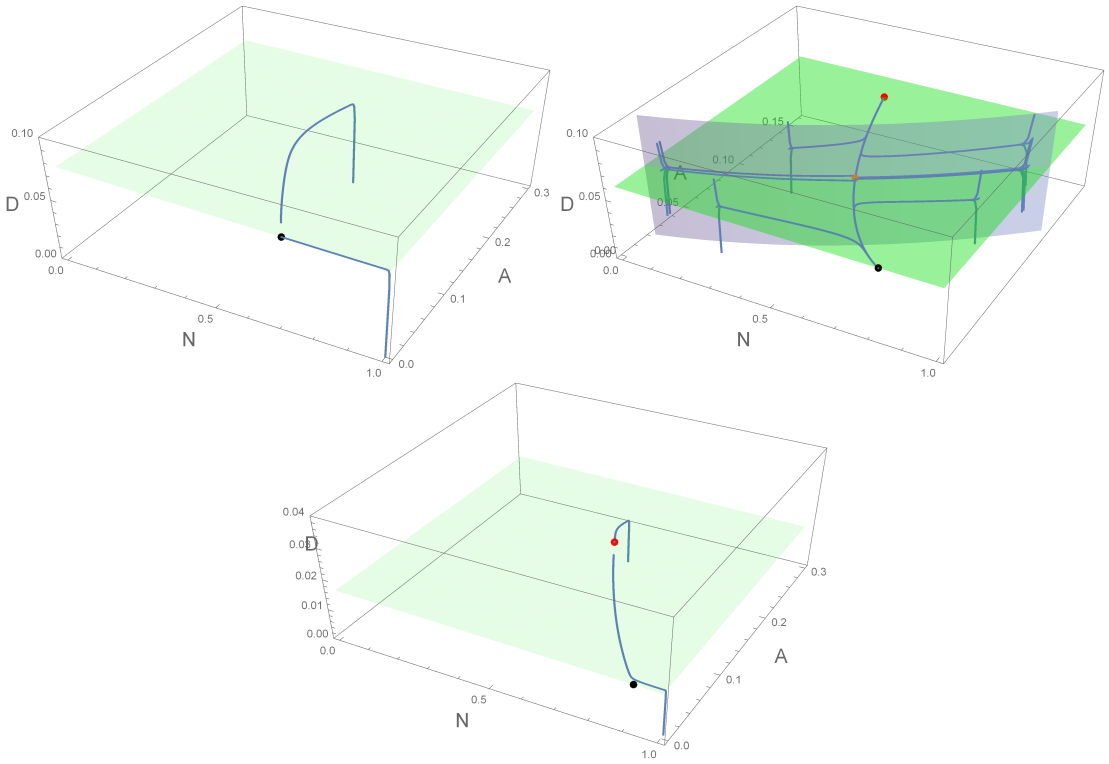


Figure 23 – Phase portraits of system (4.1) in cases A (top left), B (top right) and C (bottom). Equilibria $P_0^*$, $P_1^*$ and $P_2^*$ are represented respectively by black, red and orange points. The green surface represents surface $dD/dt = 0$. The purple surface in case B is the stable manifold of $P_1^*$.

The division of regions II and III of parameters space into regions A, B and C is showed in Figure 24. The curves which separate these regions are defined by the thresholds $\nu_1$ and $\nu_2$, which are values for which a transcritical bifurcation occurs between $P_0^*$ and some $P_i^*$, $i = 1$ or 2 (remember that $P_0^*$ has a zero eigenvalue when $\nu = \nu_i$), and by a third threshold $\nu_*$ which is a value for a saddle-node bifurcation between $P_1^*$ and $P_2^*$. Proofs and details are given in Appendix 4.A.

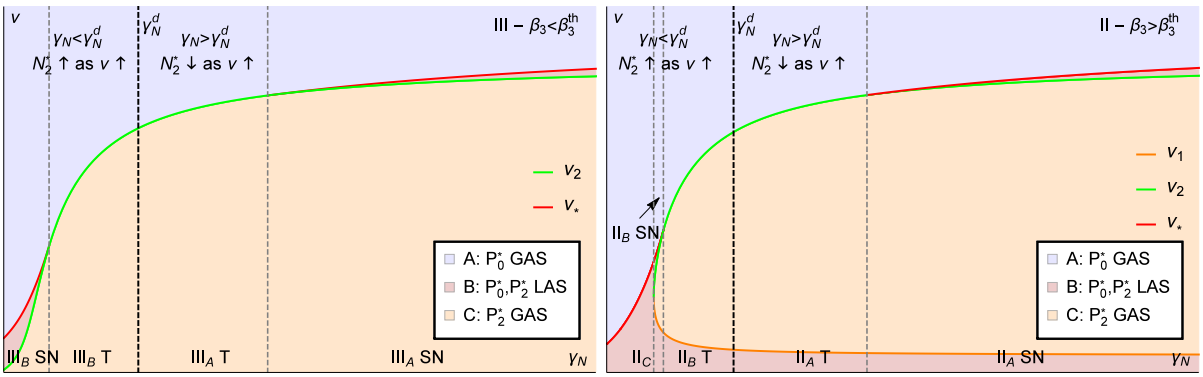


Figure 24 – On left, region III of parameter space divided in sub-regions A, B and C. On right, region II of parameter space divided in regions A, B and C.

In our analysis of the behavior of nontrivial equilibria, an important condition arose which have implications on the toxicity of the treatment. We proved that the value of $N_2^*$ is strictly increasing with respect to $\nu$ if

$$r_A\gamma_N\alpha_N < K_A\beta_1\gamma_A\alpha_A, \tag{4.18}$$

and is strictly decreasing otherwise. This condition is equivalent to

$$\gamma_N < \gamma_N^d = K_A\beta_1\alpha_A\gamma_A/r_A\alpha_N,$$

see Figure 24. This condition will have implications on the toxicity of metronomic chemotherapy, as will be commented in next Section. The behavior of nontrivial equilibria $P_i^*$ when $\nu$ increases starting from zero, in the case where this condition is satisfied and in the case it is not, is showed in Figure 25.

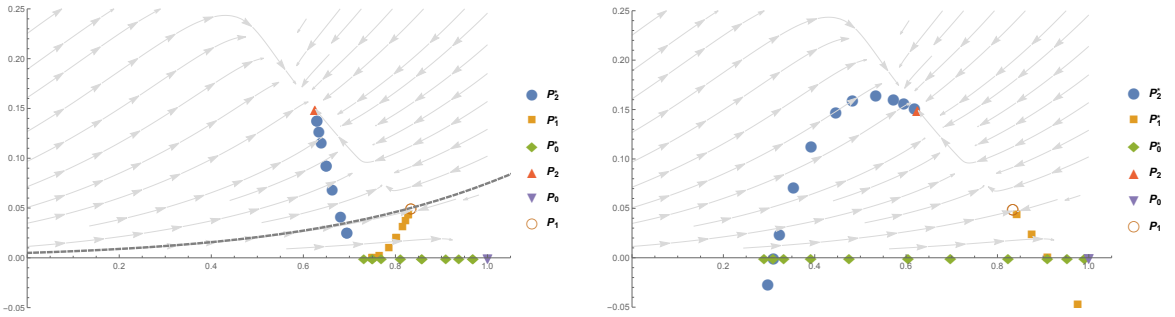


Figure 25 – These graphs show the behavior of projection nontrivial equilibria $P_1^*$ and $P_2^*$ on the $N \times A$ plane, as $\nu$ increases starting from zero. On left, the case when condition (4.18) is satisfied, and $N_2^*$ increases as $\nu$ increases. On right, this condition is not satisfied, and $N_2^*$ decreases as $\nu$ increases. These two cases correspond to diagrams ($\text{II}_A$ T) and ($\text{II}_B$ T) in Figure 26.

Our analysis also reveal that are nine qualitative distinct bifurcation diagrams of equilibria as $\nu$ varies. Each of them correspond to a vertical strip on Figure 24 (four in Region III, and five in Region II). These bifurcation diagrams are shown in Figure 26.

Finally, in Figure 27, we present how the introduction of a infusion rate $\nu > 0$ modifies the thresholds separating regions I, II and III. Compare Figures 21 and 27.

## 4.4 Discussion

Let us discuss the biological implications of the findings. Hypothetically, the scenario is the following. Before tumor detection and treatment, subsystem NA is 'running'.

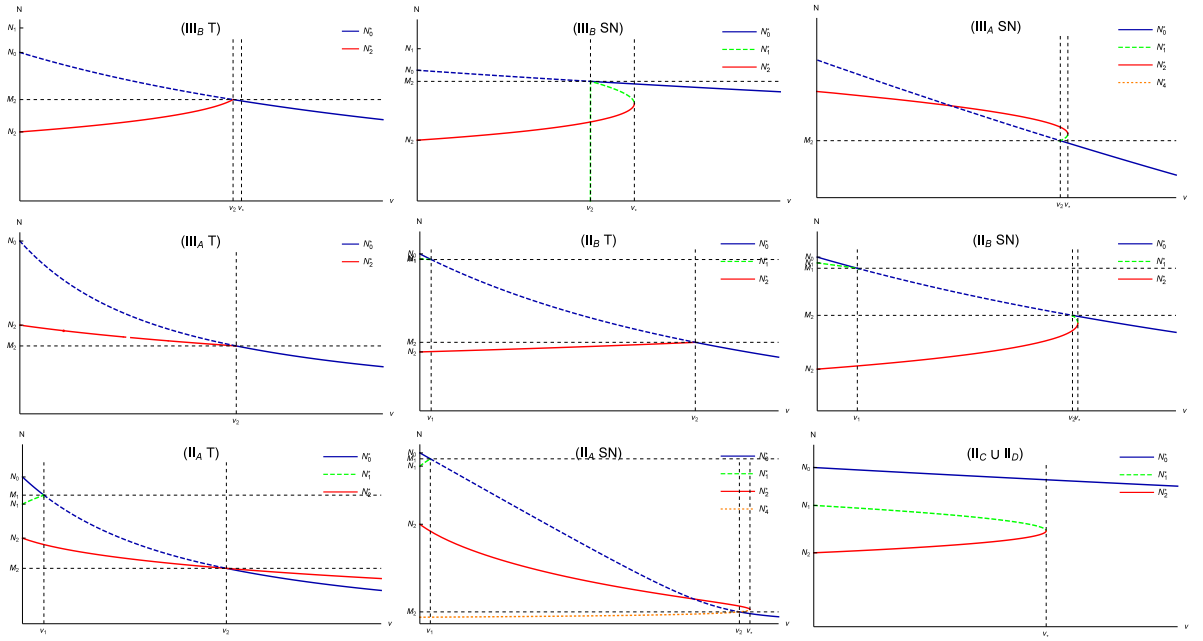


Figure 26 – Bifurcation diagrams showing behavior of coordinates $N_i^*$ of equilibrium $P_i^*$, $i = 0, 1, 2, 3, 4, 5$, of system (4.1) when $\nu$ varies. Continuous plot corresponds to stable equilibria, and dashed plot corresponds to unstable equilibria. All of these diagrams correspond to take vertical sections $\gamma_N = cte$ on the planes $\gamma_N \times \nu$ in Figure 24 (one section in each vertical strip showed in Figure 24). The label in each panel here indicates the corresponding region where the vertical section is made in Figure 24. For regions with sub-index 'A', the value of $N_2^*$ is decreasing with $\nu$ (condition (4.18) is satisfied). For regions with sub-index 'B', the value of $N_2^*$ is decreasing with $\nu$ (condition (4.18) is not satisfied). For regions with label 'T', we have a transcritical bifurcation before $P_0^*$ becomes globally stable. For regions with label 'SN', we have a saddle bifurcation before $P_0^*$ becomes globally stable.

Due to some disruption in the mechanisms of intrinsic repair system, we are in regions II or III, where the cancer equilibrium $P_2$ is stable. In region III, a tumor grows for any initial number of cancer cells. In region II a tumor will growth provided the initial number of tumor cells is high enough; cancer onset in this case depend on factors as genetic instability and exposure to carcinogenic factors. In both cases, the tumor grows and system NA approaches equilibrium $P_2$. When the tumor is detected at some time, metronomic chemotherapy starts and equation (4.1c) is 'turned on'.

### Eficacy of metronomic chemotherapy and tumor relapse after treatment

In case III, where the stability of $P_0$ was lost, analysis of $P_0^*$ reveals that there is a minimal infusion rate $\nu = \nu_2$ which must be surpassed in order to the treatment be effective, i.e., $\nu > \nu_2$ gives back the stability to the cancer free equilibrium (now a cure equilibrium) $P_0^*$. In some parameters regions, those labeled with T in Figures 24 and 26, an infusion rate above $\nu_2$ is able to make the tumor completely regrets, since $P_0^*$ is globally

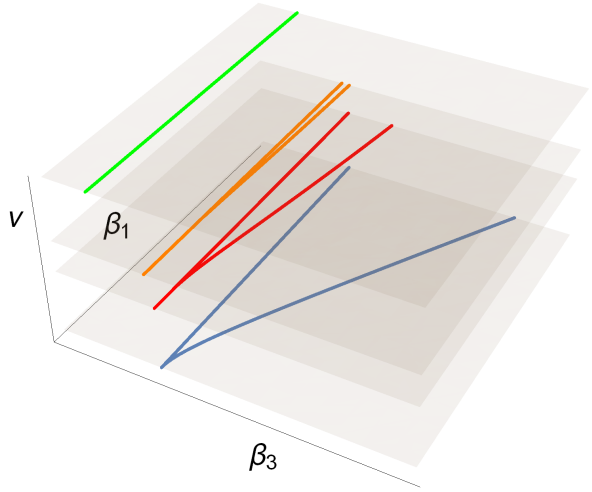


Figure 27 – Behavior of thresholds separating regions I, II and III in vertical sections $\beta_3 \times \beta_1$ as $\nu$ increases. The section with $\nu = 0$ corresponds to the plane showed in Figure 21 (left panel).

stable in these cases. On the other hand, in regions labeled with SN, if $\nu > \nu_2$ but $\nu < \nu_*$ the cancer equilibrium $P_2^*$ is stable together with $P_0^*$. Backward bifurcation diagrams occur in these cases, on the contrary to case T, where we have forward bifurcations (compare panels ($III_B$ T) and ($III_B$ SN) in Figure 26 for instance). Thus, in cases SN, metronomic therapy alone is not able to lead to tumor extinction at this level of infusion rate. There are two possibilites to achieve this goal. The first is to increasing the infusion rate until $\nu > \nu_*$, which makes $P_0^*$ globally stable. After a while, when system trajectory approaches this equilibrium, it is possible to reduce the infusion rate again to the interval $\nu_2 < \nu < \nu_*$. If this first approach of increasing $\nu$ is not possible due toxicity constraints, then the combination of metronomic chemotherapy with a procedure that decreases the initial tumor volume, like surgery or radiotherapy, may be effective, since this procedure will take the system to the basin of attraction of $P_0^*$. It is important to note that in all these cases, that tumor relapse will be observed if the treatment stops, since $P_0^* = P_0$ is unstable when $\nu = 0$ and solutions will back to $P_2$. However, if solutions get very near $P_0^*$ during the treatment phase, they will take a very long time to depart from $P_0$ and tumor relapse may be avoided for a large time.

A very similar behavior is observed in case II. The unique difference is that now the treatment can be 'turned off' after the tumor is no more detectable. This is because here the cancer free equilibrium $P_0$ is locally stable and a tumor has growth due initial conditions. However, even the tumor being undetectable, there is a risk that the number of cancer cells was high enough to the system be settled at the basin of attraction of $P_2$ when the treatment ceases. Thus, it is important that the treatment lasts the time enough to eliminate almost all cancer cells.

Summarizing, we have two kinds of cancer patients, corresponding to cases

II and III. In case II, the treatment can stops ($\nu = 0$) after tumor regression, but there is chance of relapse under much genomic instability or if treatment ceases before the tumor achieves a minimal volume. In case III, the treatment must continues indefinitely, since the disruption of the patient repair system is more severe than in case II. In order to avoid drug resistance (not modeled here) and other harmful outcomes of continued chemotherapy, it is necessary (but not necessarily possible) to change the intrinsic behavior of the repair system, through, for instance, immunostimulation (also not modeled here). However, tumor relapse may be delayed if the treatment is administered for a large time. This comparison of two kinds of patients leads suggests that those patients which presented tumor relapse after metronomic chemotherapy may be appointed to immunotherapies or return to metronomic chemotherapy if no side-effects nor drug resistance were observed.

### Toxicity

Now, we discuss the toxicity constraints of metronomic chemotherapy based on the results obtained. As the value of $N_0^*$ decreases with $\nu$, the minimal efficient infusion rate may not be possible to achieve in practice due to a high toxicity. However, condition (4.18) sheds some light in this issue, as shown in Figure 28. If this condition is satisfied, the tumor diminishes and the normal tissue recover as the treatment begins. It means that, besides eliminating the tumor the treatment also restores the normal tissue, bringing it to a healthier state than before. Thus, the thresholds $\nu_2$ or $\nu_*$ can be achieved with no side-effect. On the contrary, if condition 4.18 is not satisfied, then there is a decrease in the number of both tumor and normal cells (compare panels ($III_B$ T) and ($III_A$ T) in Figure 26 for instance). The treatment eliminates the tumor, but also brings together a toxicity that harm the normal tissue more than when it was damaged only by the presence of tumor cells. In this case, it is possible to maintain the tumor in a 'dormant state' (low, stable $A_2^*$), but with a poor state for the patient (low $N_2^*$), with $0 < \nu < \nu_2$. Thus, an analysis of what is worst need to be made.

Observing condition (4.18), we can examine tumor types were this low-toxicity may achieved more easily. We see that low values of $\gamma_N$ and $\alpha_N$ increase the chance of (4.18) be satisfied. It means that a low sensitivity of normal cells leads to a low toxicity. In the same manner, (4.18) is probably satisfied when the values $\gamma_A$ and $\alpha_A$ are high. Thus, a high sensitivity of tumor cells also leads to low toxicity. These two conditions are quite obvious, and point to the necessity of discovering high specific drugs. Let us examine the others. We see that low $r_A$ contributes to (4.18) being satisfied. This indicates that metronomic chemotherapy may have a lower toxicity when applied to slow-growing tumors. The same happens for aggressive tumors (those which cause high damage to tissue), since a high $\beta_1$ increases the chance of (4.18) being satisfied. Finally, we note that metronomic

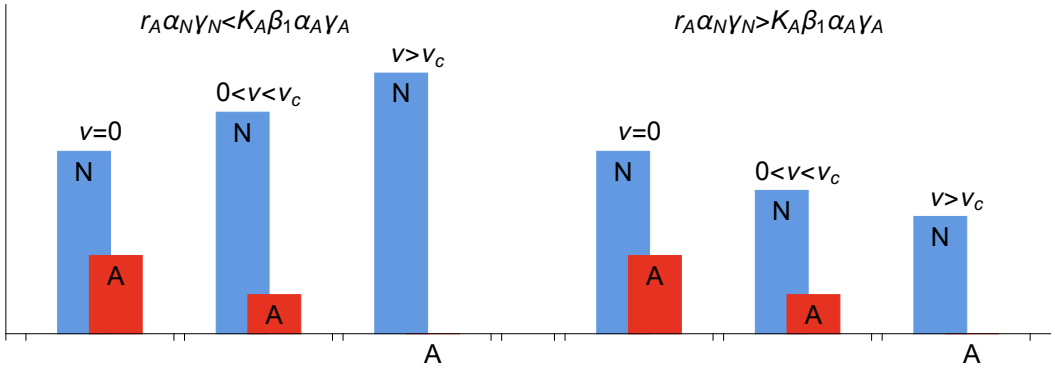


Figure 28 – This scheme shows the volumes of normal (N - blue) and cancer (A - red) cells for three different values of the infusion rate $\nu$ in cases when (4.18) is satisfied and not satisfied. The value $\nu_c = \max\{\nu_2, \nu_*\}$ is the threshold above which the cure equilibrium $P_0^*$ is globally stable (see Figure 24).

chemotherapy also may lead to low toxicity when applied to tumors with increased support capacity (high $K_A$).

## 4.5 Conclusion

In this paper we propose a minimal model for metronomic chemotherapy of an avascular tumor. The model is an ODE system which considers the populations of tumor cells and normal cells, together with the concentration of a chemotherapeutic agent. We perform a detailed mathematical analysis of this system and use the theory of competitive systems in $\mathbb{R}^3$ to establish global stability results.

Despite its simplicity, the model predicts interesting results. First, we prove that for all parameters values, there is a minimal value of the drug infusion rate above which the cancer cure equilibrium is globally stable. It can be achieved in two ways. In the first, as the drug infusion rate increases, the tumor volume decreases continuously and disappears when a threshold for the infusion rate is achieved (a transcritical bifurcation occurs in this case). In the second, the tumor decreases very slowly as the drug infusion rate increases, and does not disappears when the threshold of the previous case is surpassed. However, the cure equilibrium becomes stable, and a bistability regime emerges. As the infusion rate continues to increase, the tumor volume decreases slowly and sudden disappears when a second threshold is reached (we have a saddle-node bifurcation now). The differences among these two cases indicates the same infusion rate of metronomic chemotherapy may lead to tumor regretion in some patients, while, in others, procedures such as surgery or radiotherapy are needed before treatment, in order to decrease the initial tumor size.

Interesting, there are also two regimes with respect to the response of host tissue when the drug infusion rate changes. In the first, the number of normal cells decreases

as the drug infusion rate increases. On the other hand, in the other regime, the number of normal cells increases as the drug infusion rate increases. Thus, this second regimen clearly presents a better prognosis from the point of view of the health of the patient. We investigate the biological conditions underlying the existence of these two regimens. We concluded that the second regimen is more likely to happen in tumors with one or more of the following characteristics: slow-growing tumors, aggressive tumors (which cause high damage to normal cells), tumors with high carrying capacity, or tumors which are much more sensible to the drug than the normal cells. These conclusions can provide some insights to clinical oncologists by telling them which tumor types would respond better to metronomic chemotherapy, and which ones would require a more careful treatment.

In a recent work, Ledzewicz *et al.* proposed a minimal model for metronomic therapy considering interactions in the tumor microenvironment (106). They combined the model of angiogenic signalling of Hahnfeldt *et al.* with a model by Stepanova which consider the tumor inhibiting effects of tumor-immune system interactions (104, 133). However, their model considers drug kinetics only in the steady state, and does not take in account the drug deactivation or absorption by cells, nor its effect on normal cells, as was considered in our model. Finally, nor our model nor the model of Ledzwicz *et al.* accounts for the phenomena of immuno-surveilance regulated by $T_{REG}$ cells (91). Therefore, it would be very important to consider the dynamics of these cells explicitly and a possible extension of our work would be the adequate combination of our model with the one of Ledzwicz *et al*, in addition with the modeling of $T_{REG}$ cells dynamics.

## 4.A Proofs and mathematical details

In this Appendix, we present the proofs of results from Section 4.3.

### 4.A.1 Stability of trivial equilibrium

Solving equation (4.6) for $N_0^*$ and substituting the result in (4.7), we obtain

$$\lambda_3 = U - V = \frac{U^2 - V^2}{U + V},$$

where

$$U = l_A + \frac{\alpha_A \gamma_A \mu_N}{\alpha_N \gamma_N} + \left( \frac{\alpha_A \gamma_A}{2\alpha_N \gamma_N \tau} - \frac{\beta_3}{2\gamma_N \mu_N} \right) W, \quad V = \left( \frac{\alpha_A \gamma_A}{2\alpha_N \gamma_N \tau} + \frac{\beta_3}{2\gamma_N \mu_N} \right) \sqrt{Y},$$

$$W = \left( r_N \gamma_N - \alpha_N \gamma_N \nu - \mu_N \tau \right), \quad \text{and} \quad Y = W^2 + 4 r_N \gamma_N \mu_N \tau.$$

As $\sqrt{Y} \pm W > 0$, the denominator $U + V$ is positive. Therefore, the sign of $\lambda_3$ is the same of the numerator, which can be written as a second degree polynomial in $\nu$,

$$U^2 - V^2 = g(\nu) = a_g \nu^2 + b_g \nu + c_g, \tag{4.19}$$

with coefficients

$$
\begin{aligned}
a_g &= -\frac{\alpha_A\alpha_N\beta_3\gamma_A}{\mu_N\tau},\\
b_g &= \left(\beta_3-\beta_3^{th}\right)\left(\gamma_N-\gamma_N^s\right)\frac{\left(2r_N\alpha_A\gamma_A+\tau l_A\alpha_N\right)}{\gamma_N\mu_N\tau}+\left(\gamma_N-\gamma_N^m\right)\frac{l_A(r_N\alpha_A\gamma_A+\tau l_A\alpha_N)}{r_N\gamma_N\tau},\\
c_g &= \left(\beta_3^{th}-\beta_3\right)\frac{r_N}{\mu_N\alpha_N\gamma_N\tau}\left(r_N\alpha_A\gamma_A\gamma_N+\tau(l_A\alpha_N\gamma_N+\alpha_A\gamma_A\mu_N+\alpha_N\beta_3\tau)\right),
\end{aligned}
\tag{4.20}
$$

where

$$
\gamma_N^m=\frac{\alpha_A\gamma_A\mu_N}{l_A\alpha_N}\quad\text{and}\quad\gamma_N^s=\frac{\gamma_N^m}{1+2\dfrac{r_N\alpha_A\gamma_A}{\tau l_A\alpha_N}}<\gamma_N^m. \tag{4.21}
$$

This proofs equation (4.8), with $C_0=1/(U+V)$.

### Regions of interest by varying parameters

In order to study the signs of $g(\nu)$, we divide regions II and III in different sub-regions on the $\gamma_N\times\beta_3$ plane. These regions will also be useful for further analysis of the nontrivial equilibria. First, note that condition $\beta_1>\beta_{1,\Delta}^{th}$ for region II can be rewritten (see Figure 21, left panel) as

$$
\beta_3^{th}<\beta_3<\beta_{3,\Delta}^{th}\text{ and }\beta_1>\beta_1^{th}, \tag{4.22}
$$

where

$$
\beta_{3,\Delta}^{th}=\beta_3^{th}+\frac{K_A}{4\beta_1 r_A r_N}\left(\frac{\mu_N r_A}{K_A}-\beta_1 l_A\right)^2. \tag{4.23}
$$

Thus, the regions of interest for the mathematical analysis of system (4.1) are

$$
III=\{\beta_3<\beta_3^{th}\}\quad\text{and}\quad II=\{\beta_3^{th}<\beta_3<\beta_{3,\Delta}^{th},\ \beta_1>\beta_1^{th}\}. \tag{4.24}
$$

Now, we note that the discriminant $\Delta_g=b_g^2-4a_gc_g$ of $g(\nu)$ can be written in two ways:

$$
\Delta_g=4r_N\alpha_A\alpha_N\gamma_A\gamma_N\left(\beta_{3,\#}^{th}-\beta_3\right)\left(\frac{1}{\tau\kappa}+\frac{\beta_3}{\gamma_N\mu_N}\right)^2, \tag{4.25}
$$

and

$$
\Delta_g=\left(l_A\alpha_N\right)^2\left(\gamma_N-\gamma_N^{\%}\right)\left(\gamma_N-\gamma_N^{\#}\right)\left(\frac{1}{\tau\kappa}+\frac{\beta_3}{\gamma_N\mu_N}\right)^2, \tag{4.26}
$$

where,

$$
\beta_{3,\#}^{th}=\beta_3^{th}+\frac{\left(\kappa l_A-\mu_N\right)^2}{4\kappa r_N}\geqslant\beta_3^{th},\quad\kappa=\frac{\alpha_N\gamma_N}{\alpha_A\gamma_A} \tag{4.27}
$$

$$
\gamma_N^{\#}=\frac{\gamma_N^m}{\beta_3^{th}}\left(2\beta_3-\beta_3^{th}+\sqrt{\beta_3(\beta_3-\beta_3^{th})}\right), \tag{4.28}
$$

and

$$
\gamma_N^{\%}=\frac{\gamma_N^m}{\beta_3^{th}}\left(2\beta_3-\beta_3^{th}-\sqrt{\beta_3(\beta_3-\beta_3^{th})}\right). \tag{4.29}
$$

Let us obtain the intersection of curves $\beta_3 = \beta_{3,\Delta}^{th}$ and $\beta_3 = \beta_{3,\#}^{th}$ in the $\gamma_N \times \beta_3$ plane. Solving equation $\beta_{3,\Delta}^{th} = \beta_{3,\#}^{th}$ for $\gamma_N$, we have two solutions,

$$\gamma_N^d = \frac{K_A \beta_1 \alpha_A \gamma_A}{r_A \alpha_N}, \quad \text{and} \quad \gamma_N^e = \frac{r_A \mu_N^2 \alpha_A \gamma_A}{K_A l_A^2 \beta_1 \alpha_N}. \tag{4.30}$$

On the other hand, the intersection $\beta_{3,\#}^{th} = \beta_3^{th}$ occurs only at $\gamma_N = \gamma_N^m$. As $\beta_1 > \beta_1^{th}$ in region II, we have $\gamma_N^e < \gamma_N^m < \gamma_N^d$. Further, as $\beta_3^{th} < \beta_3 < \beta_{3,\Delta}^{th}$, from (4.25-4.29), it is possible to show that

$$\gamma_N^e < \gamma_N^{\%} < \gamma_N^m < \gamma_N^{\#} < \gamma_N^d \tag{4.31}$$

for parameters in Region II. Thus, we define the following sub-regions of regions II and III, in the $\gamma_N \times \beta_3$ plane:

$$\begin{aligned}
II_A &= \left\{\beta_1 > \beta_1^{th},\ \beta_3^{th} < \beta_3 < \beta_{3,\lambda}^{th},\ \gamma_N > \gamma_N^d\right\},\\
II_B &= \left\{\beta_1 > \beta_1^{th},\ \beta_3^{th} < \beta_3 < \beta_{3,\lambda}^{th},\ \gamma_N^{\#} < \gamma_N < \gamma_N^d\right\},\\
II_C &= \left\{\beta_1 > \beta_1^{th},\ \beta_3^{th} < \beta_3 < \beta_{3,\lambda}^{th},\ \gamma_N < \gamma_N^{\%}\right\},\\
II_D &= \left\{\beta_1 > \beta_1^{th},\ \beta_3^{th} < \beta_3 < \beta_{3,\lambda}^{th},\ \gamma_N^{\%} < \gamma_N < \gamma_N^{\#}\right\},\\
III_A &= \left\{\beta_3 < \beta_3^{th},\ \gamma_N > \gamma_N^d\right\},\\
III_B &= \left\{\beta_3 < \beta_3^{th},\ \gamma_N < \gamma_N^d\right\}.
\end{aligned} \tag{4.32}$$

These regions are shown in Figure 29. We now analyze the stability of $P_0^*$ in each of these regions.

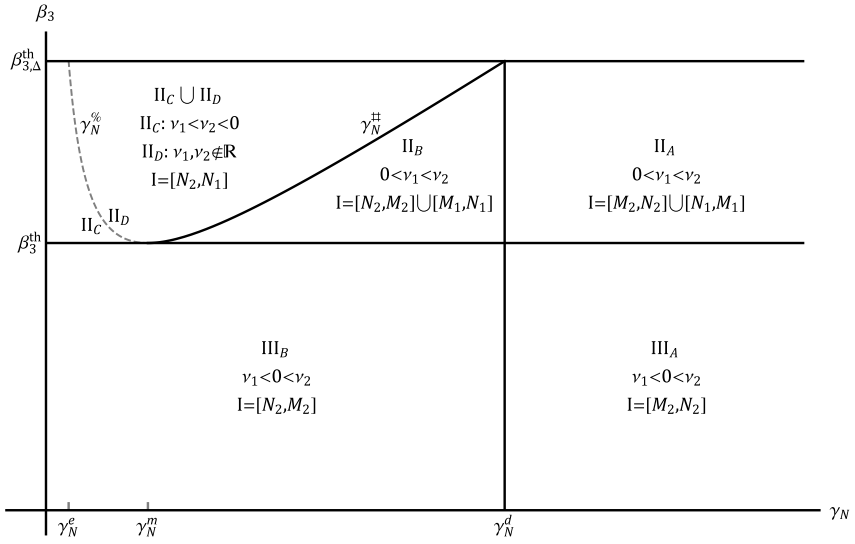


Figure 29 – The plane $\gamma_N \times \beta_3$ is divided in regions, and in each of them the feasibility interval $I$ for nontrivial equilibrium is given (see Appendix 4.A.2 below).

Region III: In both sub-regions $III_A$ and $III_B$ we have $c_g > 0$. As $a_g < 0$ it follows that $\nu_1 < 0 < \nu_2$. Thus, $g(\nu) > 0$ if $\nu_1 < \nu < \nu_2$, and $g(\nu) < 0$ otherwise. Thus, $P_0^*$ is unstable if $0 < \nu < \nu_2$, and is LAS if $\nu > \nu_2$.

Region II: In this case, we have $a_g < 0$ and $c_g < 0$. Let us analyze $b_g$ and $\Delta_g$ in each sub-region.

In sub-regions $II_A$ and $II_B$, $\gamma_N > \gamma_N^{\#}$. Therefore, $\Delta_g > 0$. Since $\gamma_N^{\#} > \gamma_N^m > \gamma_N^s$, we have $b_g > 0$. Thus, $\nu_1$ and $\nu_2$ are real and positive. Therefore, $g(\nu) > 0$ for $\nu_1 < \nu < \nu_2$, and $g(\nu) < 0$ otherwise. Thus, $P_0^*$ is LAS when $0 < \nu < \nu_1$ or $\nu > \nu_2$.

In sub-region $II_D$, $\gamma_N^{\%} < \gamma_N < \gamma_N^{\#}$. Thus, $\Delta_g < 0$ and $g(\nu)$ has no real root. Since $a_g < 0$, $g(\nu) < 0$ for all $\nu > 0$. Therefore, $P_0^*$ is LAS for all $\nu > 0$.

Finally, in sub-region $II_C$, we have $\gamma_N < \gamma_N^{\%} < \gamma_N^m$. We claim that $b_g < 0$. In fact, it is immediate from (4.20) if $\gamma_N < \gamma_N^s$. When $\gamma_N^s < \gamma_N < \gamma_N^m$, we have that $b_g < 0$ if, and only if,

$$\beta_3 < \beta_{3,b}^{th} = \beta_3^{th} + \frac{(\gamma_N^m - \gamma_N) l_A \mu_N \left(r_N \alpha_A \gamma_A + \tau l_A \alpha_N\right)}{\left(\gamma_N - \gamma_N^s\right) r_N \left(2 r_N \alpha_A \gamma_A + \tau l_A \alpha_N\right)}.$$

But, in this case, we have $\beta_{3,b}^{th} > \beta_{3,\#}^{th}$, since

$$\beta_{3,b}^{th} - \beta_{3,\#}^{th} = \frac{\left(\gamma_N^m - \gamma_N\right)\left(\gamma_N^m + \gamma_N\right) l_A^2 \alpha_N (2 r_N \alpha_A \gamma_A \gamma_N + \tau l_A \alpha_N \gamma_N + \alpha_A \gamma_A \mu_N \tau)}{\left(\gamma_N - \gamma_N^s\right) 4 r_N \alpha_A \gamma_A \gamma_N (2 r_N \alpha_A \gamma_A + \tau l_A \alpha_N)} > 0.$$

As $\gamma_N < \gamma_N^{\%}$, we have $\beta_3 < \beta_{3,\#}^{th}$. Therefore, condition $\beta_3 < \beta_{3,b}^{th}$ is satisfied and $b_g < 0$. Thus, $\nu_1 < \nu_2 < 0$ and $g(\nu) < 0$ for all $\nu > 0$. Therefore $P_0^*$ is LAS for all $\nu > 0$.

The union $II_C \cup II_D$ is equivalent to $\gamma_N < \gamma_N^{\#}$, while the union $II_A \cup II_B$ corresponds to $\gamma_N > \gamma_N^{\#}$. This proofs statements of Section 4.3.2 with respect stability of $P_0^*$.

## 4.A.2 Nontrivial equilibria

Setting the derivatives equal to zero in (4.1), getting $D$ from $dA/dt = 0$ with $A \neq 0$, and substituting the result in $dN/dt = 0$ and $dD/dt = 0$, we obtain

$$\begin{cases} r_N - \mu_N N - \beta_1 N A = \dfrac{\alpha_N \gamma_N}{\alpha_A \gamma_A} N \left(l_A - \dfrac{r_A}{K_A} A - \beta_3 N\right), & (4.33) \\ D = \dfrac{1}{\alpha_A \gamma_A} \left(l_A - \dfrac{r_A}{K_A} A - \beta_3 N\right), & (4.34) \\ \left(l_A - \dfrac{r_A}{K_A} A - \beta_3 N\right)\left(\gamma_A A + \gamma_N N + \tau\right) = \nu \alpha_A \gamma_A. & (4.35) \end{cases}$$

Solving (4.33) for $A$ in terms of $N$, and substituting the result in (4.34) and (4.35), we obtain the expressions of $A_i^*$ and $D_i^*$ in (4.10), and equation (4.11) for $N_i^*$, with $p(N)$, $q(N)$, $r(N)$ and $h(N)$ as given in (4.12-4.16).

Now, we show that $N_1$ and $N_2$, which are the $N$-coordinates of $P_1$ and $P_2$ and the roots of $q(N)$, satisfy $0 < N_2 < N_1$ in regions II and III. Indeed, the discriminant of $q(N)$,

$$\Delta_q = \frac{4 r_A r_N \beta_1}{K_A} \left(\beta_{3,\Delta}^{th} - \beta_3\right),$$

is positive in regions II and III. Thus $N_1$ and $N_2$ are real. By Descartes' Rule of Signs both are positive. Finally, as $A_1 < A_2$ and expression $N_i$ is decreasing with $A_i$, we have $0 < N_2 < N_1$.

The roots of the second degree polynomials $p(N)$ and $r(N)$ will be denoted, respectively, by $M_1$ and $M_2$, and $O_1$ and $O_2$. Whenever a pair of these roots is real, we label them in the order $x_2 < x_1$, for $x = M, O$.

As (4.11) is a fourth degree polynomial equation in $N$, it follows that there are at most four nontrivial equilibrium points $P_i^*$, $i = 1, 2, 3, 4$. The conditions to have a non-negative equilibrium $P_i^*$ are the following. In order to have $A_i^* > 0$ and $D_i^* > 0$, from (4.10) we conclude that $d$, $p(N_i^*)$ and $q(N_i^*)$ must have the same sign. Further, as the right side of (4.11) is positive, $r(N_i^*)$ must have the same sign of $q(N_i^*)$. Finally, since the left side of (4.34) will be positive at a feasible equilibrium, we conclude that both sides of (4.33) must be positive. This implies that the following two conditions must hold:

$$N_i^* < \frac{l_A}{\beta_3} \quad \text{and} \quad N_i^* < \frac{r_N}{\mu_N}.$$

Thus, we conclude that an equilibrium $P_i^*$ is non-negative if, and only if, $N = N_i^*$ satisfy

$$0 < N < \min\left\{\frac{r_N}{\mu_N}, \frac{l_A}{\beta_3}\right\}, \text{ and } p(N),\ q(N),\ r(N) \text{ have the same sign of } d. \tag{4.36}$$

We define $I$ as the feasibility interval, i.e., the set of values of $N$ such that (4.36) holds. The following Lemma establishes expressions for the feasibility interval in each region of parameters space. As the proof of Lemma 4.1 is a quite tedious, we postpone it to the next Appendix. The results of Lemma 4.1 are summarized in Figure 29, where $I$ is indicated in each sub-region of the parameters space.

**Lema 4.1.** *In each sub-region of parameters space, the feasibility interval $I$ is given by:*

1. *In region $III_A$, $I = [M_2, N_2]$.*
2. *In region $III_B$, $I = [N_2, M_2]$.*
3. *In region $II_A$, $I = [M_2, N_2] \cup [N_1, M_1]$.*
4. *In region $II_B$, $I = [N_2, M_2] \cup [M_1, N_1]$.*
5. *In region $II_C \cup II_D$, $I = [N_2, N_1]$.*

Now, we have all elements to analyze the existence of roots $N_i^*$ in interval $I$ at each region of the parameter space. Note that $I$ does not depends on $\nu$.

In order to analyze also the local stability of nontrivial equilibria, let us comment which bifurcations can occur with them as $\nu$ varies. Since all other parameters are kept

constant, only one-parameter bifurcations can occur (134). If we assume that a Hopf bifurcation cannot occur, then the unique possibility is a fold bifurcation. A necessary condition for this bifurcation is a zero eigenvalue of the Jacobian matrix of system (4.1) evaluated at $P_i^*$ (135, 134). This matrix can be written as

$$J(P_i^*) = \begin{bmatrix} -\dfrac{r_N}{N_i^*} & -\beta_1 N_i^* & -\alpha_N \gamma_N N_i^* \\ -\beta_3 A_i^* & -\dfrac{r_A}{K_A} A_i^* & -\alpha_A \gamma_A A_i^* \\ -\gamma_N D_i^* & -\gamma_A D_i^* & -\tau - \gamma_N N_i^* - \gamma_A A_i^* \end{bmatrix}. \tag{4.37}$$

Substituting expressions for $A_i^*$ and $D_i^*$ from (4.10), the determinant of $J(P_i^*)$ can be written as

$$\det(J(P_i^*)) = \frac{p(N_i^*)}{(dN_i^*)^2}\left(q'(N_i^*)r(N_i^*) + q(N_i^*)r'(N_i^*) - 2\frac{q(N_i^*)r(N_i^*)}{N_i^*}\right). \tag{4.38}$$

We see that a zero eigenvalue can occur only if

$$p(N_i^*) = 0, \tag{4.39}$$

or if

$$q'(N_i^*)r(N_i^*) + q(N_i^*)r'(N_i^*) = 2\frac{q(N_i^*)r(N_i^*)}{N_i^*}. \tag{4.40}$$

The first possibility, (4.39), implies in $A_i^* = 0$ and thus $P_i^*$ becomes $P_i^* = (N_i^*, 0, D_i^*)$, the same form of the trivial equilibrium $P_0^*$. Further, (4.39) also implies that $N_i^*$ is equal to some of the roots of $p(N)$, $M_1$ or $M_2$. By looking to Lemma 4.1, we see that these roots in general are extrema of the feasibility interval $I$. For these reasons, we can expect that the zero eigenvalue bifurcation which $P_i^*$ undergoes when (4.39) is satisfied, is a transcritical bifurcation between $P_i^*$, $i = 1$ or 2, and $P_0^*$.

On the other hand, let us examine the second possibility of a zero eigenvalue, equation (4.40). Two roots $N_i^*$ and $N_j^*$ will collide if the graphs of $q(N)r(N)$ and $h(N)$ intersect tangentially. It happens for some $\nu = \nu_*$ if $N = N_i^*$ and $\nu = \nu_*$ are solutions of the system consisting of equation (4.11) together with

$$q'(N_i^*)r(N_i^*) + q(N_i^*)r'(N_i^*) = 2\nu\alpha_A\gamma_A d^2 N_i^*. \tag{4.41}$$

But (4.11) and (4.41) imply in (4.40). Thus, we expect that (4.40) corresponds to a saddle-node bifurcation between two nontrivial equilibria $P_i^*$ and $P_j^*$.

Finally, we note the following. When $\nu = 0$, the entries $a_{31}$ and $a_{32}$ of the Jacobian matrix of system (4.1) are zero. Thus, for each $i = 1, 2$, two eigenvalues of $J(P_i^*)$, say, $\lambda_1$ and $\lambda_2$, are the eigenvalues of the Jacobian matrix of subsystem NA evaluated in $P_i$, while the third is $\lambda_3 = -\tau - \gamma_N N^* i - \gamma_A A_i^* < 0$. Moreover, for small enough $\nu > 0$, the signs of $\lambda_1$ and $\lambda_2$ will be preserved and, as $\nu$ increases, they will change only when one of equations (4.39) or (4.40) is satisfied.

With these remarks, let us present the behavior as $\nu$ varies for each sub-region in (4.32). It will be needed only to assume that $P_2^*$ does not undergoes a Hopf bifurcation. We illustrate the general behavior and its analysis in details for region $III_A$. At other regions, the analysis is analogous.

Region $III_A$. When $\nu = 0$, the unique root $N_i^*$ in $I$ is $N_2^* = N_2$. As stated before, as $q(N_2) = 0$, $D_2^* = 0$ and $P_2^* = (N_2^*, A_2^*, 0)$ coincides with equilibrium $P_2 = (N_2, A_2)$ of subsystem NA. As $\nu$ increases, $h(N)$ increases and then $N_2^*$ decreases inside $I$. Thus, $P_2^*$ is a perturbation of $P_2$ due the introduction of $\nu > 0$. We have two different cases as $\nu$ increases. An illustration of these cases can be seen in Figure 30.

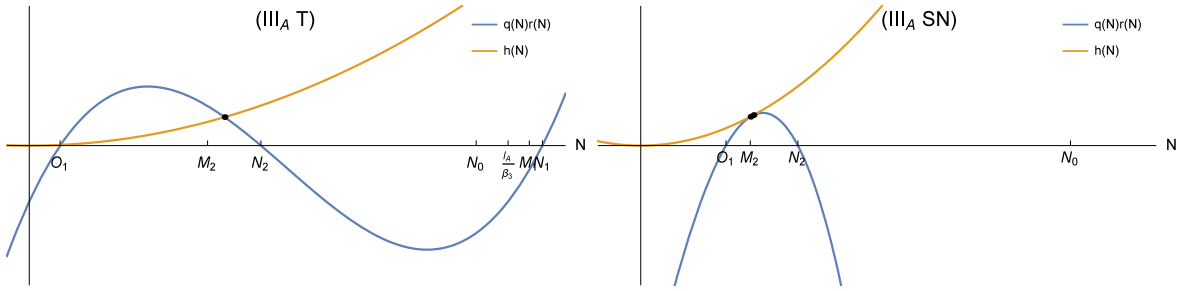


Figure 30 – Graphs of the left side $q(N)r(N)$ (blue) and the right side $h(N)$ (yellow) of equation (4.11), in function of $N$ (horizontal axis) when parameters values correspond to region $III_A$, with the feasibility interval given by $I = [M_2, N_2]$. The black dots at the intersection of these graphs correspond to feasible roots $N_i^*$ for equation (4.11). On the left panel we have case T, with a value of $\nu$ such that $0 < \nu < \nu_2$, before the transcritical bifurcation which occurs when $N_2^*$ exits the interval at $N = M_2$ and $\nu = \nu_2$. On the right panel we have case SN, with a value of $\nu$ such that $\nu_2 < \nu < \nu_*$, after the transcritical bifurcation which occurs when $N_4^* < N_2^*$ enters the interval at $N = M_2$ and $\nu = \nu_2$, and before the collision between $N_4^*$ and $N_2^*$, which occurs when $\nu = \nu_*$.

Case T: If $q(N)r(N)$ and $h(N)$ do not intersect tangentially in any $N \in I$ as $\nu$ increases, then, $N_2^*$ decreases in $I$ until reach $N_2^* = M_2$. See Figure 30, left panel. As commented before, since $M_2$ is a root of $p(N)$, we have $A_2^* = 0$ from (4.10). Thus, equilibrium $P_2^*$ becomes $P_2^* = (N_2^*, 0, D_2^*)$ and collides with the trivial equilibrium $P_0^* = (N_0^*, 0, D_0^*)$ (by the uniqueness of $P_0^*$). We claim that the value of $\nu$ such that $N_2^* = M_2 = N_0^*$, is $\nu = \nu_2$. In fact, for $\nu = \nu_2$ the third eigenvalue $\lambda_3 = 0$ of $J(P_0^*)$ is zero. Setting $\lambda_3 = 0$ in (4.7) leads to

$$(l_A - \beta_3 N_0^*)(\gamma_N N_0^* + \tau) = \alpha_A \gamma_A \nu. \tag{4.42}$$

As $N_0^*$ is a root of (4.6), we also have

$$(\gamma_N N_0^* + \tau) = \frac{\alpha_N \gamma_N \nu N_0^*}{r_N - \mu_N N_0^*}. \tag{4.43}$$

Substituting (4.43) in (4.42), we obtain

$$p(N_0^*) = \kappa N_0^*(l_A - \beta_3 N_0^*) - (r_N - \mu_N N_0^*) = 0.$$

Thus, $N_0^*$ coincides with one of the roots of $p(N)$, $M_1$ or $M_2$. As $N_0^* < r_N/\mu_N < M_1$ (see proof of Lemma 4.1), it follows that $N_0^* = M_2 = N_2^*$ when $\nu = \nu_2$, which proofs the claim. For $\nu > \nu_2$, $N_2^* < M_2$ and there is no root $N_i^*$ inside the feasibility interval $I$. Thus there is no feasible equilibrium $P_i^*$ for $\nu > \nu_2$. Of course, we see that $q(N)r(N)$ and $h(N)$ will intersect tangentially for some $\nu_* > \nu_2$, but outside $I$. Furthermore, if no Hopf bifurcation occurs with $P_2^*$, then by the previous remarks no other bifurcation will occur with $P_2^*$ until $\nu$ increases between 0 and $\nu_2$. Thus, the eigenvalues of $P_2^*$ are all negative while $0 < \nu < \nu_2$, and it is locally stable in this case.

Summarizing, we have the following. For $0 \leqslant \nu < \nu_2$, we have $M_2 < N_2^* \leqslant N_2$, $P_2^*$ is locally stable, and $P_0^*$ is unstable. For $\nu = \nu_2$, we have $N_2^* = M_2 = N_0^*$ and $P_2^* = P_0^*$, i.e., a transcritical bifurcation occurs between $P_0^*$ and $P_2^*$. For $\nu > \nu_2$ we have $N_2 \notin I$ and $P_0^*$ is stable. We label this case with 'T' because only this transcritical bifurcation occurs in this case. The bifurcation diagram of this case is shown in Figure 26, panel ($\text{III}_B$ T).

Case SN: Now, suppose that $q(N)r(N)$ and $h(N)$ intersect tangentially at some $N_i^*$ in $I$, for some $\nu = \nu_*$. Then, for $\nu < \nu_*$ sufficiently near from $\nu_*$, there are two roots of (4.11) in $I$, which we denote by $N_4^*$ and $N_2^*$, with $N_4^* < N_2^*$. See Figure 30, right panel. The root $N_2^*$ is that originated from $N_2$ when $\nu = 0$, as in the case T. The other root, $N_4^*$, is originated from $O_2$ when $\nu = 0$. As $\nu$ increases, $N_4^*$ increases outside $I$, while $N_2^*$ decreases inside $I$ and is the unique root in $I$ while $\nu < \nu_2$. For the same reasons above, $P_2^*$ is locally stable if $\nu < \nu_2$. When $\nu = \nu_2$, $N_4^*$ enters $I$ at $N_4^* = M_2$ and then $A_4^* = 0$. Clearly, we have a transcritical bifurcation between $P_4^*$ and $P_0^*$. For $\nu_2 < \nu < \nu_*$, $P_0^*$ and $P_2^*$ are locally stable, while $P_4^*$ is unstable. Indeed, since there are no other equilibria, $P_4^*$ must have a two-dimensional stable manifold which separates the basins of attraction of $P_2^*$ and $P_0^*$. When $\nu = \nu_*$, a saddle-node bifurcation occurs between $P_2^*$ and $P_4^*$. For $\nu > \nu_* > \nu_2$, $P_0^*$ becomes the unique positive equilibrium and it is globally stable. We label this case with 'SN' because the last bifurcation which occurs with $P_2^*$ is a saddle-node. The bifurcation diagram of this case is shown in Figure 26, panel ($\text{III}_A$ SN). For sake of simplifying statements in the main text and unifying results, we re-labeled the point $P_4^*$ as $P_1^*$ in this case.

Before passing to other regions, let us examine which condition distinguishes cases T and SN. A tangent intersection between $q(N)r(N)$ and $h(N)$ occurs if $N = N_*$ and $\nu = \nu_*$ are solutions of system formed by (4.11) and (4.41). Isolating $\nu$ in (4.41) and

substituting in (4.11), we obtain an equivalent system

$$\begin{cases} \nu = \dfrac{q'(N)r(N) + q(N)r'(N)}{2\alpha_A\gamma_A d^2 N}, & (4.44) \\ q(N)r(N) = \dfrac{N}{2}\left(q'(N)r(N) + q(N)r'(N)\right). & (4.45) \end{cases}$$

Thus, $N_*$ is a solution of (4.45), which does not depends on $\nu$, and $\nu_*$ is given by (4.44) with $N = N_*$. We see that what distinguishes cases T and SN is whether $N_*$ lies in interval $I$ or not. As seen in Lemma 4.1, the possibility of $N_*$ lying in $I$ will be equivalent to whether of conditions $N_* < M_i$ or $N_* > M_i$, $i = 1$ or 2, will be satisfied. Thus, the curves in parameter space which separate cases T and SN are equation (4.45) with $N = M_i$, $i = 1$ or 2. Substituting the expression for $r(N)$ in (4.45), remembering that $p(M_i) = 0$ and simplifying the result, we obtain the equation

$$H_i(\vec{\lambda}) := q'(M_i)dM_i(\gamma_N M_i + \tau) + q(M_i)(\gamma_A p'(M_i) - d\tau) = 0. \quad (4.46)$$

where $\vec{\lambda} = (r_N, \mu_N, r_A, l_A, K_A, \beta_1, \beta_3, \alpha_N, \alpha_A, \gamma_N, \gamma_A, \tau)$. Thus, for $H_i(\vec{\lambda}) > 0$ we have one of the cases SN or T, and for $H_i(\vec{\lambda}) < 0$ we have the another case. From the expressions for $I$ in Lemma 4.1, we note that only the curve $H_2 = 0$ will be of interest in region $III$, while both curves $H_1 = 0$ and $H_2 = 0$ will be of interest in region $II$. An analytical investigation of equation (4.46), with the study of which regions are divided in sub-regions $H_i < 0$ and $H_i > 0$ is out of the scope of this paper. However, using realistic parameters values, we showed numerically that these curves can intersect all sub-regions of the parameter space, except region $\mathrm{II}_C \cup \mathrm{II}D$. This result can be seen in Figure 31.

We now pass to analyzing the behavior of the nontrivial equilibria $P_i^*$ in the other sub-regions. The same mechanism of birth and death of feasible roots occurs in these regions. Thus, for sake of brevity, we only state the results. The bifurcation diagram of each case is showed in Figure 26.

Region $III_B$, $I = [N_2, M_2]$. If $\nu = 0$, we have a single root $N_2^* = N_2$, and $P_2^* = P_2$. The results are the same of region $III_A$, with the only difference that $N_2^*$ increases as $\nu$ increases. Case T: If $q(N)r(N)$ and $h(N)$ do not intersect tangentially in $I$, then $N_2^*$ increases until reach $M_2$, when $\nu = \nu_2$. A transcritical bifurcation occurs at this point and $P_2^* = P_0^*$. For $\nu > \nu_2$, $N_2^*$ leaves $I$ and $P_2^*$ is not feasible anymore. Moreover, if Hopf bifurcations do not occur then $P_2^*$ is globally stable if $\nu < \nu_2$, and $P_0^*$ is globally stable when $\nu > \nu_2$. Case SN: If, for some $\nu = \nu_* > 0$, $q(N)r(N)$ and $h(N)$ intersect tangentially in $I$, then we have the following. For $\nu < \nu_2$ there is a single feasible equilibrium, $P_2^*$. For $\nu = \nu_2$, a root $N_4^* = M_2$ enters the interval $I$. As $\nu$ increases, with $\nu_2 < \nu < \nu_*$, then $N_4^*$ decreases, with the collision between $N_2^*$ and $N_4^*$ occurring at some $\nu = \nu_*$. There is a transcritical bifurcation at $\nu = \nu_2$ and a saddle-node bifurcation at $\nu = \nu_*$. If no Hopf bifurcation occurs, then $P_2^*$ is stable and $P_4^*$ is unstable when they are positive.

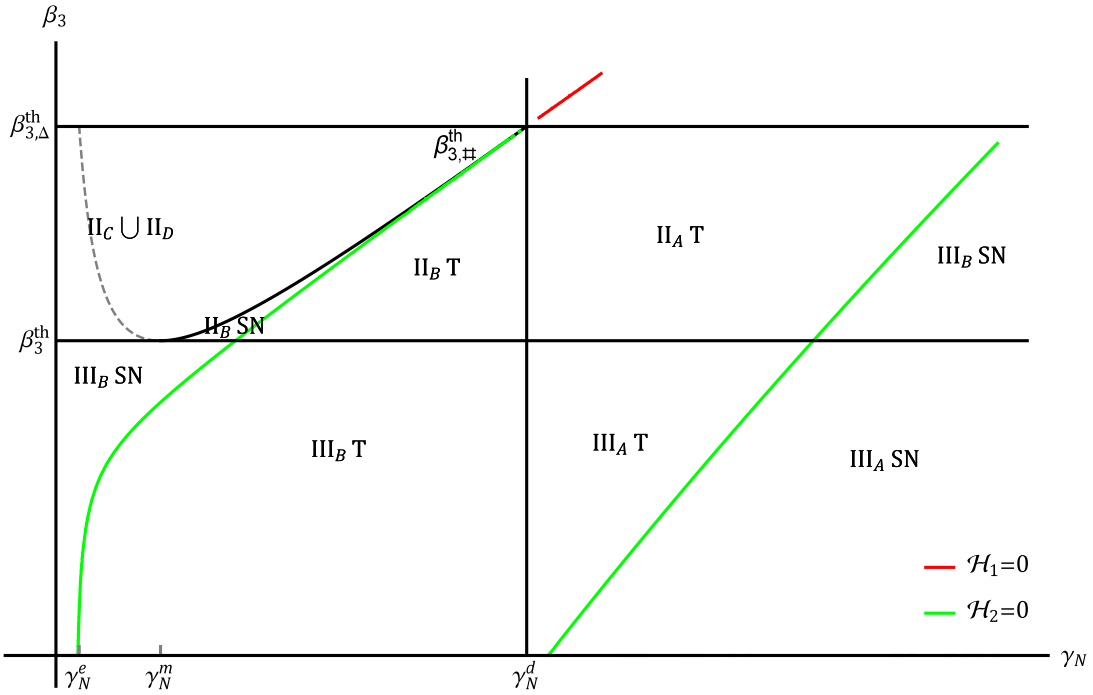


Figure 31 – The curves of $H_1 = 0$ (red) and $H_2 = 0$ (green) on the plane $\gamma_N \times \beta_3$ separate each region in two sub-regions, labeled T and SN. Both panels in Figure 24 correspond to horizontal sections in this plane.

In regions $II_A$ and $II_B$, remember that $0 < \nu_1 < \nu_2$ and that $P_0^*$ undergoes a transcritical bifurcation when $\nu = \nu_i$, $i = 1, 2$, since $\lambda_3$ is zero for these values of $\nu$. Also, as seen above, $N_0^*$ equals some of the roots of $p(N)$ when $\nu = \nu_i$, $i = 1, 2$. As $N_0^*$ is strictly decreasing with $\nu$ and as $M_2 > M_1 > 0$ in this regions, we conclude that the first transcritical bifurcation as $\nu$ increases occurs at $\nu = \nu_1$, with $N_0^* = M_1$, and the second occurs at $\nu = \nu_2$ when $N_0^* = M_2$. Now, let us consider each region separately.

Region $II_A$, $I = [M_2, N_2] \cup [N_1, M_1]$. From the proof of Lemma 4.3 below, if $a_r < 0$ we have that $0 < O_2 < M_2$ and $M_1 < O_1$. Thus, when $\nu = 0$ we have four roots for (4.11), $N_1^* = N_1$, $N_2^* = N_2$, $N_3^* = O_1$ and $N_4^* = O_2$, but only $N_1^*$ and $N_2^*$ are feasible. First, we examine the right part of the interval $I$. As $\nu$ increases, $N_1^*$ increases inside $I$ while $N_3^*$ decreases outside $I$. They will collide at some $\nu = \nu_*$, when $q(N)r(N)$ and $h(N)$ intersect tangentially. If this collision occurs outside $I$, we are in a typical T case, with a transcritical bifurcation between $P_1^*$ and $P_0^*$ occurring when $\nu = \nu_1 < \nu_*$ and $N_1^* = M_1$. If the collision occurs inside $I$, we are in a typical SN case, when a transcritical bifurcation occurs between $P_3^*$ and $P_0^*$, when $N_3^*$ enters the interval $I$ at $N = M_1$. A similar behavior is observed at the left part of the interval $I$, where $N_2^*$ decreases inside $I$ and $N_4^*$ increases outside $I$ as $\nu$ increases, with $\nu < \nu_2$. In case T, $N_2^*$ exits the interval $I$ at $N = M_2$ when $\nu = \nu_2$. In case SN, $N_4^*$ enters the interval $I$ at $N = M_4$ when $\nu = \nu_2$, and later collide with $N_2^*$ when $\nu = \nu_*$. The occurrence of cases T or SN in each part of interval $I$ is independent in each part, so we can have a total of four different cases: T-T, T-SN, SN-T, and SN-SN.

The behavior when $a_r > 0$ is very similar. The unique difference now is that $O_1 < 0$ (by the proof of Lemma 4.1 below). Thus, the root $N_3^*$ starts at $N = O_1$ when $\nu = 0$ and decreases as $\nu$ increases. A SN case cannot occur in the right part of the interval, $[N_1, M_1]$, because it would imply in the existence of two roots of (4.11) to the right of $N_1^*$, for $\nu$ slight greater than $\nu_1$ and lower than $\nu_2$. As $N_2^*$ and $N_{4*}$ are real roots for these values of $\nu$ (pertubations of $M_2$ and $O_2$), (4.11) would have at least five roots, a contradiction. So, we have only two possible cases: T-T and SN-T.

Region $II_B$, $I = [N_2, M_2] \cup [M_1, N_1]$. This case is analogous to case $II_A$, $a_r < 0$. The unique difference is that $N_2^*$ and $N_3^*$ increase while $N_1^*$ and $N_4^*$ decrease as $\nu$ increases. Again, there are four possible cases: T-T, T-SN, SN-T, and SN-SN.

Finally, in the last region, $II_C \cup II_D$, we have $I = [N_2, N_1]$ and $q(N)r(N) \geqslant 0$ in $I$. When $\nu = 0$, we have $N_2^* = N_2$ and $N_1^* = N_1$. As $\nu$ increases, $N_2^*$ increases while $N_1^*$ decreases until they collide for $\nu = \nu_*$. There is no transcritical bifurcation in this case, $P_0^*$ is always stable. If $\nu < \nu_*$, $P_2^*$ is also locally stable. For $\nu > \nu_*$, $P_0^*$ is globally stable.

### 4.A.3 Proof of Lemma 4.1

We now present the proof of Lemma 4.1. The following Lemmas will be useful.

**Lema 4.2.** *Let $M_2$ and $M_1$ be the roots of $p(N)$. Thus, $M_2$ and $M_1$ are complex in region $II_D$, and are real and positive in all other regions of the parameters space.*

*Proof.* The discriminant $\Delta_p$ of $p(N)$ is given by

$$\Delta_p = 4\kappa r_N \left(\beta_{3,\#}^{th} - \beta_3\right) = \left(\frac{l_A \alpha_N}{\alpha_A \gamma_A}\right)^2 \left(\gamma_N - \gamma_N^{\%}\right)\left(\gamma_N - \gamma_N^{\#}\right). \tag{4.47}$$

The Lemma follows from (4.26), (4.32) and from the Descartes' Rule of Signs applied to $p(N)$. □

**Lema 4.3.** *Denote the roots of $r(N)$ by $O_1$ and $O_2$. Then*

1. *In regions $III_B$, $II_B$ and $II_C$, $r(N) < 0$, for all $N \in (0, M_2] \cup [M_1, \infty)$.*
2. *In region $II_D$, $r(N) < 0$ for all $N \geqslant 0$.*
3. *In region $III_A$ and $II_A$, $r(N) > 0$ for all $N \in [M_2, M_1]$.*

*Proof.*

1. In regions $III_B$, $II_B$ and $II_C$, we have $d < 0$ and $p(N) < 0$ in $(-\infty, M_2) \cup (M_1, \infty)$, with $0 < M_2 < M_1$. Thus, from (4.14), $r(N) < \gamma_A p(N) \leqslant 0$ for all $N \in (0, M_2] \cup [M_1, \infty)$.
2. In region $II_D$, we have $p(N) < 0$ for all $N$ and $d < 0$. Thus, $r(N) \leqslant \gamma_A p(N) < 0$ for all $N \geqslant 0$.

3. In regions $III_A$ and $II_A$ we have $d > 0$ and then, $r(N) > \gamma_A p(N)$. Thus, the leading coefficient $a_r$ of $r(N) = a_r N^2 + b_r N + c_3$ may be positive or negative. If $a_r < 0$, then

$$r(0) = \gamma_A p(0) < 0,\ r(M_i) = dM_i(\gamma_N M_i + \tau) > 0,\ i = 1, 2,\ r(\infty) = -\infty.$$

Thus, the roots of $r(N)$ satisfy $O_2 \in [0, M_2]$, $O_1 \in [M_1, \infty)$, and $r(N) > 0$ for all $N \in [M_2, M_1]$. On the other hand, if $a_r > 0$, then $r(-\infty) = \infty$. Therefore, $O_2 \in [0, M_2]$, $O_1 \in (-\infty, 0]$, and $r(N) > 0$ for all $N > O_2$. Thus $r(N) > 0$ for all $N \in [M_2, M_1]$.

□

*Proof of Lemma 4.1.* First, we define the following expressions:

$$f_i(N) = s(N) - y_i l(N),\ i = 1, 2 \tag{4.48}$$
$$s(N) = N(l_A - \beta_3 N), \tag{4.49}$$
$$l(N) = r_N - \mu_N N, \tag{4.50}$$
$$y_1 = \frac{1}{\kappa} > 0, \tag{4.51}$$
$$y_2 = \frac{r_A}{K_A \beta_1} > 0. \tag{4.52}$$

Thus, $p(N)$ and $q(N)$ are written in terms of $f_1(N)$ and $f_2(N)$ as

$$p(N) = \kappa f_1(N) \text{ and } \ q(N) = -\beta_1 f_2(N). \tag{4.53}$$

The roots $M_1$ and $M_2$ of $p(N)$ are the roots of $f_1(N)$, and the roots $N_1$ and $N_2$ of $q(N)$ are the roots of $f_2(N)$. Note that

$$f_i(0) = -r_N y_i,\ i = 1, 2 \tag{4.54}$$
$$f_i(r_N/\mu_N) = (r_N/\mu_N)^2(\beta_3^{th} - \beta_3),\ i = 1, 2 \tag{4.55}$$
$$f_i(l_A/\beta_3) = \frac{y_i r_N}{\beta_3}(\beta_3^{th} - \beta_3),\ i = 1, 2 \tag{4.56}$$
$$f_i(+\infty) = -\infty,\ i = 1, 2 \tag{4.57}$$
$$f_1(N) - f_2(N) = \mu_N(y_2 - y_1)(r_N/\mu_N - N), \tag{4.58}$$
$$d = \beta_1 \left(\frac{y_2}{y_1} - 1\right) = \frac{\alpha_N r_A}{\alpha_A \gamma_A K_A}\left(\gamma_N - \gamma_N^D\right), \tag{4.59}$$
$$f_i(N) = -\beta_3 N^2 + (lA + y_i \mu_N)N - y_i r_N. \tag{4.60}$$

We start with region III. As $r_N/\mu_N < l_A/\beta_3$, $I$ is contained in $[0, r_N/\mu_N]$. Since $f_i(0) < 0 < f_i(r_N/\mu_N)$ and $f_i(l_A/\beta_3) > 0 > f_i(\infty)$, the roots $x_1$ and $x_2$ of $f_i(N)$, with $x = M$ for $i = 1$, and $x = N$ for $i = 2$, satisfy

$$0 < x_2 < r_N/\mu_N < l_A/\beta_3 < x_1. \tag{4.61}$$

Thus, we have $0 < M_2, N_2 < r_N/\mu_N$. We now consider sub-regions $III_A$ and $III_B$ separately.

In sub-region $III_A$ we have $d > 0$. Thus, from (4.59), $y_2 > y_1$. Also, from (4.58), we have $f_1(N) > f_2(N)$ for $0 < N < r_N/\mu_N$. Therefore, as $0 < N_2 < r_N/\mu_N$, from (4.54) we have

$$f_1(0) < 0 = f_2(N_2) < f_1(N_2).$$

Thus, the root $M_2$ of $f_1(N)$ lies in the interval $(0, N_2)$. As $d > 0$, we conclude that $I$ must be such that $p(N)$, $q(N)$ and $r(N)$ are positive. From Lemma 4.3, $r(N) > 0$ in $[M_2, M_1]$. From (4.53), conditions $p(N), q(N) > 0$ correspond to $f_2(N) < 0 < f_1(N)$. From (4.60), we see that both $f_i(N)$ have negative leading coefficient. Since $f_2(N) < f_1(N)$ in the interval $[0, r_N/\mu_N]$, we conclude that $I = [M_2, N_2]$ in this case.

In sub-region $III_B$, we have $d < 0$ and $y_2 < y_1$. From (4.58), it follows that $f_2(N) > f_1(N)$ for $0 < N < r_N/\mu_N$. As $0 < M_2 < r_N/\mu_N$, we have

$$f_2(0) < 0 = f_1(M_2) < f_2(M_2).$$

In this case, the root $N_2$ of $f_2(N)$ lies in the interval $[0, M_2]$. By an analogous reasoning with the previous case, as $d < 0$, $I$ is such that $f_1(N) < 0 < f_2(N)$, what lead us to $I = [N_2, M_2]$.

We now pass to region II. From Lemma 4.3, $0 < N_2 < N_1$. As $N_i = r_N/(\mu_N + A_i)$ and $A_i > 0$, we have $N_i < r_N/\mu_N$, $i = 1, 2$. Further, $l_A/\beta_3 < r_N/\mu_N$, since $\beta_3 > \beta_3^{th}$. As $s(N) \leqslant 0$ for $N \geqslant l_A/\beta_3$, and $l(N) > 0$ for $N < r_N/\mu_N$, it follows that

$$f_2(N) = s(N) - y_2 l(N) < 0, \text{ for } l_A/\beta_3 \leqslant N < r_N/\mu_N.$$

Thus, the roots $N_2 < N_1$ of $f_2(N)$ occur before $l_A/\beta_3$. Therefore, we have

$$0 < N_2 < N_1 < l_A/\beta_3 < r_N/\mu_N. \tag{4.62}$$

It remains to analyse positions of roots $M_i$ of $f_1(N)$ and $p(N)$.

In sub-region $II_A$, we have $d > 0$ and $y_2 > y_1$. Thus, $f_1(N) > f_2(N)$ if $N \in (0, r_N/\mu_N)$. Therefore,

$$f_1(0) < 0 = f_2(N_2) < f_1(N_2) \text{ and } f_1(N_1) > f_2(N_1) = 0 > f_1(l_A/\beta_3).$$

Thus, the roots $M_i$ of $f_1(N)$ satisfy

$$0 < M_2 < N_2 < N_1 < M_1 < l_A/\beta_3 < r_N/\mu_N. \tag{4.63}$$

As $d > 0$, $I$ must be such that $f_1(N) > 0 > f_2(N)$ in $I$. Finally, from Lemma 4.3, we conclude that $I = [M_2, N_2] \cup [N_1, M_1]$.

In regions $II_B$ and $II_C$, we have $d < 0$, $y_1 > y_2$, and $0 < M_2 < M_1$. From (4.58), we have

$$f_1(N) < f_2(N) \text{ for } N \in (0, r_N/\mu_N), \text{ and } f_1(N) > f_2(N) \text{ for } N > r_N/\mu_N. \tag{4.64}$$

As $f_2(N) \leqslant 0$ when $N \in [0, N_2) \cup (N_1, r_N/\mu_N]$, we see from (4.64) that there are two possibilities to where the roots of $f_1(N)$ occur: either they occur in $(N_2, N_1)$, or in $(r_N/\mu_N, \infty)$. Now note the following. As $f_1(N)$ is a second degree polynomial in $N$ with negative leading coefficient, its derivative $f_1'(N)$ changes its sign only once, from positive to negative. We calculate the derivative in $N = l_A/\beta_3$ and analyze each case separately. We have

$$f_1'(l_A/\beta_3) = \frac{l_A}{\beta_3}(\gamma_N^m - \gamma_N).$$

In sub-region $II_B$, we have $\gamma_N > \gamma_N^m$, which implies that $f_1'(l_A/\beta_3)$ is negative. So $f_1'(N)$ will not change its sign as $N$ increases. As $f_1(l_A/\beta_3) < 0$, it means that $f_1(N) < 0$ for $N > l_A/\beta_3$. Therefore, the roots $M_2 < M_1$ must occur before $l_A/\beta_3$. Since $l_A/\beta_3 < r_N/\mu_N$, we have the first option above, i.e., the roots occur in $(N_2, N_1)$. Therefore,

$$0 < N_2 < M_2 < M_1 < N_1 < l_A/\beta_3 < r_N/\mu_N. \tag{4.65}$$

As $d < 0$ the feasibility interval is such that $f_1(N) < 0 < f_2(N)$, what lead us to $I = [N_2, M_2] \cup [M_1, N_1]$.

In sub-region $II_B$, $\gamma_N < \gamma_N^m$. Thus, $f_1'(l_A/\beta_3) > 0$. Now, as $f_1(l_A/\beta_3) < 0$, we have $f_1(N) < 0$ for $N < l_A/\beta_3$. Therefore, the roots $M_2 < M_1$ must occur after $l_A/\beta_3$, what lead us to the second option, since $N_2 < l_A/\beta_3$. Thus, $M_2 < M_1$ occur in $(r_N/\mu_N, \infty)$. Therefore,

$$0 < N_2 < N_1 < l_A/\beta_3 < r_N/\mu_N < M_2 < M_1. \tag{4.66}$$

Again, the feasibility interval is such that $f_1(N) < 0 < f_2(N)$, but, in this case, as it must be contained in $[0, l_A/\beta_3]$, we have $I = [N_2, N_1]$.

In sub-region $II_D$, we have $\Delta_p < 0$. Thus $f_1(N)$ and $p(N)$ have complex roots $M_1$ and $M_2$, and are always negative. As $d < 0$, $I$ must be such that $f_1(N) < 0 < f_2(N)$ for $N \in (0, r_N/\mu_N)$. Therefore $I = [N_2, N_1]$. □

# 5 An alternative approach to modeling and optimizing cancer chemotherapy

*Abstract*. Despite the widely use of chemotherapeutic treatments against cancer in last fifty years, questions concerning which are the best scheduling strategies remains unsolved. In this paper, we investigate the implications of using a simple approach to modeling and optimizing chemotherapy. By using parametrized forms for the function which describes treatment, we are able to reproduce a variety of realistic dosage regimes, and the optimization problem is restricted to a finite dimensional space. These features are illustrated by applying this approach to a simple model for tumor growth. Based on numerical simulations, we discuss how different treatment indicators may be calculated in order to compose an objective functional encompassing aspects such as toxicity, drug constraints, recovery time and risk of tumor relapse. Two toxicity measures are considered, one which considers the total number of host cells killed by treatment, and other which tracks the health level of the patient during the treatment. Numerical experiments are performed varying the interval between doses, doses intensities and the number of doses in each treatment. The results indicate that maximum tolerated dose regimes minimize recovery time, risk of tumor relapse and the total number of cells killed by treatment, but has harmful effects on the health of the patient during the treatment. On the contrary, metronomic schedules present best performance only with respect to the health level during the treatment. This paper illustrates the potential biological and mathematical advantages of this approach if applied to more complex models for specific tumor types.

*Keywords*: Maximum tolerated dose; Metronomic chemotherapy; Optimal treatments; Differential equations.

## 5.1 Introduction

Despite being the major treatment against cancer in the last fifty years, the use of chemotherapy did not achieved a satisfactory stage yet (100, 86, 101). It remains the quests for the best schedules of treatment, the combination with other therapies which have different targets, the elucidation of the role of cytotoxic agents in the immune response and many other specific features of each tumor type (17, 100).

In the last fifteen years, there has been a changing in the paradigm that regimes of maximum tolerated dose (MTD - administration of high and spaced in time doses) are the best ones, and recent clinical studies have been evaluated and showed that

metronomic schedules (administration of low and frequent doses) has presenting promising results, largely due to its anti-angiogenic effects (102, 86, 101). However, other more recent studies have shown that metronomic treatment must be at a sufficient high dose and also sufficiently spaced in time to induce a strong antitumor immune response which contributes to tumor regression (136). Therefore, it appears that an optimization problem remains unsolved, and even unformulated, due to the several effects of cytotoxic drugs on the tumor microenvironment which remain to be elucidated.

Mathematical models have joined this quest for optimizing cancer treatment very long ago. The majority of these mathematical studies in optimizing cancer therapy use the optimal control approach (118, 126, 123, 117, 125, 50, 124, 127, 137). The goal of this paper is to explore how the use of a simple approach to model chemotherapy may lead to advantages on the tasks of defining criteria for optimal treatments and finding them in fact. The approach is illustrated in a toy model for cancer growth and treatment. But our point of view is that the same ideas can be used in other more specific and complex models, focusing in particular types of cancer.

While the optimal control approach deals with the problem to find, at an infinite dimensional function space, a function $v(t)$, of any form, which minimizes an objective functional like $\Phi$, the approach of this work reduces the function space to a finite dimensional one, by restricting the form of $v(t)$ to a simple form which reproduces traditional protocols and their variations. Three advantages of this approach over the optimal control one can be commented. First, the optimal control approach sometimes encounters solutions that are difficult to implement in practice, since they predict irregular time intervals between doses, or very specific time-dependent dosages. On the contrary, the present approach seeks optimal solutions in a space of more realistic protocols, and solutions are more easily implementable from the medical point of view. Second, the search for an optimal treatment protocol in a finite dimensional space avoid many numerical and mathematical issues encountered in the infinite dimensional case of the optimal control approach. On the other hand, it is expected that solutions of the optimal control approach give best (lower) values of the objective functional to be minimized, since the search is in a large space. Third, our approach allow us to define several quantities that can be taken in account when searching for the optimal solution. In other words, our approach allows to the inclusion of several features of interest for cancer treatment in the objective functional. In general, the objective functional of the optimal approach includes a small number of these features, and the complexity of the problems increase a lot by adding other features to the functional.

This paper is organized as follows. In Section 5.2 a mathematical model for tumor growth and parametric modeling for chemotherapeutic protocols are presented. Section 5.3 concerns the asymptotic behavior of the model. In Section 5.4, some numerical

simulations and their biological implications are discussed. In Section 5.5, we define criteria for optimal treatments and perform numerical experiments to compare different scheduling regimes. Finally, in Section 5.6 we discuss the results and point future research directions.

## 5.2 Modeling of chemotherapeutic treatments

The model we consider in this paper is given by the following system of differential equations:

$$\frac{dN}{dt} = r_N - \mu_N N - \beta_1 NA - \alpha_N \gamma_N DN, \tag{5.1a}$$

$$\frac{dA}{dt} = r_A A\left(1 - \frac{A}{K_A}\right) - \beta_3 NA - (\mu_A + \epsilon_A)A - \alpha_A \gamma_A DA, \tag{5.1b}$$

$$\frac{dD}{dt} = v(t) - \gamma_A DA - \gamma_N DN - \tau D. \tag{5.1c}$$

In this system, $N$ represents the normal cells at a given tissue of the human body, $A$ stands for tumor cells in this tissue, and $D$ represents the concentration of a cytotoxic drug used to treat this tumor. Similar versions of this model were presented and studied in other papers, thus we discuss its hypothesis very briefly (87, 130, 138).

The vital dynamics of normal cells is described by a constant flux term $r_N$ representing the formation of new normal cells as an intrinsic property of the tissue aiming to maintain its architecture and a homeostatic state, together with a natural mortality $\mu_N$. On the other hand, as tumor cells have a certain independent, but limited growth, a logistic term is used together with natural mortality $\mu_A$ and an extra mortality $\epsilon_A$ due to apoptosis. Competition parameters $\beta_1$ and $\beta_3$ encompass in a simple manner the many interactions among tumor and tissue cells. Parameters $\gamma_N$ and $\gamma_A$ represent the rates of drug absorption and deactivation by normal and cancer cells, and $\alpha_N$ and $\alpha_N$ are the rates of death of cells due to the drug, according to the log-kill hypothesis.

Now, the modeling of the treatment function $v(t)$ is presented. The protocols commonly used in clinical practice have a robust and easily implementable schedule, with the doses values being almost the same, or the treatment consisting of cycles comprising some sequence of prescribed doses (136, 99). In order to mimic these protocols, we consider functional forms for $v(t)$ parametrized by a few parameters which are allowed to vary. The first functional form that can be assumed for $v(t)$ is

$$v(t) = \sum_{i=1}^{n_d} \rho_i \delta(t - T_i), \tag{5.2}$$

where $\delta(t)$ represents the Dirac Delta function. With this expression, the treatment is described by a sequence of $n_d$ doses, each with quantity $\rho_i$ (in milligrams) being given at time $T_i$. This pulse functional form describes exactly the case of treatments administered

by oral way, where the chemotherapeutic agent is given at a single time. For treatments by infusion on blood stream, the administration lasts from minutes or hours, but this interval of time is small when compared with the interval between the doses and with the time of physiological response of the patient. Thus, these kinds of treatment can also be roughly considered as instantaneous doses. This assumption is commonly done in many mathematical models. If the infusion time is an important variable, this approach also covers these situations by substituting the Dirac deltas $\delta(t - T_i)$ in (5.2) by

$$\frac{1}{I_T}\left(H(t - T_i) - H(t - T_i - I_T)\right),$$

where $H$ is the Heaviside function and $I_T$ stands for the infusion time. For simplicity we will not consider this case here.

Expression (5.2) allows to describe many possible pulse protocols, since the values of each $\rho_i$ and $T_i$ can vary, but this generality does not occur in standard chemotherapy, where the given doses are the same, or cyclically repeated. To reproduce and compare these simpler protocols, more implementable at clinician routine, but still allowing some generality, we consider that the treatment consists of cycles which are repeated periodically. Thus, the treatment is modeled by

$$v(t) = \sum_{i=0}^{n_c-1} c(t - iT - T_0). \tag{5.3}$$

Here, we have $n_c$ cycles $c(t)$ with period of $T$ days, the first starting at day $T_0$.

To construct the cycles $c(t)$, we must consider the maximum tolerated dose (MTD) which can be administered each $T$ days. This is a specific property of each medicine, and depends on the toxicity and side effects resulting from the treatment. It will be denoted as a function $m(T)$. We assume that $m(T)$ is linear with respect to $T$, i.e.,

$$m(T) = \rho T,$$

where $\rho$ is the average daily maximum tolerated dose. But, other expressions may be considered, like $m(T) = c_1 T/(c_2 + T)$, since, there is a saturation effect in $m(T)$ when the time interval $T$ is very large.

We assume that each cycle $c(t)$ gives at most a quantity $m(T)$ during the cycle period, distributed in a sequence of $n_d$ doses, given at days $T_1$, $T_2$, ... , $T_{n_d}$, along the cycle period, from day 0 to day $T$. Each dose gives a proportion $\sigma_i$ of the maximum cycle dose $m(T)$. Thus we have

$$c(t) = \sum_{i=1}^{n_d} \sigma_i \, m(T) \, \delta(t - T_i), \tag{5.4}$$

where $0 \leqslant T_1 < T_2 < ... < T_{n_d} \leqslant T$, $0 \leqslant \sigma_1, \sigma_2, ..., \sigma_{n_d} \leqslant 1$ and $\sigma_1 + \sigma_2 + ... + \sigma_{n_d} \leqslant 1$. If equality holds in this last condition, the treatment prescribes the MTD in each cycle.

Expressions (5.3) and (5.4) allow us to reproduce standard treatment schedules. For example, a treatment which gives the MTD each week, during 16 weeks, is described by parameters

$$n_c = 16, \quad T = 7, \quad n_d = 1, \quad \sigma_1 = 1, \quad T_1 = 0. \tag{5.5}$$

Another example is given by

$$n_c = 6, \quad T = 21, \quad n_d = 3, \quad \sigma_1 = \sigma_2 = 0.5, \quad \sigma_3 = 0, \quad T_1 = 0, \quad T_2 = 7, \quad T_3 = 14. \tag{5.6}$$

In this case, the treatment comprises 18 weeks divided in 6 cycles of 3 weeks. Each cycle gives the MTD in two weekly equal doses, which are followed by a rest period of one week with no dose.

## 5.3 Asymptotic behavior

Since $v(t) = 0$ for $t > t_F = T_0 + n_C T$, it is easy to see that solutions of system (5.1) approach solutions of system (5.1a-5.1b) with $D = 0$. Therefore, the treatment only move the points in the phase space and do not alters the global dynamics of the system. This fact has interesting consequences from the point of view of ecological resilience applied to tumor growth and treatment. See (130) for a discussion.

Thus, it is enough to understanding the asymptotic behavior of system (5.1a-5.1b) with $D = 0$, which will be referred as the NA subsystem. Let us briefly present previous results concerning the analysis of this system (130, 87). It has a trivial equilibrium

$$P_0 = \left(\frac{r_N}{\mu_N}, 0\right) \tag{5.7}$$

and up to two nontrivial equilibria (CE)

$$P_1 = (N_1, A_1), \quad \textit{and} \quad P_2 = (N_2, A_2),$$

where $A_1$ and $A_2$ are the roots of the second degree equation

$$\beta_1 \frac{r_A}{K_A} A^2 + \left(\mu_N \frac{r_A}{K_A} - \beta_1 l_A\right) A + (r_N \beta_3 - l_A \mu_N) = 0.$$

Further, this subsystem presents three possible parameters regimes:

I) If $\beta_3 > \beta_3^{th}$ and $\beta_1 < \beta_{1,\Delta}^{th}$, $P_0$ is globally stable.

II) If $\beta_3 > \beta_3^{th}$ and $\beta_1 > \beta_{1,\Delta}^{th}$, $P_0$ and $P_2$ are locally stable. Equilibrium $P_1$ is a saddle point whose stable manifold is the separatrix between the basins of attraction of $P_0$ and $P_2$.

III) If $\beta_3 < \beta_3^{th}$, $P_2$ is globally stable.

Expressions for thresholds $\beta_3^{th}$, $\beta_1^{th}$ and $\beta_{1,\Delta}^{th}$ can be found in (130, 87).

## 5.4 Numerical simulations

We now deal with the simulation of system (5.1) in order to stimulate the defining of criteria for effectiveness, efficiency and low-toxicity of protocols. These criteria will be used in the next section to optimize treatments. We perform numerical simulations only in regimes II and III of subsystem $NA$, which the ones of interest for applying treatment, since regime I corresponds to a healthy person. In all simulations, we used parameters values presented in Table 2. These values were obtained from data in literature according procedures described in (130, 87).

Table 2 – Parameters description and values adopted in simulations.

| Parameter | Description | Value |
|---|---|---|
| $\mu_N$ | $1/\mu_N$ is the lifetime of a normal cell | $0.01$ day$^{-1}$ |
| $r_N$ | total constant reproduction of normal cells | $10^6$ cell day$^{-1}$ |
| $r_A$ | tumor growth rate | $0.05$ day$^{-1}$ |
| $K_A$ | tumor carrying capacity | $0.75 \times 10^8$ cells |
| $\mu_A$ | natural mortality rate of cancer cells | $0.01$ day$^{-1}$ |
| $\epsilon_A$ | extra mortality rate of cancer cells | $0.01$ day$^{-1}$ |
| $\beta_1$ | cancer cells aggressiveness | $0.40 \times 10^{-9}$ cell$^{-1}$day$^{-1}$ |
| $\beta_3^{II}$ | tissue response to cancer cells - case II | $0.28 \times 10^{-9}$ cell$^{-1}$day$^{-1}$ |
| $\beta_3^{III}$ | tissue response to cancer cells - case III | $0.32 \times 10^{-9}$ cell$^{-1}$day$^{-1}$ |
| $\gamma_N$ | drug absorption rate by normal cells | $0.18 \times 10^{-8}$ cell$^{-1}$day$^{-1}$ |
| $\gamma_A$ | drug absorption rate by cancer cells | $0.3 \times 10^{-8}$ cell$^{-1}$day$^{-1}$ |
| $\alpha_N$ | death rate of normal cells due chemotherapy | $0.3 \times 10^8$ cell mg$^{-1}$ |
| $\alpha_A$ | death rate of cancer cells due chemotherapy | $0.5 \times 10^8$ cell mg$^{-1}$ |
| $\tau$ | drug decay rate | $2.5$ day$^{-1}$ |

We present results of simulation of protocols (5.5) and (5.6) in cases II and III. Since $P_2$ is globally stable in regime III, we may expect that no solution will lead to complete tumor regression. On the other hand, in case II we have bistability and may expect some solutions that lead to cure. Initial conditions are $(N(0), A(0)) = P_2$ and $D(0) = 0$, meaning that the cancer of our hypothetical patient has attained a dangerous stationary size, which needs urgently to be treated, since, on the contrary it can evolve to more a malignant and lethal tumor and the patient will die soon. In order to simulate a small initial period without treatment, we use the value $T_0 = 7$ in all simulations. Since each drug has a specific dosage, the value of $\rho$ depends on the drug and the tumor type. We adopt a value $\rho = 0.71$ mg/day, which corresponds to 5 milligrams per week. If another values were adopted, the quantitative results below would change, but the overall qualitative behaviour and its implications would still be valid.

Figures 32 and 33 show simulations of protocols (5.5) and (5.6) in case III, with two values of $n_c$ in each protocol: $n_c = 12$ (dashed lines) and $n_c = 24$ (continuous lines) for protocol (5.5) and $n_c = 6$ (dashed lines) and $n_c = 12$ (continuous lines) for protocol (5.6).

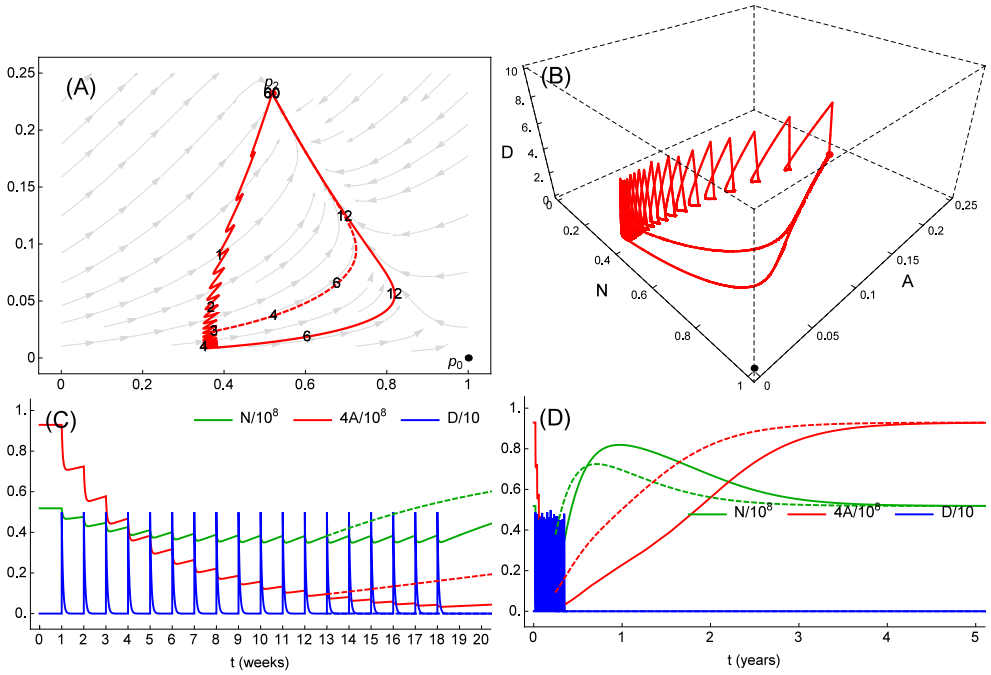


Figure 32 – Solutions of system (5.1) when parameters correspond to case II and protocol (5.5). The numbers on panel (A) indicate the time (in months) in which the solution was at each point.

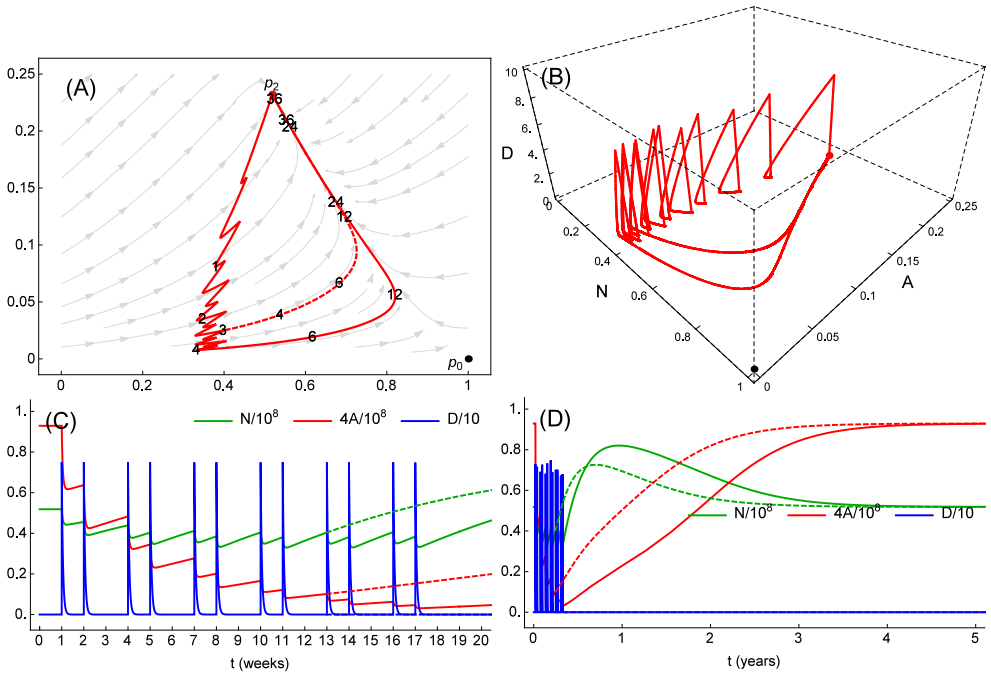


Figure 33 – Solutions of system (5.1) when parameters correspond to case II and protocol (5.6). The numbers on panel (A) indicate the time (in months) in which the solution was at each point.

As expected, in all simulations of case III, we see the relapse of cancer after some time. As the doses are applied, cancer cells are killed and solutions get near the

$N$ axis. After the treatment, they move in direction to $P_0$. But it is a saddle-point, and this transient of apparent cure is due the proximity with the stable manifold of $P_0$. After getting near $P_0$, solutions spend a long time to pass through this point and began to come back to $P_2$. This recurrence rate increases as the number of doses given increases.

Figures 34 and 35 show, respectively, simulations of protocols (5.5) and (5.6) applied in case II. Each figure show simulations of these protocols with three different numbers of cycles applied: $n_c = 11$ (dotted lines), $n_c = 12$ (dashed lines), and $n_c = 16$ (continuous lines) for protocol (5.5), and $n_c = 3$ (dotted lines), $n_c = 4$ (dashed lines), and $n_c = 6$ (continuous lines) for protocol (5.5). The time $t_C$ at which the trajectory crosses the separatrix is indicated in panel (C) of each Figure.

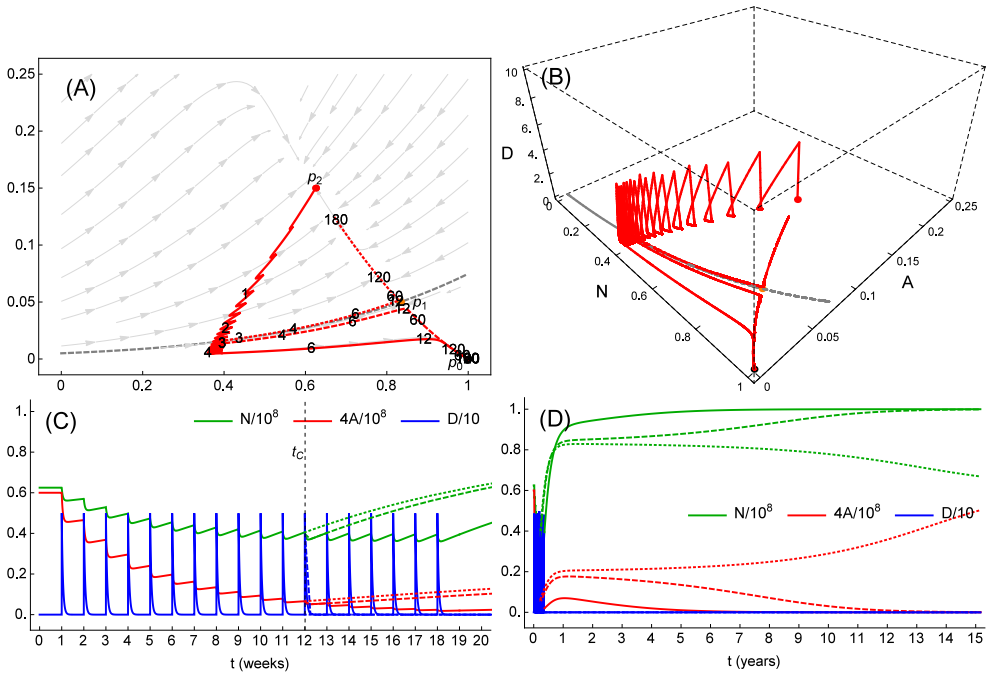


Figure 34 – Solutions of system (5.1) when parameters correspond to case II and protocol (5.5). The numbers on panel (A) indicate the time (in months) in which the solution was at each point.

On the contrary to case III, on case II some treatments are effective (lead to cure). It happens if the treatment diminishes the number of cancer cells enough to move the trajectory to the basin of attraction of $P_0$. Treatment (5.5) is effective with $n_c \geqslant 12$, and it is ineffective if $n_c \leqslant 11$. Similar facts happen for protocol (5.6), which is effective for $n_c \geqslant 4$, and ineffective if $n_c \leqslant 3$.

A closer look to Figures 34 and 35 reveals some interesting facts about effective treatments and give us another insights.

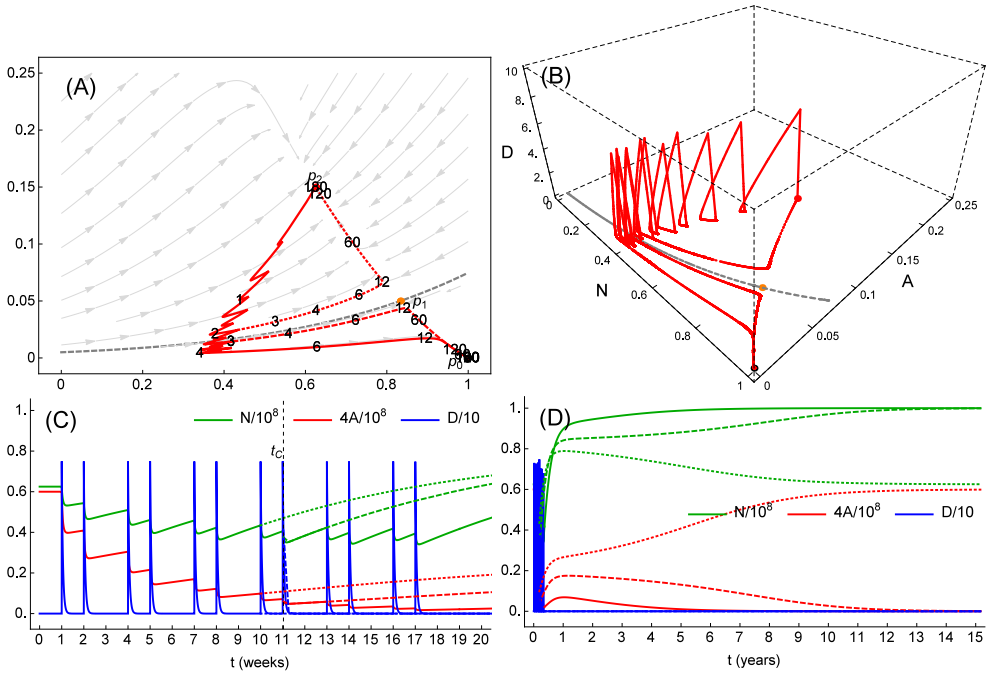


Figure 35 – Solutions of system (5.1) when parameters correspond to case II and protocol (5.6). The numbers on panel (A) indicate the time (in months) in which the solution was at each point.

First, we conclude that given a prescribed form of the cycle (5.4), there exists a minimal number of these cycles, which will be denoted by $n_c^{min}$, that must be administered by the treatment in order to it be effective. Most important, this minimal number is patient-specific, since the position of $P_1$ and of the separatrix depend on the values of $\beta_1$ and $\beta_3$ which may be a little different for two patients with similar tumors. It lead us to the conclusion that it is important to, by some way, assess the cancer aggressiveness and the condition of immune system for each patient and take this information in account when designing the treatment.

Second, we focus in the transient period of about one year after the treatment. At this period, it is difficult to distinct between the behaviour of the 'minimal cure solution' (that with $n_c = n_c^{min}$, dashed lines) and the 'last non-cure solution' (that with $n_c = n_c^{min} - 1$, dotted lines). This resemblance occurs because when the treatment ceases, both solutions are very near the separatrix, one at each side, and it takes a long time to the solutions pass trough the saddle point $P_1$. Only after passing trough $P_1$ they take distinct ways. Even in treatments with more cycles than the minimum necessary (continuous lines), this transient period with a small growth of cancer cells is observed. From the medical point of view it implies that the short-term response to the treatment can be different from the long-term response. Thus, monitoring of patients must be precise and continued after the treatment.

Further, we also note that there is a risk of tumor relapse even after effective

treatments, if they give the minimal number of doses or a few more. In fact, trajectories of these treatments are very near the separatrix and can be shifted by random fluctuations that can occur at any real system. These fluctuations can be caused by changes in the patient's health during the treatment, or an increase in mutations of cancer cells, or by acquired drug-resistance by these cells. So, a effective and safe treatment must give some additional doses in order to damp small disturbances and ensure the long-term recovery.

Another advantage of prolonged treatments can be depicted by looking the time that solutions take to pass through $P_1$ and reach $P_2$. While minimal cure solutions spend more than 10 years to attain the stationary state $P_2$, cure solutions with a greater number of cycles take much less time to reach the cure state. This means that a prolonged treatment leads to a smaller recovery time.

We also see that the during this worst phase of the treatment, the population of normal cells attain very low levels, about 35% of the natural size, and 55% of the initial size before the beginning of the treatment. The more prolonged is the treatment, lower is this level. So, tissue's health can suffer high damage during treatments and it may be a complication.

Finally, we look at the period of time ranging from the beginning of the treatment until the time the solutions cross the separatrix. We observe that initial doses are very successful in decrease the tumor size, while in the second half of the treatment, when trajectories are near the separatrix, there is an enormous difficult to diminish the number of cancer cells, with each dose killing very few cells. Looking the phase portraits (A) and (B) in each Figure, we see that at this stage, the solution is squeezed in a zig-zag fashion inside a narrow strip along the separatrix. Looking to panel (C) in each Figure, we see that the last doses after the crossing time have a very small killing effect on cancer cells. From the medical point of view, this fact can implicate that facing resistance in the diminishing of cancer cells during treatment may be a signal that the treatment is near the transition between non-cure and cure long-term expectancy, and, with a little more persistence, it will leads to cure. Of course, it is only a hypothesis and may be false, since this model does not account for acquired drug-resistance, which is an explanation for tumor persistence.

## 5.5 Optimal treatment strategies

The above results shed some light on model behavior and on what may be expected of an effective treatment with low toxicity. Based on the previous discussion, we define some indicators to quantify specific features of each protocol, in order to compare and classify the various possible treatments, allowing us to choose those that would be the best ones. We take in account the following features: side effects, recovery time, likely of

tumor relapse and total amount of drug.

In order to account for the side effects, we define $N_\dagger$ as the number of normal cells killed by the chemotherapeutic agent by the treatment:

$$N_\dagger = \int_0^\infty \gamma_N \alpha_N N(t) D(t) dt.$$

We also define $N_{\min}$ as

$$N_{\min} = \min\{N(t),\, t \geqslant 0\}.$$

It is a different indicator for side effects which tracks the level of health of the patient during the treatment.

Another indicator we define is

$$R = \left((r_N/\mu_N - N(t_F))^2 + A(t_F)^2\right)^{1/2}.$$

where $t_F = T_0 + n_c T$ is the final time of the treatment. $R$ measures the distance of the solution $(N(t), A(t))$ at time $t_F$ from point $P_0$. As seen in Figures 34 and 35, treatments that end at more distant points from the separatrix lead to a smaller recovery time. Also, treatments that end very near from the separatrix offer more risk of cancer re-incidence, since small perturbations can move the solution to the basin of attraction of $P_2$. Thus, $R$ is a indicator of the recovery time and relapse risk.

Finally, we count the total drug given by the treatment, since it can be a limitation due the high cost of some drugs. This quantity is given by

$$D_\Sigma = \int_0^\infty v(t) dt = n_c \rho T(\sigma_1 + ... + \sigma_{n_d}).$$

For convenience of the reader, the meaning of parameters in treatment expressions (5.3-5.4) and the indicators defined above are summarized in Table 3.

Table 4 shows the value of the indicators above calculated for protocols (5.5) and (5.6). Note that all values of $N_\dagger$ and $A_\dagger$ are greater than the initial values $N(0)$ and $A(0)$, implicating that an effective treatment basically renews the entire tissue.

### 5.5.1 Experimental results of an *in silico* lab

With indicators defined above, we can construct a functional to classify the various possible effective protocols. Given a cycle form, which is defined by variables $T$, $n_d$, $T_1, ..., T_{n_d}$, $\sigma_1, ..., \sigma_{n_d}$, a treatment consisting of $n_c \geqslant n_c^{min}$ cycles is applied, and we calculate the following functional:

$$\Phi(T, n_d, T_1, ..., T_{n_d}, \sigma_1, ..., \sigma_{n_d}, n_c) = w_1 N_\dagger + w_2(N_0 - N_{\min}) + w_3 R + w_4 D_\Sigma,$$

where $w_i$ are weighting factors. The first and second terms measure the side effects of the treatment, the third term intends to measure the recovering time of the patient and the

Table 3 – Treatment parameters and treatment indicators.

| Parameter/Quantity | Meaning |
|---|---|
| $\rho$ | daily MTD |
| $m(T) = \rho T$ | MTD which can be given in $T$ days |
| $n_c$ | number of cycles of the treatment |
| $n_d$ | number of doses in each cycle |
| $T_0$ | starting day of the treatment |
| $T$ | period of each cycle |
| $T_i$ | day in which the $i^{th}$ dose is given in each cycle |
| $\sigma_i$ | fraction of $m(T)$ which is given in the $i^{th}$ dose |
| $n_c^{\min}$ | minimal number of cycles for a protocol be effective |
| $t_C$ | crossing time |
| $N_\dagger$ | number of normal cells killed by chemotherapy |
| $A_\dagger$ | number of cancer cells killed by chemotherapy |
| $N_{\min}$ | minimum number of normal reached during the treatment |
| $t_F$ | final day of the treatment |
| $R$ | distance of solution at the end of treatment from the point $P_0$ |
| $D_\Sigma$ | total drug given by treatment |

Table 4 – Values of treatment indicators for protocols (5.5) and (5.6).

| | $n_c$ cycles | $t_L$ days | $t_C$ days | $t_F$ days | $N_\dagger$ $10^8$ cells | $A_\dagger$ $10^8$ cells | $N_{\min}$ $10^8$ cells | $D_\Sigma$ mg | $N_R$ - | $A_R$ - |
|---|---|---|---|---|---|---|---|---|---|---|
| (5.5) | 12 | 84 | 84.1 | 91 | 0.61 | 0.176 | 0.37 | 60.0 | 0.84 | 0.04 |
| (5.5) | 16 | 112 | 84.1 | 119 | 0.79 | 0.187 | 0.36 | 80.0 | 0.90 | 0.02 |
| (5.6) | 4 | 84 | 77.2 | 91 | 0.61 | 0.174 | 0.35 | 60.0 | 0.84 | 0.04 |
| (5.6) | 6 | 126 | 77.2 | 133 | 0.88 | 0.189 | 0.34 | 90.0 | 0.92 | 0.01 |

relapse risk, and the last term describes the need to minimize the total amount of drug given. Of course, if one is interested in minimizing only one of the indicators above, the weights $w_i$ can all be chosen to be zero, excepted the one corresponding the quantity of interest.

With this, we have, roughly speaking, an *in silico* lab where different treatments can be compared. One can test many different treatment protocols varying some key parameters of $v(t)$ and then assess their effects in features of interest or solve an optimization problem (minimize $\Phi$) in a finite dimensional space of parameters of interest which are allowed to vary, while other parameters are kept constant.

We now present results concerning the comparison of various protocols and the seek for optimal ones. As cure is not possible in case III, we focus the applying of short-term treatments on case II. Due the difficult of calibrating the weights $w_i$, at this initial stage we do not perform an optimization of the functional $\Phi$, but only present the variation on indicators above when some treatment parameters vary.

In order to better understand the differences between protocols, we introduce two quantities. The first is the total duration of the treatment, denoted by $t_\Delta$, and given by

$$t_\Delta = n_c T.$$

The second quantity we introduce defined as the 'average infusion rate' of a given protocol, denoted by $\bar{v}$, and given by the ratio between the total drug given, $D_\Sigma$, and the total duration, $t_\Delta$. Thus,

$$\bar{v} = \frac{D_\Sigma}{t_\Delta} = \frac{n_c \rho T(\sigma_1 + ... + \sigma_{n_d})}{n_c T} = \rho(\sigma_1 + ... + \sigma_{n_d}).$$

Let us present the result of different experiments.

### Experiment I

In the first experiment, we assess the differences between treatments that give the same amount of drug and last the same time, but have different cycle periods, each cycle having a single doses. We consider 10 different treatments that last 120 days, each with period given by $T = 1, 2, 3, 4, 5, 6, 8, 10, 12, 15$ (divisors of 120), and number of cycles given by $n_c = 120/T$. The cycles are described by $n_d = 1$, $\sigma_1 = 1$, $T_1 = 0$. The total amount of drug given by all protocols is the same, $D_\Sigma = 85.71$ mg, and also the average infusion rate, $\bar{v} = 0.71$ mg/day. Results are shown in Figure 36.

On the one hand, low values of $T$ mimic metronomic therapy, with the lower value, $T = 1$ day, prescribing 120 daily doses of 0.71 mg. On the other hand, large values of $T$ resemble standard chemotherapy, with spaced, higher doses. The treatment with the larger value gives 8 doses of 10.71 mg, one each $T = 15$ days. From Figure 36, we conclude that the greater is the interval between doses, the lesser are the values of $N_\dagger$ and $R$, implicating that treatment regimes with more spaced and higher doses kill less cells and have a faster recovery and less recurrence risk, compared with regimes of frequent, lower doses. On the other hand, the health of the patient during treatment is more protected by metronomic therapy regimes, since the value of $N_{\min}$ increases when $T$ decreases.

### Experiment II

In Experiment I, the effects of changing $T$ and $n_c$ simultaneously were assessed. In order to deepen these results and examine the effects of varying $T$ and $n_c$ separately, we perform a second experiment. We run protocols with periods $T = 1, 2, 3, \ldots, 120$ and number of cycles $n_c = 4, 5, 6, \ldots, 30$ satisfying $n_c T \leqslant 120$. The cycles are described by $n_d = 1$, $T_1 = 0$, and $\sigma_1 = 120/(n_c T)$. Thus, each protocol prescribes cycles with a single dose at day 0, with absolute value $\sigma_1 m(T) = \sigma_1 \rho T = 120\rho/n_c$ mg. The total amount of

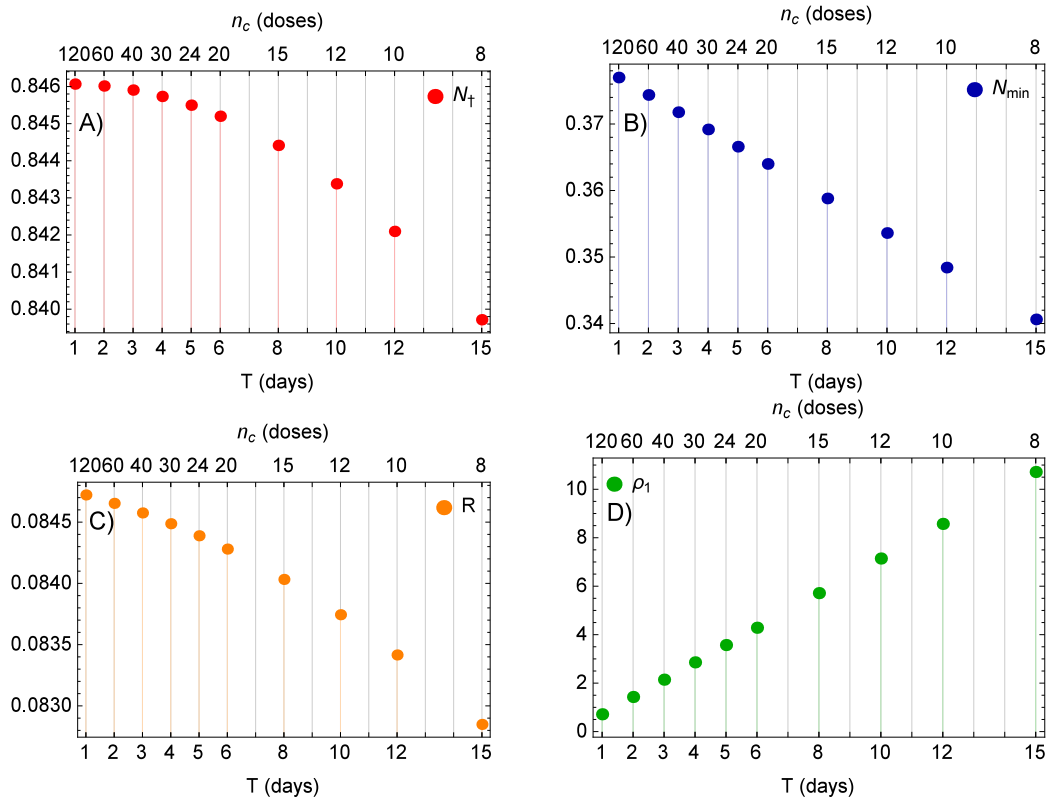


Figure 36 – Results from simulations in Experiment I.

drug is the same for all protocols, and the same of Experiment I, $D_\Sigma = n_c \rho T \sigma_1 = 85.71$. The average infusion rate for each protocol is $\bar{v} = 85.71/(n_c T)$ mg/day. Results are shown in Figure 37.

Suppose that the period $T$ between the doses (cycles) is fixed and $n_c$ vary. Then, we have different protocols that dilute the total amount of drug in different numbers of doses. If this number increases, the quantity of drug given in each dose decreases and also the average infusion rate. We see that more diluted and prolonged regimes (with more doses) have the same features of metronomic regimes in Experiment I, with greater values of $N_\dagger$, $R$ and $N_{\min}$. Now, suppose that $n_c$ is fixed and $T$ vary. In this case, all protocols have the same number of doses, and the same absolute value for each dose, but the interval $T$ between the doses vary. As $T$ increases, the average infusion rate $\bar{v}$ decreases and the values of $N_\dagger$, $R$ and $N_{\min}$ increase. Thus, in this case, more spaced regimes have the same effects of metronomic regimes, on the contrary to Experiment I. Therefore, we conclude that it is not the interval of time $T$ itself that reproduces features of metronomic regimes when it is low, but the key quantity is the average infusion rate $\bar{v}$: the lower $\bar{v}$, the greater $N_\dagger$, $R$ and $N_{\min}$; and, for different protocols with the same average infusion rate, the case of Experiment I, metronomic regimes are more similar to those regimes with greater number of doses.

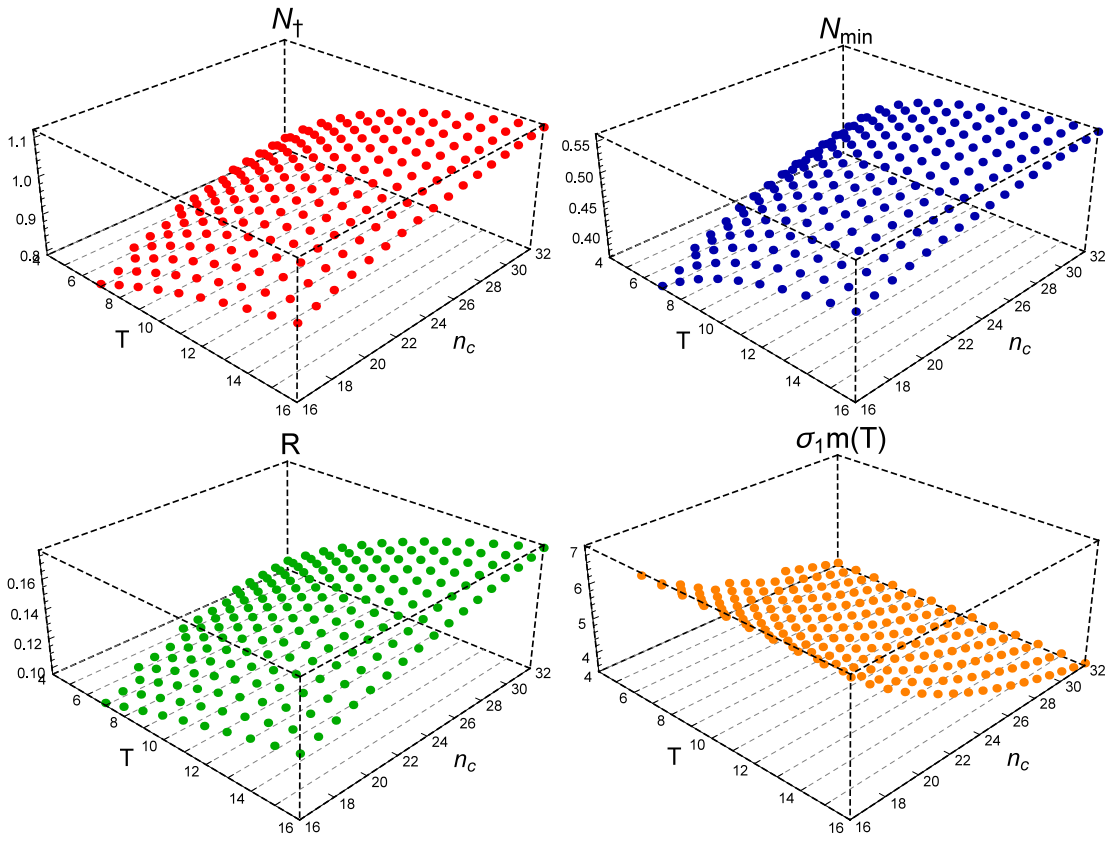


Figure 37 – Results from simulations in Experiment II.

### Experiment III

We now turn attention to treatments with cycles comprising two different doses. We simulate treatments with different values of $T \in \{2, 4, 6, 8, 10, 12, 20, 24, 30\}$ and $\sigma_1 \in [0, 1]$. Each cycle is given by $n_d = 2$, $\sigma_2 = 1 - \sigma_1$, $T_1 = 0$ and $T_2 = T/2$. Thus, each cycle gives the MTD and the doses are given at the beginning and at half the cycle. Each protocol gives $n_c = 120/T$ doses and lasts 120 days. Thus, the quantity of drug and the average infusion rate of all protocols are the same, $D_\Sigma = 85.71$ mg and $\bar{v} = 0.71$ mg/day. Results are show in Figure 38.

With $T$ fixed and $\sigma_1$ varying, the maximum values of $N_\dagger$, $N_{\min}$ and $R$ occur when $\sigma_1 = 0.5$, implicating that $\sigma_2 = 0.5$, while the minimum values of these quantities occur when $\sigma_1 = 0$ or 1, and then, $\sigma_2 = 1$ or 0. Therefore, regimes with more equally distributed doses present the features of metronomic regimes. When $\sigma_1$ is fixed and $T$ varies, the same results of Experiment I are observed: $N_\dagger$, $N_{\min}$ and $R$ increase when $T$ decreases.

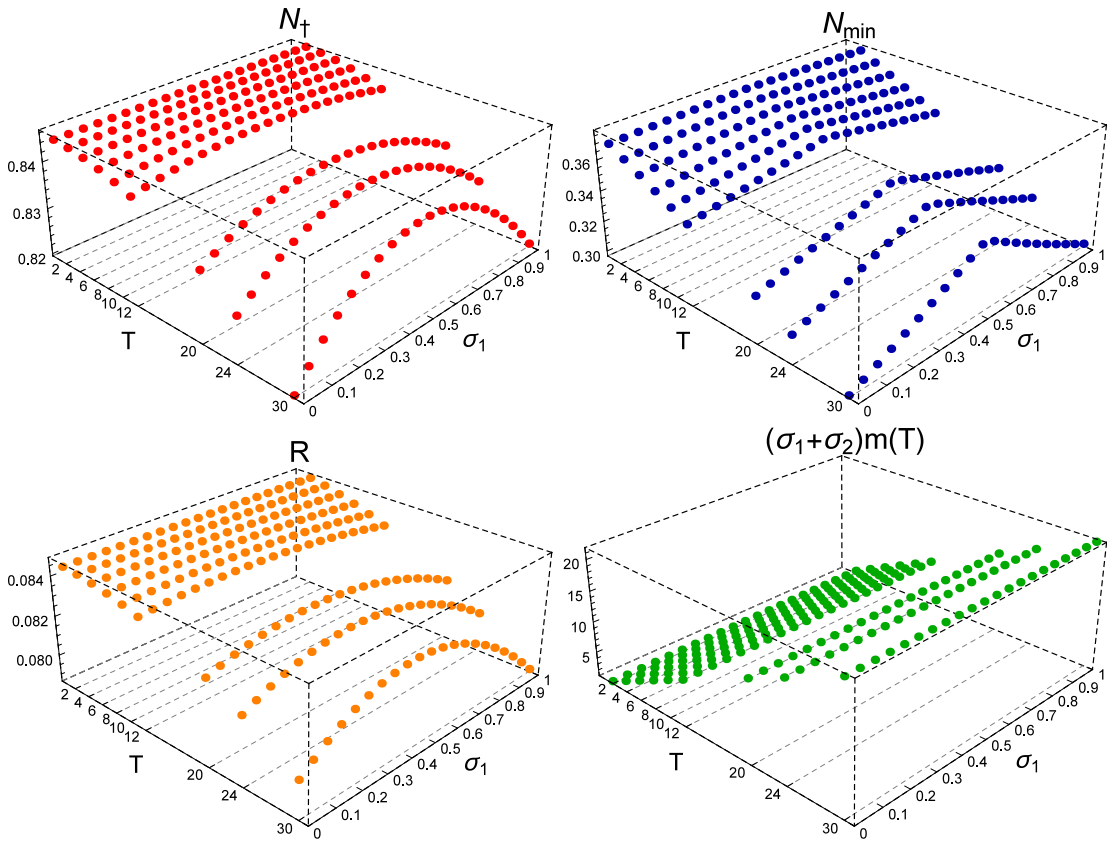


Figure 38 – Results from simulations in Experiment III.

### Experiment IV

Finally, we asses the effect of three different doses in each cycle. In this Experiment, all treatments consist of $n_c = 6$ cycles of $T = 21$ days, each with $n_d = 3$ weekly doses ($T_1 = 0$, $T_2 = 7$ and $T_3 = 14$). The proportions of the first and second doses, $\sigma_1$ and $\sigma_2$, vary in the interval $\in [0, 1]$, with the restriction $\sigma_1 + \sigma_2 \leqslant 1$, and the proportion of the third dose is $\sigma_3 = 1 - \sigma_1 - \sigma_2$, implicating that the treatment gives the MTD in each cycle. The total duration, total drug given, and the average infusion rate are the same in all treatments: $t_\Delta = 126$ days, $D_\sigma = 90$ mg and $\bar{v} = 0.71$ mg/day. Results are shown if Figure 39.

Results are very similar to those of the previous Experiment. The maximum values of $N_\dagger$, $N_{\min}$ and $R$ occur when $\sigma_1 = \sigma_2 = \sigma_3 = 1/3$, and the minimum occur at the vertices, where one of the doses is maximal and the other two are zero. The absolute minimum of $R$ occur at $\sigma_1 = 1$, $\sigma_2 = 0$, since this protocol starts to apply the maximal dose before protocol with $\sigma_1 = 0$, $\sigma_2 = 1$, or with $\sigma_1 = 0$, $\sigma_2 = 0$.

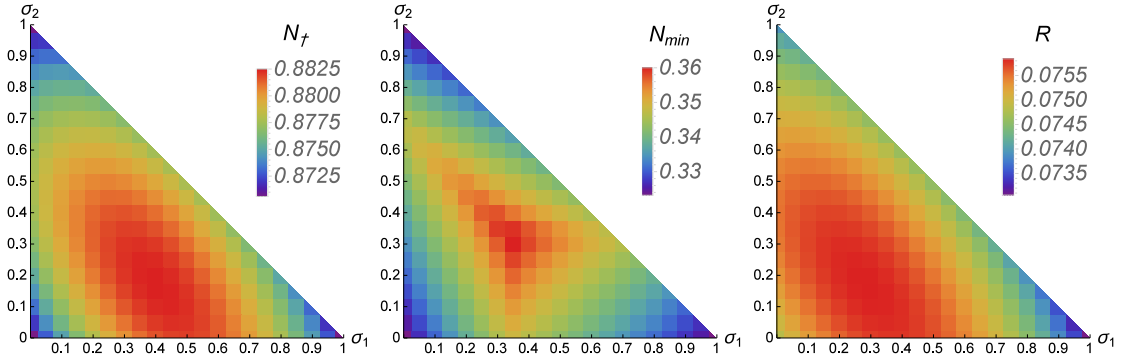


Figure 39 – Results from simulations in Experiment IV.

## 5.6 Discussion

In this paper we propose an approach to modeling and optimizing cancer therapies based on parametric functional forms for treatment functions. This approach restricts the functional space of treatments to more real and implementable protocol schedules and also simplifies the mathematical problem of optimizing treatments. The approach in this paper focus on chemotherapy but may be extended to other therapies, such as radiotherapy or immunotherapies.

We apply this modeling of treatments to a simple model for tumor growth and perform numerical simulations. The results of these simulations allow us to observe different features of effective treatments. We introduce indicators for measuring side effects, recovery time, risk of tumor relapse and total drug given. These indicators are easily calculated for each solution of the system of differential equations. In particular, two different indicators of side effects are considered. One of these accounts for the total number of tissue cells killed by the treatment, a posterior and global indicator. On the other hand, the other indicator tracks the instantaneous health level of the tissue during the treatment period, a local indicator.

We then illustrate how an objective functional encompassing all these indicators may be constructed and then applied to optimization methods in finite dimensional spaces in order to find the best protocols according to these criteria. This approach allows for considering multiples features of tumor treatment which in general are considered individually in optimal control problems. However, the choice of weights in the functional expression is not a straightforward task.

Some experiments were performed to compare different schedules regimes. We considered experiments varying the interval between doses, doses intensities and the number of doses in each treatment cycle. In all these experiments we see a duality between metronomic scheduling and MTD scheduling concerning the two indicators of side effects. In all experiments, we observe that metronomic scheduling minimizes the side effects

during the treatment, but maximizes the total size effects. On the other hand, protocols with higher and more spaced doses minimize the indicator accounting for the total side effects and maximize the instantaneous side effects. In other words, due to the almost constant infusion rate, metronomic regimes present a more smooth passage towards the cure equilibrium and the tissue maintain higher health levels, but this smoothness implies in the killing of more cells during the entire period of treatment.

Our numerical experiments also indicated that MTD regimes minimize the recovery time and the risk of tumor relapse. These results show the importance of a correct choice for the optimality criteria, and also illustrate the problem of choosing the weights correctly when combining these criteria.

The approach presented here may be applied to more specific models for tumor treatment which explicitely consider important interactions within the tumor microenvironment, such as the role of innate immune response, the role of angiogenesis, drug resistance, and etc. We believe that the application of this approach to a specific tumor type will shed some light on the issue of dose scheduling and may serve as a beacon to clinicians. In this case, a careful choice for the quantities of interest to optimizing and a study of how to combine these quantities correctly will be necessary.

# 6 Conclusão e perspectivas futuras

Nesta tese, foram desenvolvidos e analisados modelos matemáticos para a fase inicial e tratamento de tumores.

No Capítulo 2, estudamos e modelamos a fase inicial, abordando a formação de um tumor como um processo multipasso onde alterações genéticas transformam uma célula normal e suas descendentes em um tumor avascular. A análise do modelo proposto indica que o surgimento de uma população de células mutantes com fenótipo mais agressivo, a partir de células mutantes menos adaptadas, abre espaço no tecido para a sobrevivência destas células menos adaptadas, o que leva à formação de um tumor heterogêneo. Além disso, apesar de ser um modelo simples que não contempla toda a complexidade do câncer, as simulações numéricas com parâmetros baseados na literatura exibiram resultados quantitativos de acordo com o observado na realidade. De fato, vimos que pequenas alterações nas taxas de apoptose ou de mutações alteram o tempo necessário para o tumor alcançar um tamanho clinicamente detectável, diminuindo este tempo de 80 para 5 anos.

No Capítulo 3, estudamos de um ponto de vista diferente um modelo simples para crescimento tumoral. Apesar de ser muito conhecido na Ecologia e já contar com um certo ferramental matemático teórico, o ponto de vista da Resiliência Ecológica é pouco abordado e aplicado em modelos matemáticos. De fato, os conceitos de Latitude, Precariedade e Resistência de um ponto de equilíbrio estável, relacionados à sua bacia de atração, estão definidos há algum tempo na literatura, mas poucas vezes foram aplicados quantitativamente a modelos matemáticos, e os métodos para calculá-los ainda são incipientes. Neste Capítulo, propusemos métodos alternativos que são mais precisos e possuem menos custo computacional. Além disso, acreditamos que a discussão sobre o surgimento e tratamento de câncer como transições críticas pode colaborar no entendimento sobre a doença, especialmente ao fato de que a recidiva tumoral após aplicação de tratamentos pode estar ligada à existência de uma instabilidade intrínsica dos sistemas celulares do paciente, sendo assim necessário considerar terapias que possibilitam a criação de uma estabilidade mínima para evitar tal recidiva.

O Capítulo 4 de certa forma tenta apresentar uma solução simplificada para este problema. Analisamos como a manutenção de um regime de tratamento contínuo de longo prazo, via quimioterapia metronômica, descrita por um termo de infusão constante, pode devolver a estabilidade intrínsica perdida pelo sistema de reparo natural. É uma solução simplificada, pois fatores como resistência à droga e angiogênese não foram considerados. Para análise deste modelo de três dimensões, utilizamos ferramentas da Teoria dos Sistemas Competitivos em $\mathbb{R}^3$. Com isto, foi possível obter resultados de estabilidade global, e realizar

uma análise do modelo em todo o seu espaço de parâmetros. Ao realizar esta análise, uma condição sobre os parâmetros apareceu naturalmente, possuindo uma interessante interpretação biológica. Quando os parâmetros satisfazem esta condição, o tratamento com quimioterapia metronômica, além de diminuir o número de células tumorais, restabelece a população de células normais do tecido. Por outro lado, quando esta condição não é satisfeita, o tratamento diminui o número de ambas populações celulares. Um exame de quando esta condição tem mais chances de ser satisfeita indica que a quimioterapia metronômica seria mais recomendada para tumores de crescimento lento, tumores com alta capacidade de suporte e tumores altamente competitivos.

Finalmente, no Capítulo 5, apresentamos uma abordagem para modelar e otimizar protocolos de tratamento por quimioterapia. Por restringir a forma dos protocolos de tratamento a um espaço de dimensão finita, esta abordagem traz vantagens no processo de encontrar protocolos ótimos, e também do ponto de vista prático, pois os protocolos reproduzidos são aqueles utilizados de fato na rotina clínica e também as soluções encontradas, sendo as mesmas facilmente implementadas. Outra vantagem desta abordagem é que a busca pelo melhor protocolo pode levar em diversos aspectos da aplicação de um protocolo de tratamento, como toxicidade, custo financeiro, risco de recidiva e tempo de recuperação, pois estes fatores podem ser calculados para cada protocolo e combinados em um único funcional objetivo. Contudo, surge a dificuldade de calibrar pesos para combinação de todos estes fatores. Realizamos experimentos numéricos variando o intervalo entre doses, intensidades das doses e número de doses diferentes em cada ciclo. Todos os resultados indicaram que regimes metronômicos (doses frequentes e baixas) são os que mantêm a saúde do paciente em um melhor nível durante o tratamento, mas são os regimes de dose máxima tolerada (doses altas e espaçadas no tempo) que minimizam o risco de recidiva e tempo de recuperação. Acreditamos que a abordagem apresentada neste Capítulo é promissora e pode ser aplicada em modelos mais completos, podendo ajudar de fato na busca de melhores protocolos de tratamento.

Para desenvolvimento desta tese foram consultadas diversas referências sobre a Biologia do Câncer. Pudemos constatar como a complexidade desta doença emerge da combinação de aspectos envolvendo alterações genéticas e rotas de sinalização intracelulares com aspectos extracelulares, como as várias interações intercelulares no tecido tumoral. Além disso, chama atenção a existência de tantos mecanismos intrincados apresentados pelas células do corpo humano para evitar e controlar o crescimento de células mutantes. Ainda, chega-se ao final desta tese acreditando que realmente é possível que a Matemática Aplicada auxilie no combate ou, pelo menos, no controle do câncer. Contudo, para que os modelos alcancem resultados que de fato possam influenciar decisões ou testes clínicos, percebemos que é essencial uma forte colaboração interdisciplinar com médicos e biólogos.

A seguir, apresentamos duas linhas diferentes de perspectivas para trabalhos

futuros.

## O papel das células T reguladoras na progressão tumoral

A primeira delas trata de modelar o papel das células T reguladoras na evasão tumoral da imunovigilância (91). Pesquisas recentes tem mostrado que estas células são recrutadas pelo tumor para o microambiente tumoral e então inibem a resposta imune ao tumor, desempenhada por células T citotóxicas e outras. Esta inibição da resposta imune parece ser essencial para o desenvolvimento do tumor e foi apontada como um *Hallmark* emergente do câncer (19). Apesar de existirem inúmeros modelos matemáticos descrevendo a resposta imune ao câncer (94), poucos tem tratado destas descobertas recentes (139). Temos elaborado um modelo neste contexto e o apresentamos a seguir.

O modelo considera inicialmente as populações de células tumorais ($T$), células T citotóxicas no local do tumor ($E$), células T reguladoras no local do tumor ($R$), células T citotóxicas na corrente sanguínea ($E_B$), células T reguladoras na corrente sanguínea ($R_B$). Supomos que as células T na corrente sanguínea são recrutadas ao local do tumor quando encontram com células tumorais, de acordo com a lei de ação de massas:

$$\frac{dT}{dt} = aT\left(1 - bT\right) - d_1 TE, \tag{6.1a}$$

$$\frac{dE}{dt} = c_1 E_B T - \mu_E E - d_2 TE - d_3 RE, \tag{6.1b}$$

$$\frac{dR}{dt} = c_2 R_B T^2 - \mu_R R, \tag{6.1c}$$

$$\frac{dE_B}{dt} = r_E - \mu_E E - c_1 E_B T, \tag{6.1d}$$

$$\frac{dR_B}{dt} = r_R - \mu_R R_B - c_2 R_B T^2. \tag{6.1e}$$

Contudo, assumimos que o recrutamento das células T reguladoras tem uma dependência não-linear do número de células tumorais, descrita pelo termo $c_2 R_B T^2$. Com isto, o recrutamento é baixo quando o tumor é pequeno. Aplicando a hipótese de que as células T na corrente sanguínea, $E_B$ e $R_B$, estão em equilíbrio quase-estacionário,

$$\frac{dE_B}{dt} = 0, \quad \frac{dR_B}{dt} = 0 \Longrightarrow E_B = \frac{r_E}{\mu_E + c_1 T}, \; R_B = \frac{r_R}{\mu_R + c_2 T^2}.$$

obtemos o sistema reduzido:

$$\frac{dT}{dt} = aT\left(1 - bT\right) - d_1 TE, \tag{6.2a}$$

$$\frac{dE}{dt} = \frac{r_E c_1 T}{\mu_E + c_1 T} - \mu_E E - d_2 TE - d_3 RE, \tag{6.2b}$$

$$\frac{dR}{dt} = \frac{r_R c_2 T^2}{\mu_R + c_2 T^2} - \mu_R R. \tag{6.2c}$$

Uma versão adimensional deste sistema é dada por:

$$\frac{dT}{dt} = \alpha T\,(1-T) - \beta_1 TE, \tag{6.3a}$$

$$\frac{dE}{dt} = \frac{\rho_1 T}{1+\rho_1 T} - E - \beta_2 TE - \beta_3 RE, \tag{6.3b}$$

$$\frac{dR}{dt} = \delta\left(\frac{\rho_2 T^2}{1+\rho_2 T^2} - R\right), \tag{6.3c}$$

onde

$$\bar{T} = bT,\ \bar{E} = \frac{\mu_E E}{r_E},\ \bar{R} = \frac{\mu_R R}{r_R},\ \bar{t} = \mu_E t,$$

e os parâmetros adimensionais são

$$\alpha = \frac{a}{\mu_E},\ \rho_1 = \frac{c_1}{b\mu_E},\ \beta_1 = \frac{d_1 r_E}{\mu_E^2},\ \rho_2 = \frac{c_2}{b^2\mu_R},\ \beta_2 = \frac{d_2}{\mu_E b},\ \beta_3 = \frac{d_3 r_R}{\mu_E \mu_R},\ \delta = \frac{\mu_R}{\mu_E}.$$

Os pontos de equilíbrio deste sistema são:

1. $P_0 = (0,0,0)$, que é sempre instável, e
2. $P = (T,E,R) = \left(T, \alpha\beta_1^{-1}(1-T), \dfrac{\rho_2 T^2}{1+\rho_2 T^2}\right)$, onde $T$ é raiz da equação

$$\frac{\beta_1}{\alpha}\frac{\rho_1 T(1+\rho_2 T^2)}{(1+\rho_1 T)(1-T)} = \left(1+\beta_2 T(1+\rho_2 T^2) + \beta_3\rho_2 T^2\right). \tag{6.4}$$

É possível mostrar que a equação (6.4) sempre possui ou uma ou três raízes reais entre 0 e 1. Portanto, o sistema sempre possui ou um ou três pontos de equilíbrio não trivais. Diagramas de bifurcação indicam a ocorrência de histerese para alguns valores dos parâmetros, como mostra a Figura 40. Esta Figura mostra como os parâmetros $\rho_2$ (recrutamento das células T reguladoras) $\beta_3$ (taxa de inativação da resposta imune pelas células T reguladoras) influenciam na progressão tumoral. Para valores baixos destes parâmetros, o tumor possui um tamanho muito pequeno, correspondendo a um tumor controlado pela resposta imune. À medida que estes parâmetros aumentam, o volume do tumor quase não se altera. Quando cada um destes parâmetros ultrapassa certo limiar, este estado controlado do tumor desaparece e então o tumor alcança um tamanho muito maior. Devido ao efeito da histerese, mesmo que estes parâmetros diminuam um pouco, o tumor ainda continua neste tamanho.

Além do papel na imunoevasão tumoral, tem sido evidenciado que as células T reguladoras também contribuem para a angiogênese tumoral (91). Assim, supondo que a vascularização tumoral é descrita implicitamente pelo parâmetro $K = b_1$, investigamos o comportamento quando $K$ varia. Os resultados podem ser vistos na Figura 41. No primeiro gráfico, para certos valores dos parâmetros, observamos a não-ocorrência de histerese.

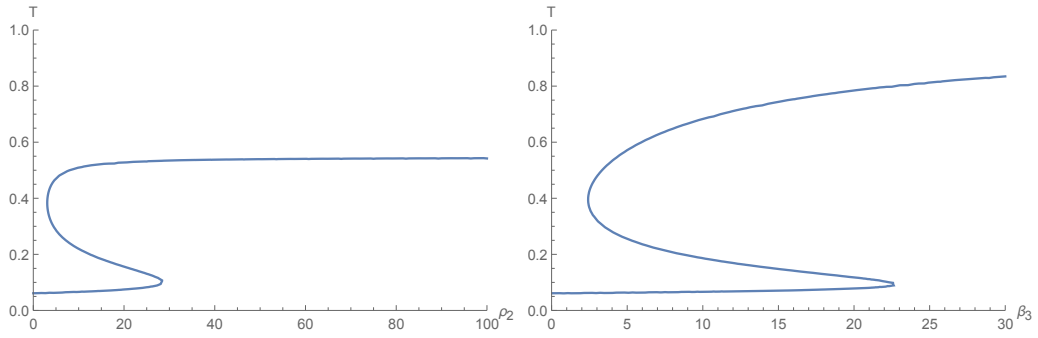


Figura 40 – Diagramas de bifurcação dos pontos de equilíbrio não-triviais do sistema (6.3) mostrando ocorrência de histerese. Eixo vertical: células tumorais $T$. Eixo horizontal: parâmetros $\rho_2$ (esquerda) e $\beta_3$ (direita).

Contudo, à medida que $K$ aumenta, o volume tumoral diminui até um certo valor e depois aumenta rapidamente. No segundo gráfico, para outros valores dos parâmetros, vemos um forte efeito de histerese à medida que $K$ varia.

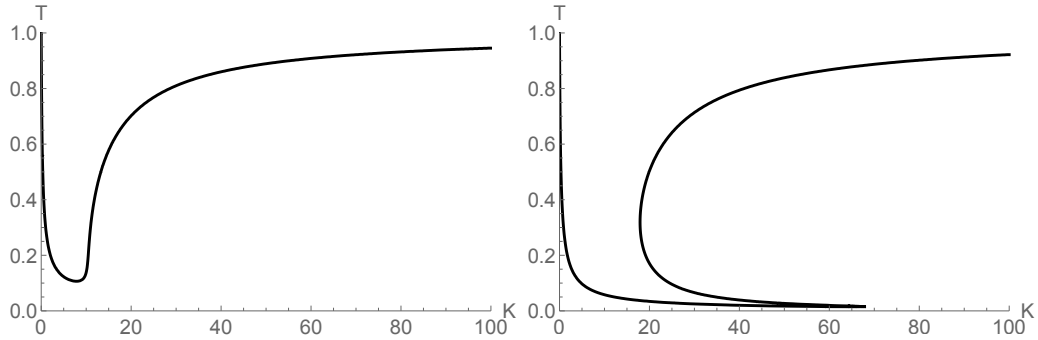


Figura 41 – Diagramas de bifurcação dos pontos de equilíbrio não-triviais do sistema (6.3) mostrando ocorrência de histerese. Eixo vertical: células tumorais $T$. Eixo horizontal: capacidade de suporte do tumor $K = b^{-1}$.

Assim, uma possível extensão do modelo apresentado acima é considerar explicitamente a dinâmica angiogênica. Um possível modelo seria o seguinte:

$$\frac{dT}{dt} = r_T T\left(1 - \frac{T}{K_T + \alpha V}\right) - d_1 TE, \tag{6.5}$$

$$\frac{dE}{dt} = \frac{r_E(c_1 + e_1 V)T}{\mu_E + c_1 T} - \mu_E E - d_2 TE - d_3 RE, \tag{6.6}$$

$$\frac{dR}{dt} = \frac{r_R(c_2 + e_2 V)T^2}{\mu_R + c_2 T^2} - \mu_R R, \tag{6.7}$$

$$\frac{dV}{dt} = \frac{\eta RV}{\kappa + V} - \mu_V V. \tag{6.8}$$

Neste caso, células T reguladoras promovem a angiogênese por meio a formação de uma vasculatura $V$, e esta nova vasculatura alimenta o tumor com mais nutrientes e oxigênio (termo $\alpha V$), mas também traz mais células T, reguladoras e citotóxicas, para o microambiente do tumor (termos $e_1 V$ e $e_2 V$).

## Avaliação de combinação de tratamentos em tumores angiogênicos

Uma segunda linha de pesquisa para trabalhos futuros é a aplicação da abordagem apresentada no Capítulo 5 a modelos mais completos considerando tumores específicos. Por exemplo, tumores como gliobastoma e câncer coloretal são tumores angiogênicos que tem sido tratados com combinação de quimioterápicos com inibidores de angiogênese. Assim, pode-se incluir angiogênese tumoral naquele modelo, introduzindo-se uma equação para a neovascularização, descrita por $V$. Além disso, a dosagem de um tratamento quimioterápico é limitada pela toxicidade que este causa em células do organismo que, em geral, não são as células do órgão onde o tumor se desenvolve. Portanto, a toxicidade é avaliada em uma população de células normais $N_2$ que não interage diretamente com o tumor, ao contrário das células normais do tecido, descritas por $N_1$. Além do efeito dos inibidores angiogênicos (descritos por $I$) pode-se considerar também os efeitos de radioterapia nas populações celulares, descritos pelos termos $g_i(t)$. Assim, teríamos o sistema:

$$\frac{dN_1}{dt} = r_N - \mu_N N_1 - \beta_1 N_1 A - \alpha_N \gamma_N D N_1 - g_1(t), \tag{6.9}$$

$$\frac{dA}{dt} = r_A A\left(1 - \frac{A}{K_A + kV}\right) - \beta_3 N A - (\mu_A + \epsilon_A)A - \alpha_A \gamma_A D A - g_2(t), \tag{6.10}$$

$$\frac{dV}{dt} = bA - dVA - \mu_V V - \kappa\eta I V - g_3(t), \tag{6.11}$$

$$\frac{dD}{dt} = v_D(t) - \gamma_A D A - \gamma_{N_1} D N_1 - \gamma_{N_2} D N_2 - \tau_D D, \tag{6.12}$$

$$\frac{dI}{dt} = v_I(t) - \eta I V - \tau_I I, \tag{6.13}$$

$$\frac{dN_2}{dt} = r_N - \mu_N N_2 - \alpha_{N_2}\gamma_{N_2} D N_2 - g_4(t). \tag{6.14}$$

$$\tag{6.15}$$

Aplicando a abordagem do Capítulo 5, podemos parametrizar as funções que descrevem os tratamentos ($v_D(t)$, $v_I(t)$, $g_i(t)$) e combinar diversos índices como toxicidade, custo total do tratamento, risco de recidiva, tempo de recuperação para buscar quais seriam as combinações ótimas de tratamento.

# Referências

1 JEMAL, A.; SIEGEL, R.; WARD, E.; HAO, Y.; XU, J.; THUN, M. J. Cancer statistics, 2009. *CA: a Cancer Journal for Clinicians*, Wiley Online Library, v. 59, n. 4, p. 225–249, 2009.

2 MACKEY, M. C.; MAINI, P. K. What has mathematics done for biology? *Bulletin of Mathematical Biology*, Springer, v. 77, n. 5, p. 735–738, 2015.

3 COHEN, J. E. Mathematics is biology's next microscope, only better; biology is mathematics' next physics, only better. *PLoS Biology*, Public Library of Science, v. 2, n. 12, p. e439, 2004.

4 ARAUJO, R. P.; MCELWAIN, D. S. A history of the study of solid tumour growth: the contribution of mathematical modelling. *Bulletin of Mathematical Biology*, Springer, v. 66, n. 5, p. 1039–1091, 2004.

5 MARTINS, M. L.; Ferreira Jr, S. C.; VILELA, M. J. Multiscale models for the growth of avascular tumors. *Physics of Life Reviews*, Elsevier, v. 4, n. 2, p. 128–156, 2007.

6 BYRNE, H. M. Dissecting cancer through mathematics: from the cell to the animal model. *Nature Reviews Cancer*, Nature Publishing Group, v. 10, n. 3, p. 221–230, 2010.

7 BYRNE, H. M.; ALARCON, T.; OWEN, M. R.; WEBB, S.; MAINI, P. K. Modelling aspects of cancer dynamics: a review. *Philosophical Transactions of the Royal Society A: Mathematical, Physical and Engineering Sciences*, The Royal Society, v. 364, n. 1843, p. 1563–1578, 2006.

8 ROOSE, T.; CHAPMAN, S. J.; MAINI, P. K. Mathematical models of avascular tumor growth. *Siam Review*, SIAM, v. 49, n. 2, p. 179–208, 2007.

9 LOWENGRUB, J. S.; FRIEBOES, H. B.; JIN, F.; CHUANG, Y.; LI, X.; MACKLIN, P.; WISE, S.; CRISTINI, V. Nonlinear modelling of cancer: bridging the gap between cells and tumours. *Nonlinearity*, IOP Publishing, v. 23, n. 1, p. R1–R91, 2010.

10 BELLOMO, N.; LI, N. K.; MAINI, P. K. On the foundations of cancer modelling: selected topics, speculations, and perspectives. *Mathematical Models and Methods in Applied Sciences*, World Scientific, v. 18, n. 04, p. 593–646, 2008.

11 REJNIAK, K. A.; ANDERSON, A. R. Hybrid models of tumor growth. *Wiley Interdisciplinary Reviews: Systems Biology and Medicine*, Wiley Online Library, v. 3, n. 1, p. 115–125, 2011.

12 GATENBY, R. A.; MAINI, P. K. Mathematical oncology: cancer summed up. *Nature*, Nature Publishing Group, v. 421, n. 6921, p. 321–321, 2003.

13 ANDERSON, A. R.; QUARANTA, V. Integrative mathematical oncology. *Nature Reviews Cancer*, Nature Publishing Group, v. 8, n. 3, p. 227–234, 2008.

14 ZHANG, L.; WANG, Z.; SAGOTSKY, J. A.; DEISBOECK, T. S. Multiscale agent-based cancer modeling. *Journal of Mathematical Biology*, Springer, v. 58, n. 4-5, p. 545–559, 2009.

15 BELLOMO, N.; PREZIOSI, L. Modelling and mathematical problems related to tumor evolution and its interaction with the immune system. *Mathematical and Computer Modelling*, Elsevier, v. 32, n. 3, p. 413–452, 2000.

16 CLAIRAMBAULT, J. Can theorems help treat cancer? *Journal of Mathematical Biology*, Springer, p. 1–4, 2013.

17 BENZEKRY, S.; PASQUIER, E.; BARBOLOSI, D.; LACARELLE, B.; BARLÉSI, F.; ANDRÉ, N.; CICCOLINI, J. Metronomic reloaded: theoretical models bringing chemotherapy into the era of precision medicine. In: ELSEVIER. *Seminars in Cancer Biology*. [S.l.], 2015. v. 35, p. 53–61.

18 HANAHAN, D.; WEINBERG, R. A. The hallmarks of cancer. *Cell*, Elsevier Science, v. 100, n. 1, p. 57–70, 2000.

19 _____. Hallmarks of cancer: the next generation. *Cell*, Elsevier, v. 144, n. 5, p. 646–674, 2011.

20 WEINBERG, R. *The biology of cancer*. [S.l.]: Garland Science, 2013.

21 BARRETT, J. C. Mechanisms of multistep carcinogenesis and carcinogen risk assessment. *Environmental Health Perspectives*, National Institute of Environmental Health Science, v. 100, p. 9, 1993.

22 FOULDS, L. The experimental study of tumor progression: a review. *Cancer Research*, AACR, v. 14, n. 5, p. 327–339, 1954.

23 NOWELL, P. C. The clonal evolution of tumor cell populations. *Science*, American Association for the Advancement of Science, v. 194, n. 4260, p. 23–28, 1976.

24 SPENCER, S. L.; BERRYMAN, M. J.; GARCIA, J. A.; ABBOTT, D. An ordinary differential equation model for the multistep transformation to cancer. *Journal of Theoretical Biology*, Elsevier, v. 231, n. 4, p. 515–524, 2004.

25 ASHKENAZI, R.; GENTRY, S. N.; JACKSON, T. L. Pathways to tumorigenesis-modeling mutation acquisition in stem cells and their progeny. *Neoplasia*, Elsevier, v. 10, n. 11, p. 1170–IN6, 2008.

26 GENTRY, S. N.; JACKSON, T. L. A mathematical model of cancer stem cell driven tumor initiation: implications of niche size and loss of homeostatic regulatory mechanisms. *PLoS One*, v. 8, p. e71128, 2013.

27 STIEHL, T.; MARCINIAK-CZOCHRA, A. Mathematical modeling of leukemogenesis and cancer stem cell dynamics. *Mathematical Modelling of Natural Phenomena*, Cambridge Univ Press, v. 7, n. 01, p. 166–202, 2012.

28 SOLÉ, R. V.; DEISBOECK, T. S. An error catastrophe in cancer? *Journal of Theoretical Biology*, Elsevier, v. 228, n. 1, p. 47–54, 2004.

29 MICHOR, F.; HUGHES, T. P.; IWASA, Y.; BRANFORD, S.; SHAH, N. P.; SAWYERS, C. L.; NOWAK, M. A. Dynamics of chronic myeloid leukaemia. *Nature*, Nature Publishing Group, v. 435, n. 7046, p. 1267–1270, 2005.

30 MICHOR, F. Mathematical models of cancer stem cells. *Journal of Clinical Oncology*, American Society of Clinical Oncology, v. 26, n. 17, p. 2854–2861, 2008.

31 NAGY, J. D. Competition and natural selection in a mathematical model of cancer. *Bulletin of Mathematical Biology*, Springer, v. 66, n. 4, p. 663–687, 2004.

32 ENDERLING, H.; CHAPLAIN, M. A.; ANDERSON, A. R.; VAIDYA, J. S. A mathematical model of breast cancer development, local treatment and recurrence. *Journal of Theoretical Biology*, Elsevier, v. 246, n. 2, p. 245–259, 2007.

33 JOHNSTON, M. D.; EDWARDS, C. M.; BODMER, W. F.; MAINI, P. K.; CHAPMAN, S. J. Mathematical modeling of cell population dynamics in the colonic crypt and in colorectal cancer. *Proceedings of the National Academy of Sciences*, National Acad Sciences, v. 104, n. 10, p. 4008–4013, 2007.

34 MARCINIAK-CZOCHRA, A.; KIMMEL, M. Reaction-difusion model of early carcinogenesis: The effects of influx of mutated cells. *Mathematical Modelling of Natural Phenomena*, Cambridge Univ Press, v. 3, n. 07, p. 90–114, 2008.

35 BELLOMO, N.; DELITALA, M. From the mathematical kinetic, and stochastic game theory to modelling mutations, onset, progression and immune competition of cancer cells. *Physics of Life Reviews*, Elsevier, v. 5, n. 4, p. 183–206, 2008.

36 GENTRY, S. N.; ASHKENAZI, R.; JACKSON, T. L. A maturity-structured mathematical model of mutation, acquisition in the absence of homeostatic regulation. *Mathematical Modelling of Natural Phenomena*, Cambridge Univ Press, v. 4, n. 03, p. 156–182, 2009.

37 DELCASTILLO, T.; IGNACIO, J. On a mathematical model of tumor growth based on cancer stem cells. *Mathematical Biosciences and Engineering (MBE)*, American Institute of Mathematical Sciences, v. 10, n. 1, p. 263–278, 2013.

38 TOMLINSON, I. P.; BODMER, W. F. Failure of programmed cell death and differentiation as causes of tumors: some simple mathematical models. *Proceedings of the National Academy of Sciences*, National Acad Sciences, v. 92, n. 24, p. 11130–11134, 1995.

39 D'ONOFRIO, A.; TOMLINSON, I. P. A nonlinear mathematical model of cell turnover, differentiation and tumorigenesis in the intestinal crypt. *Journal of Theoretical Biology*, Elsevier, v. 244, n. 3, p. 367–374, 2007.

40 SPENCER, S. L.; GERETY, R. A.; PIENTA, K. J.; FORREST, S. Modeling somatic evolution in tumorigenesis. *PLoS Computational Biology*, v. 2, n. 8, p. e108, 2006.

41 ABBOTT, R. G.; FORREST, S.; PIENTA, K. J. Simulating the hallmarks of cancer. *Artificial Life*, MIT Press, v. 12, n. 4, p. 617–634, 2006.

42 ENDERLING, H.; HAHNFELDT, P. Cancer stem cells in solid tumors: Is 'evading apoptosis'a hallmark of cancer? *Progress in Biophysics and Molecular Biology*, Elsevier, v. 106, n. 2, p. 391–399, 2011.

43 VAINSTEIN, V.; KIRNASOVSKY, O. U.; KOGAN, Y.; AGUR, Z. Strategies for cancer stem cell elimination: Insights from mathematical modeling. *Journal of Theoretical Biology*, Elsevier, v. 298, p. 32–41, 2012.

44 FUMIÃ, H. F.; MARTINS, M. L. Boolean network model for cancer pathways: predicting carcinogenesis and targeted therapy outcomes. *PLoS One*, Public Library of Science, v. 8, n. 7, p. e69008, 2013.

45 RODRIGUEZ-BRENES, I. A.; KOMAROVA, N. L.; WODARZ, D. Tumor growth dynamics: insights into evolutionary processes. *Trends in Ecology & Evolution*, Elsevier, v. 28, n. 10, p. 597–604, 2013.

46 WICHA, M. S.; LIU, S.; DONTU, G. Cancer stem cells: an old idea—a paradigm shift. *Cancer Research*, AACR, v. 66, n. 4, p. 1883–1890, 2006.

47 REYA, T.; MORRISON, S. J.; CLARKE, M. F.; WEISSMAN, I. L. Stem cells, cancer, and cancer stem cells. *Nature*, Nature Publishing Group, v. 414, n. 6859, p. 105–111, 2001.

48 GATENBY, R. A. Models of tumor-host interaction as competing populations: implications for tumor biology and treatment. *Journal of Theoretical Biology*, Elsevier, v. 176, n. 4, p. 447–455, 1995.

49 GATENBY, R. A.; GAWLINSKI, E. T. A reaction-diffusion model of cancer invasion. *Cancer Research*, AACR, v. 56, n. 24, p. 5745–5753, 1996.

50 PILLIS, L. G. de; RADUNSKAYA, A. A mathematical tumor model with immune resistance and drug therapy: an optimal control approach. *Computational and Mathematical Methods in Medicine*, Taylor & Francis, v. 3, n. 2, p. 79–100, 2001.

51 MCGILLEN, J. B.; GAFFNEY, E. A.; MARTIN, N. K.; MAINI, P. K. A general reaction–diffusion model of acidity in cancer invasion. *Journal of Mathematical Biology*, Springer, v. 68, n. 5, p. 1199–1224, 2014.

52 SIMONS, B. D.; CLEVERS, H. Strategies for homeostatic stem cell self-renewal in adult tissues. *Cell*, Elsevier, v. 145, n. 6, p. 851–862, 2011.

53 MORRISON, S. J.; KIMBLE, J. Asymmetric and symmetric stem-cell divisions in development and cancer. *Nature*, Nature Publishing Group, v. 441, n. 7097, p. 1068–1074, 2006.

54 KUZNETSOV, V. A.; MAKALKIN, I. A.; TAYLOR, M. A.; PERELSON, A. S. Nonlinear dynamics of immunogenic tumors: parameter estimation and global bifurcation analysis. *Bulletin of Mathematical Biology*, Springer, v. 56, n. 2, p. 295–321, 1994.

55 PILLIS, L. G. de; RADUNSKAYA, A. E.; WISEMAN, C. L. A validated mathematical model of cell-mediated immune response to tumor growth. *Cancer Research*, AACR, v. 65, n. 17, p. 7950–7958, 2005.

56 FEDI, P.; TRONICK, S.; AARONSON, S. Growth factors. *Cancer Medicine*, Baltimore, MD: Williams and Wilkins, p. 41–64, 1997.

57 SHERR, C. J. Principles of tumor suppression. *Cell*, Elsevier, v. 116, n. 2, p. 235–246, 2004.

58 YANG, H. M. Mathematical modeling of solid cancer growth with angiogenesis. *Theoretical Biology and Medical Modelling*, BioMed Central Ltd, v. 9, n. 2, 2012.

59 BARTEK, J.; BARTKOVA, J.; LUKAS, J. Dna damage signalling guards against activated oncogenes and tumour progression. *Oncogene*, Nature Publishing Group, v. 26, n. 56, p. 7773–7779, 2007.

60 DANIAL, N. N.; KORSMEYER, S. J. Cell death: critical control points. *Cell*, Elsevier, v. 116, n. 2, p. 205–219, 2004.

61 FINN, O. J. Cancer immunology. *New England Journal of Medicine*, Mass Medical Soc, v. 358, n. 25, p. 2704–2715, 2008.

62 GATENBY, R. A.; GAWLINSKI, E. T. The glycolytic phenotype in carcinogenesis and tumor invasion insights through mathematical models. *Cancer Research*, AACR, v. 63, n. 14, p. 3847–3854, 2003.

63 GATENBY, R. A.; GAWLINSKI, E. T.; GMITRO, A. F.; KAYLOR, B.; GILLIES, R. J. Acid-mediated tumor invasion: a multidisciplinary study. *Cancer Research*, AACR, v. 66, n. 10, p. 5216–5223, 2006.

64 TOMLINSON, I. P.; NOVELLI, M. R.; BODMER, W. F. The mutation rate and cancer. *Proceedings of the National Academy of Sciences*, National Acad Sciences, v. 93, n. 25, p. 14800–14803, 1996.

65 JACKSON, A. L.; LOEB, L. A. The mutation rate and cancer. *Genetics*, Genetics Soc America, v. 148, n. 4, p. 1483–1490, 1998.

66 LOEB, L. A. Mutator phenotype may be required for multistage carcinogenesis. *Cancer Research*, AACR, v. 51, n. 12, 1991.

67 NEGRINI, S.; GORGOULIS, V. G.; HALAZONETIS, T. D. Genomic instability—an evolving hallmark of cancer. *Nature Reviews Molecular Cell Biology*, Nature Publishing Group, v. 11, n. 3, p. 220–228, 2010.

68 SALK, J. J.; FOX, E. J.; LOEB, L. A. Mutational heterogeneity in human cancers: Origin and consequences. *Annu. Rev. Pathol. Mech. Dis*, v. 5, p. 51–75, 2010.

69 ANDERSON, B.; JACKSON, J.; SITHARAM, M. Descartes' rule of signs revisited. *American Mathematical Monthly*, JSTOR, p. 447–451, 1998.

70 CANTRELL, R. S.; COSNER, C. Practical persistence in ecological models via comparison methods. *Proceedings of the Royal Society of Edinburgh: Section A Mathematics*, Cambridge Univ Press, v. 126, n. 02, p. 247–272, 1996.

71 STROGATZ, S. H. *Nonlinear dynamics and chaos: with applications to physics, biology and chemistry*. [S.l.]: Perseus publishing, 2001.

72 WILLEMS, J. L. *Stability theory of dynamical systems*. [S.l.]: Nelson London, 1970.

73 FOLKMAN, J. What is the evidence that tumors are angiogenesis dependent? *Journal of the National Cancer Institute*, Oxford University Press, v. 82, n. 1, p. 4–7, 1990.

74 SCHABEL, F. M. Concepts for systemic treatment of micrometastases. *Cancer*, Wiley Online Library, v. 35, n. 1, p. 15–24, 1975.

75 RUGGIERO, R. A.; BUSTUOABAD, O. D. The biological sense of cancer: a hypothesis. *Theoretical Biology and Medical Modelling*, v. 3, p. 43, 2006.

76 HOLLING, C. S. Resilience and stability of ecological systems. *Annual Review of Ecology and Systematics*, JSTOR, p. 1–23, 1973.

77 MAY, R. M. Thresholds and breakpoints in ecosystems with a multiplicity of stable states. *Nature*, v. 269, n. 5628, p. 471–477, 1977.

78 SCHEFFER, M.; CARPENTER, S.; FOLEY, J. A.; FOLKE, C.; WALKER, B. Catastrophic shifts in ecosystems. *Nature*, Nature Publishing Group, v. 413, n. 6856, p. 591–596, 2001.

79 FOLKE, C. Resilience: The emergence of a perspective for social–ecological systems analyses. *Global Environmental Change*, Elsevier, v. 16, n. 3, p. 253–267, 2006.

80 MENCK, P. J.; HEITZIG, J.; MARWAN, N.; KURTHS, J. How basin stability complements the linear-stability paradigm. *Nature Physics*, Nature Publishing Group, v. 9, n. 2, p. 89–92, 2013.

81 MEYER, K. A dynamical systems framework for resilience in ecology. *arXiv preprint arXiv:1509.08175*, 2015.

82 WALKER, B.; HOLLING, C. S.; CARPENTER, S. R.; KINZIG, A. Resilience, adaptability and transformability in social–ecological systems. *Ecology and Society*, v. 9, n. 2, p. 5, 2004.

83 MITRA, C.; KURTHS, J.; DONNER, R. V. An integrative quantifier of multistability in complex systems based on ecological resilience. *Scientific Reports*, Nature Publishing Group, v. 5, 2015.

84 TOMASETTI, C.; VOGELSTEIN, B. Variation in cancer risk among tissues can be explained by the number of stem cell divisions. *Science*, American Association for the Advancement of Science, v. 347, n. 6217, p. 78–81, 2015.

85 WU, S.; POWERS, S.; ZHU, W.; HANNUN, Y. A. Substantial contribution of extrinsic risk factors to cancer development. *Nature*, Nature Publishing Group, v. 529, n. 7584, p. 43–47, 2016.

86 KERBEL, R. S.; KAMEN, B. A. The anti-angiogenic basis of metronomic chemotherapy. *Nature Reviews Cancer*, Nature Publishing Group, v. 4, n. 6, p. 423–436, 2004.

87 FASSONI, A. C.; YANG, H. M. Modeling dynamics for oncogenesis encompassing mutations and genetic instability. *preprint*, 2016.

88 SARAPATA, E. A.; PILLIS, L. de. A comparison and catalog of intrinsic tumor growth models. *Bulletin of Mathematical Biology*, Springer, v. 76, n. 8, p. 2010–2024, 2014.

89 KERBEL, R. S. Tumor angiogenesis. *New England Journal of Medicine*, Mass Medical Soc, v. 358, n. 19, p. 2039–2049, 2008.

90 VIVIER, E.; UGOLINI, S.; BLAISE, D.; CHABANNON, C.; BROSSAY, L. Targeting natural killer cells and natural killer t cells in cancer. *Nature Reviews Immunology*, Nature Publishing Group, v. 12, n. 4, p. 239–252, 2012.

91 FACCIABENE, A.; MOTZ, G. T.; COUKOS, G. T-regulatory cells: key players in tumor immune escape and angiogenesis. *Cancer Research*, AACR, v. 72, n. 9, p. 2162–2171, 2012.

92 FASSONI, A. C.; TAKAHASHI, L. T.; SANTOS, L. J. dos. Basins of attraction of the classic model of competition between two populations. *Ecological Complexity*, Elsevier, v. 18, p. 39–48, 2014.

93 FASSONI, A. C.; MARTINS, M. L. Mathematical analysis of a model for plant invasion mediated by allelopathy. *Ecological Complexity*, Elsevier, v. 18, p. 49–58, 2014.

94 EFTIMIE, R.; BRAMSON, J. L.; EARN, D. J. Interactions between the immune system and cancer: a brief review of non-spatial mathematical models. *Bulletin of Mathematical Biology*, Springer, v. 73, n. 1, p. 2–32, 2011.

95 STUPP, R.; MASON, W. P.; BENT, M. J. V. D.; WELLER, M.; FISHER, B.; TAPHOORN, M. J.; BELANGER, K.; BRANDES, A. A.; MAROSI, C.; BOGDAHN, U. et al. Radiotherapy plus concomitant and adjuvant temozolomide for glioblastoma. *New England Journal of Medicine*, Mass Medical Soc, v. 352, n. 10, p. 987–996, 2005.

96 SCHEFFER, M.; CARPENTER, S. R.; DAKOS, V.; NES, E. H. van. Generic indicators of ecological resilience: inferring the chance of a critical transition. *Annual Review of Ecology, Evolution, and Systematics*, Annual Reviews, v. 46, p. 145–167, 2015.

97 CHIANG, H.-D.; HIRSCH, M. W.; WU, F. F. Stability regions of nonlinear autonomous dynamical systems. *Automatic Control, IEEE Transactions on*, IEEE, v. 33, n. 1, p. 16–27, 1988.

98 ABARBANEL, H. D.; BROWN, R.; KENNEL, M. B. Variation of lyapunov exponents on a strange attractor. *Journal of Nonlinear Science*, Springer, v. 1, n. 2, p. 175–199, 1991.

99 SCHILLER, J. H.; HARRINGTON, D.; BELANI, C. P.; LANGER, C.; SANDLER, A.; KROOK, J.; ZHU, J.; JOHNSON, D. H. Comparison of four chemotherapy regimens for advanced non–small-cell lung cancer. *New England Journal of Medicine*, Mass Medical Soc, v. 346, n. 2, p. 92–98, 2002.

100 LEAF, C. Why we're losing the war on cancer (and how to win it). *Fortune*, TIME INC, v. 149, n. 5, p. 42–55, 2004.

101 PASQUIER, E.; KAVALLARIS, M.; ANDRÉ, N. Metronomic chemotherapy: new rationale for new directions. *Nature Reviews Clinical Oncology*, Nature Publishing Group, v. 7, n. 8, p. 455–465, 2010.

102 HANAHAN, D.; BERGERS, G.; BERGSLAND, E. Less is more, regularly: metronomic dosing of cytotoxic drugs can target tumor angiogenesis in mice. *The Journal of Clinical Investigation*, Am Soc Clin Investig, v. 105, n. 8, p. 1045–1047, 2000.

103 KERBEL, R. S. Inhibition of tumor angiogenesis as a strategy to circumvent acquired resistance to anti-cancer therapeutic agents. *Bioessays*, Wiley Online Library, v. 13, n. 1, p. 31–36, 1991.

104 HAHNFELDT, P.; PANIGRAHY, D.; FOLKMAN, J.; HLATKY, L. Tumor development under angiogenic signaling a dynamical theory of tumor growth, treatment response, and postvascular dormancy. *Cancer Research*, AACR, v. 59, n. 19, p. 4770–4775, 1999.

105 D'ONOFRIO, A.; GANDOLFI, A. Tumour eradication by antiangiogenic therapy: analysis and extensions of the model by hahnfeldt et al.(1999). *Mathematical Biosciences*, Elsevier, v. 191, n. 2, p. 159–184, 2004.

106 SCHÄTTLER, H.; LEDZEWICZ, U.; AMINI, B. Dynamical properties of a minimally parameterized mathematical model for metronomic chemotherapy. *Journal of Mathematical Biology*, Springer, p. 1–26, 2015.

107 PILLIS, L. G. de; GU, W.; RADUNSKAYA, A. E. Mixed immunotherapy and chemotherapy of tumors: modeling, applications and biological interpretations. *Journal of Theoretical Biology*, Elsevier, v. 238, n. 4, p. 841–862, 2006.

108 PINHO, S. T.; BACELAR, F. S.; ANDRADE, R. F.; FREEDMAN, H. I. A mathematical model for the effect of anti-angiogenic therapy in the treatment of cancer tumours by chemotherapy. *Nonlinear Analysis: Real World Applications*, Elsevier, v. 14, n. 1, p. 815–828, 2013.

109 SACHS, R. K.; HLATKY, L. R.; HAHNFELDT, P. Simple ode models of tumor growth and anti-angiogenic or radiation treatment. *Mathematical and Computer Modelling*, Elsevier, v. 33, n. 12, p. 1297–1305, 2001.

110 STAMPER, I. J.; OWEN, M. R.; MAINI, P. K.; BYRNE, H. M. Oscillatory dynamics in a model of vascular tumour growth-implications for chemotherapy. *Biology Direct*, BioMed Central Ltd, v. 5, n. 1, p. 27, 2010.

111 COJOCARU, L.; AGUR, Z. A theoretical analysis of interval drug dosing for cell-cycle-phase-specific drugs. *Mathematical Biosciences*, Elsevier, v. 109, n. 1, p. 85–97, 1992.

112 PANETTA, J. C. A mathematical model of periodically pulsed chemotherapy: tumor recurrence and metastasis in a competitive environment. *Bulletin of Mathematical Biology*, Springer, v. 58, n. 3, p. 425–447, 1996.

113 _____. A mathematical model of drug resistance: heterogeneous tumors. *Mathematical Biosciences*, Elsevier, v. 147, n. 1, p. 41–61, 1998.

114 LEDZEWICZ, U.; SCHÄTTLER, H. Analysis of a cell-cycle specific model for cancer chemotherapy. *Journal of Biological Systems*, World Scientific, v. 10, n. 03, p. 183–206, 2002.

115 LAKMECHE, A.; ARINO, O. Nonlinear mathematical model of pulsed-therapy of heterogeneous tumors. *Nonlinear Analysis: Real World Applications*, Elsevier, v. 2, n. 4, p. 455–465, 2001.

116 HOLDER, A. B.; RODRIGO, M. R. Model for acid-mediated tumour invasion with chemotherapy intervention ii: Spatially heterogeneous populations. *Mathematical Biosciences*, Elsevier, v. 270, p. 10–29, 2015.

117 SWAN, G. W. Role of optimal control theory in cancer chemotherapy. *Mathematical Biosciences*, Elsevier, v. 101, n. 2, p. 237–284, 1990.

118 MARTIN, R. Optimal control drug scheduling of cancer chemotherapy. *Automatica*, Elsevier, v. 28, n. 6, p. 1113–1123, 1992.

119 COSTA, M. I.; BOLDRINI, J. L.; BASSANEZI, R. C. Drug kinetics and drug resistance in optimal chemotherapy. *Mathematical Biosciences*, Elsevier, v. 125, n. 2, p. 191–209, 1995.

120 _____. Chemotherapeutic treatments involving drug resistance and level of normal cells as a criterion of toxicity. *Mathematical Biosciences*, Elsevier, v. 125, n. 2, p. 211–228, 1995.

121 COSTA, M. I.; BOLDRINI, J. L. Conflicting objectives in chemotherapy with drug resistance. *Bulletin of Mathematical Biology*, Springer, v. 59, n. 4, p. 707–724, 1997.

122 BOLDRINI, J. L.; COSTA, M. I. Therapy burden, drug resistance, and optimal treatment regimen for cancer chemotherapy. *Mathematical Medicine and Biology*, IMA, v. 17, n. 1, p. 33–51, 2000.

123 PANETTA, J. C.; FISTER, K. R. Optimal control applied to cell-cycle-specific cancer chemotherapy. *SIAM Journal on Applied Mathematics*, SIAM, v. 60, n. 3, p. 1059–1072, 2000.

124 PILLIS, L. G. de; RADUNSKAYA, A. The dynamics of an optimally controlled tumor model: A case study. *Mathematical and Computer Modelling*, Elsevier, v. 37, n. 11, p. 1221–1244, 2003.

125 LEDZEWICZ, U.; SCHÄTTLER, H. Antiangiogenic therapy in cancer treatment as an optimal control problem. *SIAM Journal on Control and Optimization*, SIAM, v. 46, n. 3, p. 1052–1079, 2007.

126 ENGELHART, M.; LEBIEDZ, D.; SAGER, S. Optimal control for selected cancer chemotherapy ode models: A view on the potential of optimal schedules and choice of objective function. *Mathematical Biosciences*, Elsevier, v. 229, n. 1, p. 123–134, 2011.

127 LEDZEWICZ, U.; AMINI, B.; SCHÄTTLER, H. Dynamics and control of a mathematical model for metronomic chemotherapy. *Mathematical Biosciences and Engineering (MBE)*, v. 12, n. 6, p. 1257–1275, 2015.

128 LORZ, A.; LORENZI, T.; CLAIRAMBAULT, J.; ESCARGUEIL, A.; PERTHAME, B. Modeling the effects of space structure and combination therapies on phenotypic heterogeneity and drug resistance in solid tumors. *Bulletin of Mathematical Biology*, Springer, v. 77, n. 1, p. 1–22, 2015.

129 BILLY, F.; CLAIRAMBAULT, J.; FERCOQ, O. Optimisation of cancer drug treatments using cell population dynamics. In: *Mathematical Methods and Models in Biomedicine*. [S.l.]: Springer, 2013. p. 265–309.

130 FASSONI, A. C.; YANG, H. M. An ecological resilience perspective on cancer: insights from a toy model. *preprint*, 2016.

131 LAKSHMIKANTHAM, V.; LEELA, S. *Differential and integral inequalities: theory and applications*. [S.l.]: Academic press, 1969. v. 1.

132 SMITH, H. L. *Monotone dynamical systems: an introduction to the theory of competitive and cooperative systems*. [S.l.]: American Mathematical Soc., 2008.

133 STEPANOVA, N. Course of the immune reaction during the development of a malignant tumor. *Biophysics*, v. 24, n. 1, p. 220–235, 1980.

134 GUCKENHEIMER, J.; HOLMES, P. *Nonlinear oscillations, dynamical systems, and bifurcations of vector fields*. [S.l.]: Springer Science & Business Media, 1983. v. 42.

135 KUZNETSOV, Y. A. *Elements of applied bifurcation theory*. [S.l.]: Springer, 1998. v. 112.

136 CHEN, C.-S.; DOLOFF, J. C.; WAXMAN, D. J. Intermittent metronomic drug schedule is essential for activating antitumor innate immunity and tumor xenograft regression. *Neoplasia*, Elsevier, v. 16, n. 1, p. 84–W27, 2014.

137 BENZEKRY, S.; HAHNFELDT, P. Maximum tolerated dose versus metronomic scheduling in the treatment of metastatic cancers. *Journal of Theoretical Biology*, Elsevier, v. 335, p. 235–244, 2013.

138 FASSONI, A. C.; YANG, H. M. Minimal model for metronomic chemotherapy in avascular tumors: global dynamics and medical implications. *preprint*, 2016.

139 ROBERTSON-TESSI, M.; EL-KAREH, A.; GORIELY, A. A model for effects of adaptive immunity on tumor response to chemotherapy and chemoimmunotherapy. *Journal of Theoretical Biology*, Elsevier, v. 380, p. 569–584, 2015.